DECONSTRUCTING THE TUMOUR MICROENVIRONMENT: THE ROLE OF FIBRONECTIN

By Frankie Vanterpool

Submitted in fulfilment of the requirements
for the degree of Doctor of Philosophy in
Biomedical Engineering

School of Engineering
College of Science and Engineering
University of Glasgow

September 2017

Abstract

Cancer is a worldwide issue affecting millions and the need for understanding specific mechanisms linked to its progression has never been higher. One of the biggest challenges in cancer research is the complexity of the tumour microenvironment (TME) which not only consists of cancerous cells, but auxiliary lymphocytes, macrophages, blood vessels and the extracellular matrix (ECM). There is therefore a need to unravel the impact of these specific components on cancer cells by deconstructing their environment. In this study, we aim to understand fundamental cell-ECM interactions by breaking down the complex TME to its building blocks: the cancer cell and the ECM.

We use poly(alkyl acrylates) material surfaces which have been shown to direct the organisation of fibronectin (FN), a key ECM protein, upon adsorption to study cell behaviour such as adhesion, growth, migration and drug resistance. Here we show that poly(methyl acrylate) (PMA) and poly(ethyl acrylate) (PEA) are able to organise FN into globular and fibrillar conformations respectively upon adsorption, thus exposing or concealing specific integrin binding domains such as the RGD cell binding domain and the PHSRN synergy sequence.

With these conditions, we assess: cell adhesion through studying attachment, focal adhesion formation and single cell traction on the surface of the polymers; cell migration by looking at the speed of gap closure in wound healing assays; drug resistance by studying cytotoxicity of a well-established anticancer drug in docetaxel as well as PND-1186 (VS-4718) which is a novel drug currently in phase 1 clinical trials; and intracellular signalling by quantifying protein expressions of focal adhesion kinase (FAK). Furthermore, we conduct a preliminary study of cancer cells in a highly tuneable poly ethylene glycol (PEG)-based 3D system functionalised with the RGD cell binding domain. We analyse hydrogel stability, cell viability and cell invasion.

We demonstrate that upon adsorption to the polymers the fibrillar and globular forms of FN lead to the PHSRN synergy sequence being more exposed on PEA compared to PMA respectively. This is shown to have significant impact on cell anchorage, mediated primarily by the RGD domain of FN via integrin $\alpha_v\beta_3$, and cell motility which is mediated by both the RGD and PHSRN sequences via integrin $\alpha_5\beta_1$.

We also demonstrate that although this 2D model provides essential information for cell-ECM interactions, it does not take into account the 3D environment. We show that cells are able to interact with the proposed PEG-based hydrogel and that it can be fine-tuned by altering gel stiffness and functional components independently.

Overall, the methods and systems used in this study have allowed for a better understanding of the material-protein and the cell-protein interfaces and how they affect cell behaviour in regard to adhesion, migration and invasion.

Table of contents

List of Tables

List of Figures

Acknowledgments

I would first and foremost like to thank God for giving me the strength and grace to carry out this project for the past 4 years. I would also like to thank my family, especially my parents, Frankie and Sylvia Vanterpool, for always encouraging me to go as far as possible in my education. My wife, Amanda, who has been a constant support and help to me, being patient during the long days and nights at work. My supervisors, Professor Manuel Salmerón-Sanchez, Dr Philipp Seib and Dr Marco Cantini who have been extremely patient with me all while encouraging me and always pushing me in the right direction. Lastly, I would like to thank the University of Glasgow, Strathclyde University, and the ERC who funded this project through HealinSynergy 306990.

Author’s declaration

“I declare that, except where explicit reference is made to the contribution of others, this thesis is the result of my own work and has not been submitted for any other degree at the University of Glasgow or any other institution”

Frankie Artwin Vanterpool

List of abbreviations

2D: 2 Dimensional

3D: 3 Dimensional

ACA: Advancing contact angle

AFM: Atomic force microscopy

BCA: Bicinchoninic acid

BME: Biomedical engineering

DMEM: Dulbecco's modified eagle's medium

DMSO: Dimethyl sulfoxide

DPBS: Dulbecco's phosphate buffer saline

ECM: Extracellular matrix

ELISA: Enzyme-linked immunosorbent assay

FAs: Focal adhesions

FAAS: Focal adhesion analysis sever

FAK: Focal Adhesion Kinase

FBS: Foetal bovine serum

FN: Fibronectin

MAL: Maleimide

MEM: Modified eagle's medium

MMP: Matrix metalloproteinase

MTT: 3-(4,5-dimethylthiazol-2-yl)-2,5-diphenyltetrazolium bromide

P/S: Penicillin/Streptomycin

PBS: Phosphate buffer saline

PEA: Poly (ethyl acrylate)

PEG: Polyethylene glycol

PEG4MAL: 4-arm PEG-Maleimide

PMA: Poly (methyl acrylate)

PHSCN: Pro-His-Ser-Arg-Asn amino acid sequence

PHSCO: Pro-His-Ser-Arg-Pyl amino acid sequence

PHSRN: Pro-His-Ser-Arg-Asn amino acid sequence

RCA: Receding contact angle

RGD: Arg-Gly-Asp amino acid sequence

RGE: Arg-Gly-Glu amino acid sequence

SCA: Static contact angle

TCP: Tissue culture plastic

TME: Tumour microenvironment

WCA: Water contact angle

1 Introduction

1.1 An overview of biomedical engineering

1.1.1 Introduction and brief history

The field of biomedical engineering (BME) is a rapidly growing area of research that has evolved over the past few decades. The term describes an interdisciplinary science in which mechanical, chemical and electrical engineering principles are used for a vast array of medical and biological applications such as bioinformatics, biomedical optics, medical devices, biomechanics and tissue engineering, among others[1, 2].

On a cellular level, the evolution of the area of BME has allowed the development of cellular and molecular biomechanics, which studies the conversion of mechanical stimuli to biological responses, as well as synthetic biology which is the design and construction of biological models such as modified amino acids and nucleotides, and custom-designed proteins and enzymes among others[3, 4]. Both interdisciplinary fields have been used to gain further understanding in cellular behaviour with research, diagnostic, therapeutic and preventative applications. The development of biosensors in the medical field has allowed more precise ways of diagnosing infectious diseases, identifying patients prone to heart failure, and are proving to be a powerful tool in cancer diagnosis through the detection of cancer-related biomarkers. Recent studies have shown that the use of engineered surfaces can affect cell adhesion, migration and proliferation, highlighting the importance of cell-material and cell-protein interactions and the dependence of the extracellular matrix[5].

1.1.2 Biological functions

These studies demonstrate how biomedical engineering is useful in understanding biological functions due to their naturally complex nature. Standard studies of cells are carried out *in vitro* with the use of tissue culture plastic (TCP), with the focus being on one cell line and understanding the physiological response as a response to different external stimuli i.e. drugs, enzymes, etc. This simplified model has shown its limitations with the fact that cells *in vivo* have very different configurations and external stimuli compared to cells on TCP. In natural conditions for a vast majority of tissue cells are in a 3-dimensional setting surrounded by other cells of

the same line, different cell types and the ECM providing them with much different biological and mechanical stimuli[6, 7].

Many 2D models of tissue culture take into account proteins of the ECM such as fibronectin, collagen, vitronectin, laminin, etc. with the addition of foetal bovine serum to allow cell adhesion and spreading[8-10]. However, these models ignore the influence of paracrine and endocrine signalling of other cell types which secrete essential proteins such as growth factors necessary for cell development. BME seeks to improve these models with the use of polymers and hydrogels that can be used to mimic *in vivo* conditions (Figure 1).

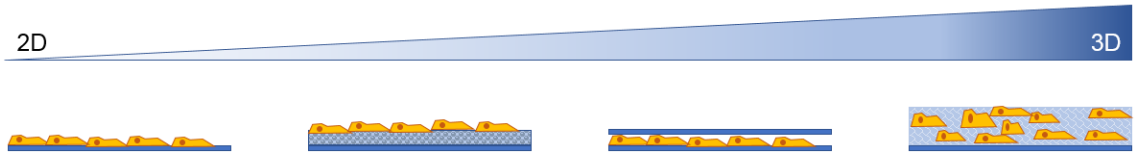

Traditional cell culture	Culture on hydrogels	Sandwich culture	Culture within hydrogels
Standard cell culture on TCP Cell-protein interactions	Mechanostransduction Cell traction	Apical and basal stimuli of cells	Cell-ECM interactions Migration Degradation/invasion

Figure 1: Applications of cell culture from 2D to 3D. Traditional cell culture is carried out on standard TCP or glass that are treated with ECM proteins allowing cell adhesion and studying specific cell-protein interactions. Cells cultured on top of hydrogels allow for the study of cell traction, looking at the mechanotransduction of forces between the cell and its close environment. Sandwich cultures are used to study the effects of apical and basal stimuli of cells. Cells cultured inside of hydrogels are used to study cells in a fully 3D setting.

Polymers are used and fine-tuned to replicate the stiffness of the natural cellular environment and study the influence of stiffness on cell behaviour. Many biomaterial surfaces are used in cell culture depending on the aim of the study. 2D hydrogels are used to provide a substrate that is not super physiologically stiff such as plastic or glass[11, 12]. This allows cells to have a less aberrant phenotypes such as flat cells with a large amount of stress fibres. It is well documented that substrate stiffness has a significant impact on cell behaviour such as differentiation and proliferation[12] so biomaterials such as polyacrylamide (PAA), collagen, alginate, polyethylene glycol (PEG), and hyaluronic acid (HA) are useful to study cells in an environment

with more controlled, physiologically relevant stiffness'[13, 14]. Furthermore, it is possible to control the proteins cells are exposed to using these biomaterials. Adhesive ligands such as RGD can be cross-linked to the majority of these substrates if they do not present any natural binding sequences[11] as well as other protein sequences of interest. This allows a more in depth understanding of specific cell-protein interactions.

Co-culture systems grow two distinct cell types, often separated by a physical boundary while allowing the transfer of proteins and molecules, to understand their interaction and the influence of one cell line on the other. Sandwich cultures are developed to provide both basal and apical stimuli to cells. Hydrogels are used with ECM protein components in order to grow cells in a 3D environment[11, 15-18].

These methods all present their respective advantages and inconveniences with a study of several of them being useful to gain a more complete understanding of biological functions.

1.1.3 Applications in cancer research

The study of cancer is a representative example in understanding the limitations of simple 2D systems on TCP and the need for more innovative methods. Tumours are complex organs within the body composed of not only the cancer cells themselves, but of various auxiliary cell types such as neoplastic cells, fibroblasts, immune cells and endothelial cells[19] (Figure 2). These are all maintained by blood vessels that irrigate them and held together by the ECM. This protective and nurturing environment provides cancer cells with the opportunity to proliferate, spread, and develop resistance to several drugs. A large number of studies now show the link between cancer treatment resistance and components of the tumour microenvironment (TME). For example, breast cancer cells develop resistance to tamoxifen, a selective oestrogen receptor modulator, via fibronectin and the β1 integrin[20, 21]. Moreover, the use of tamoxifen has been shown to increase the expression of an ECM gene cluster. This example is among many that show that the tumour's response to therapy is modulated by the TME.

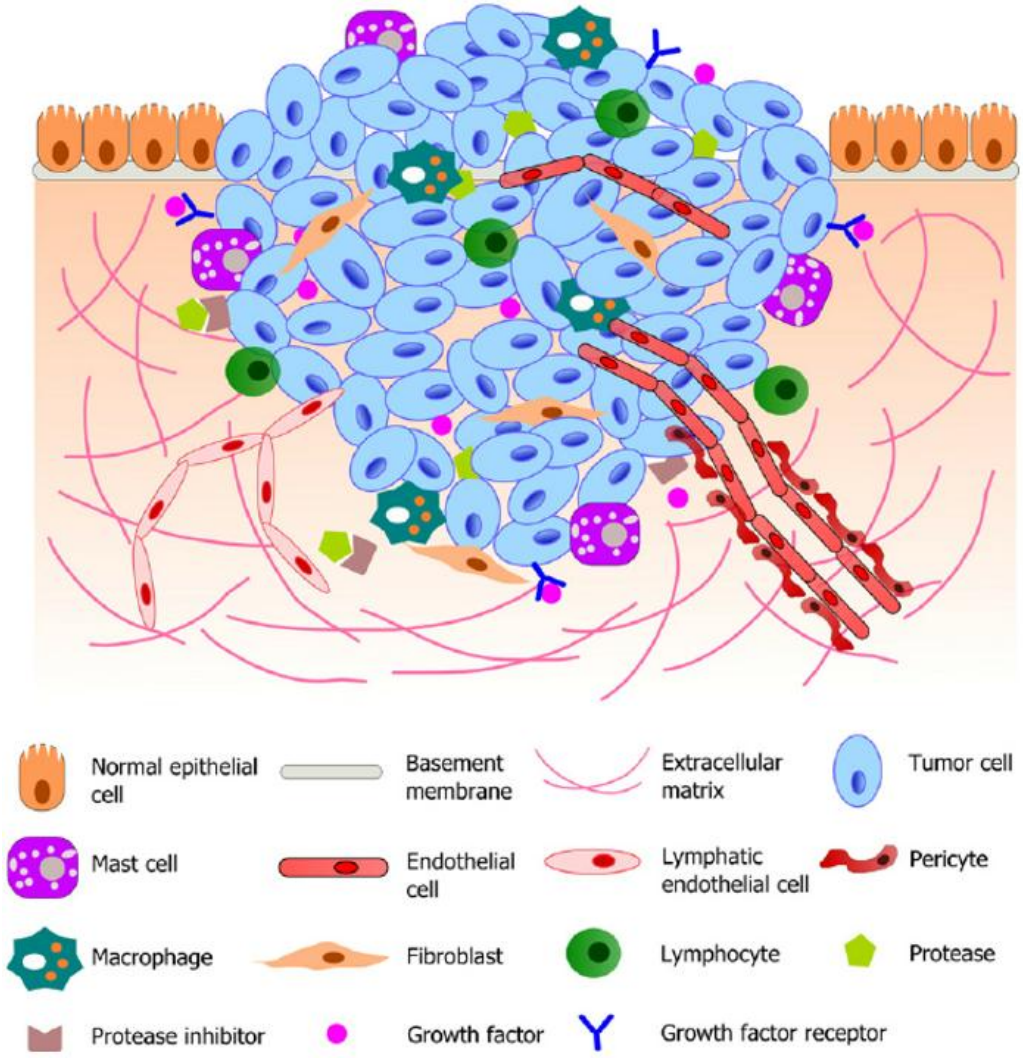

Figure 2: Schematic illustration of a typical TME. Tumour cells are surrounded and protected by diverse auxiliary cell types (such as endothelial and epithelial cells, fibroblasts, macrophages, and lymphocytes) and ECM proteins (such as collagen, fibronectin, laminin...*etc.*). Image from Xian Xu 2014[19] (© 2014, Elsevier).

Until recently, the *in vitro* study of cancer cells has failed to realise the importance of the TME and take into account the complex factors needed to fully understand cancer. Cells are grown on tissue culture treated polystyrene but this simplified model does not consider key factors of the cells environment such as accessory cells and ECM proteins. More and more studies are being carried out using biomimetic models of components of the TME and the ECM. Electrospun fibres are used due to their structural and topological similarities with the ECM and are a promising tool in understanding cancer cell migration but also for bone and neural

regenerative applications[22-24]. More *in vivo* like approaches are also being used with 3D culture models that take into consideration structural and mechanical properties not replicable in a 2D system. These systems are however not yet perfected as there is still limited special organisation and interaction between cells which does not allow a better understanding of mechanisms involving cell-cell and cell-ECM interactions. The 3D system is preferably used to better understand cell migration and not simplified interactions.

Many *in vitro* tumour models are currently being looked at to understand the mechanisms involved in cancer progression such as growth, migration, metastasis and drug resistance in order to develop novel therapies and screen potential drug candidates. There are 4 main models which are used to screen drug candidates and understand metastasis: transwell-based models, spheroids, hybrid models, and, tumour-microvessel models[25].

Transwell-based models are widely used for invasion and migration assays[26, 27] which consist of analysing the movement of the cells from one area to another either spontaneously or with the help of an external stimuli such as gradients in media, substrate stiffness or electrical fields. Migration deals with cell movement on the surface of a substrate (in the 2D context) or within a substrate (in the 3D context), whereas invasion consists of the ability of cells to penetrate a 3D ECM substrate. Transwell-based assays exist for both types of behaviours and are able to assess and compare the metastatic potential of different cell types with combinations of various ECM proteins, drugs and treatments, as well as gene modification. This method has the advantage of being relatively low-cost and high throughput but due to the fact that only single-cell motility is taken into account, it has little physiological relevance.

Spheroids are grown in suspension or in 3D ECM. They are multicellular aggregates that represent avascular tumour nodules or micro-metastases[25, 28]. They are used primarily for drug testing, proliferation, angiogenesis, as well as the effects of hypoxia on metastasis and tumour progression. This model helps understand cell-cell and cell-matrix interactions in a 3D setting as well as the tumour's interaction with its environment. Although being more expensive and needing more preparation time than 2D models, a clear advantage of spheroids is the ability to mimic *in vivo* tumours with nutrient and proliferation gradients with the development of necrotic cores[28, 29].

Hybrid models are a compromise between the elaborate TME and a straightforward *in vitro* model, consisting of properties observed in transwell and spheroid systems. For example, *ex vivo* tumour sections can be collected from patients by biopsy and embedded into an ECM substrate to determine an adequate chemotherapy treatment or even to study proliferation (Brown 2004, Xu 2013). 3D invasion models are studied by seeding cancerous cells on the surface of an ECM substrate and tracking individual movements and trajectories of cells through the hydrogel which gives insight into the effects of matrix stiffness and composition on cell adhesion and invasion[30, 31]. These techniques are useful for fine-tuning the TME and using patient-specific cells which can lead to patient specific treatment approaches but do not mimic the *in vivo* effect of angiogenesis and vasculature formation.

Tumour microvessel models take into account a commonly overlooked but rapidly growing area of interest in cancer studies[32], the supplementation of oxygen and nutrients to the tumour allowing proliferation and eventually metastasis through the formation and development of blood vessels. According to Butler *et al.* the endothelial cells that line blood vessels secrete factors that promote and repress tumour growth[33] highlighting their importance in cancer proliferation. This model is used to study the interaction between cancer cells and the microvessel, more specifically metastatic components such as intravasation into the vessel and extravasation out of the vessel.

Although many of these models are able to mimic some physiological factors such as vascularisation, invasion, degrees of hypoxia and their role in tumour progression, the study of fundamental cell-cell and cell-protein interactions proves to be difficult from a quantitative point of view. These basic interactions are important in understanding how cancer cells survive, divide and recruit other cells using ECM proteins.

1.2 The ECM

The extracellular matrix (ECM) is a complex structure of proteoglycans which form a hydrated gel filling up most of the intercellular space and various fibrous proteins such as collagen, fibronectin and laminin among others[34]. These components, produced mainly by fibroblast and other connective tissue cells are essential for holding together the cells of multicellular organisms in tissues and organs [34]. The ECM bridges between cells, provides mechanical support to tissues and is a source of signalling cues that are important for cell survival, proliferation, differentiation and migration[35, 36]. It is a highly dynamic network that communicates with cells through bi-directional integrin signalling, in conjunction with growth factors, that is inside-out (cells being able to rearrange the external ECM environment) and outside-in (ECM proteins being able to direct cell behaviour). Moreover, the ECM provides mechanical signalling with the cells being able to sense differences in ECM stiffness and respond accordingly[37].

According to J. Engel and M. Chiquet, the ECM is made up of multidomain proteins that sometimes act in a concerted fashion forming lateral interactions that allow the formation of fibres and a network[38]. Of the many domains in ECM proteins, cadherin, epidermal growth factors, TGF-β (transforming growth factor) and RGD binding domains are among the most notable. These proteins are highly involved in the signalling processes of many growth factors such as TGF-β, VEGF (vascular endothelial growth factor), and, EGF (epidermal growth factor)[39]. Collagen is secreted primarily by connective tissue cells and is the major protein of the ECM, making up to 25% of total protein mass in mammals[40]. Well documented disorders such as Marfan syndrome are linked to mutations and alterations to this structural ECM protein[41]. Fibronectin (FN), a specialized ECM protein, is one of the most studied due to its known implication in cell binding via the RGD domain and is thus essential in understanding cell-protein interaction.

1.2.1 Fibronectin

Fibronectin is synthesised in many cell types although it is primarily produced by fibroblasts and mesenchymal cells. Besides the ECM, FN can also be found in the plasma (necessary for wound healing)[42], synthesised by hepatocytes. It is a dimeric glycoprotein consisting of two subunits of 220-270 kDa and one of the main components of the ECM contributing in cell interactions and regulating cell growth

and migration[43-45]. This protein consists of a multimodular structure made up principally of three types of amino acid repeat domains termed FN-I, FN-II and FN-III (Figure 3). FN monomers consist of 12 FN-I, 2 FN-II and 15-17 FN-III repeats responsible for binding with other ECM proteins such as collagen and fibrin, other FN molecules to form networks, integrins presented at the cell surface, and growth factors[43].

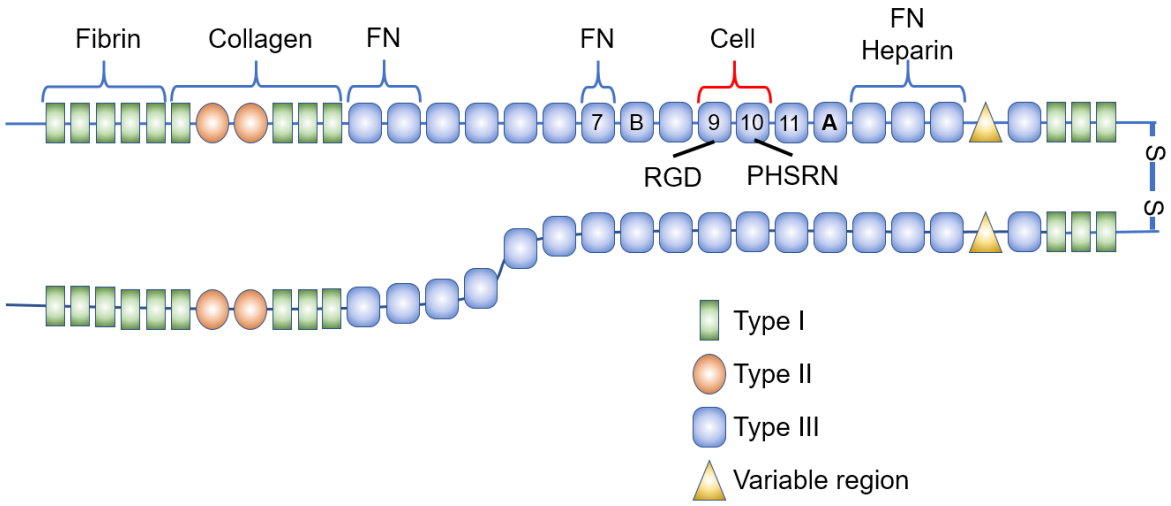

Figure 3: Structure of a fibronectin dimer with different repeat domain types and binding sites. Fibronectin is formed of repeat types I, II and III as well as a variable region. These repeats serve as binding sites for other ECM proteins such as fibrin and collagen. A cell binding site is located on the 9th and 10th type III repeat (FN-III$_{9\text{-}10}$) via PHSRN and RGD sequences respectively. Image adapted from Hynes, R.O. *et al*.[46]

Among the domains on FN, the Arg-Gly-Asp (RGD) cell binding domain is one of the most important as it binds cells via the α5β1 and αvβ3 integrins[47]. Another important domain in cell binding is the PHSRN synergy sequence that increases cell binding via the α5β1 integrin[48-50]. These domains are very close, at about 30 Å in distance from each other[51, 52] and are responsible for integrin binding and the formation of focal adhesions (FAs), anchor points of the cell in the ECM (Figure 4). Although it is largely believed that the RGD domain is essential for cell binding, some studies have shown that cells attach to FN when the RGD domain is deactivated but attachment decreases when the PHSRN domain is deactivated [47-49, 52]. Furthermore, studies have shown that cells also bind to FN using the selectively expressed $\alpha_v\beta_6$ integrin[53] and that the inhibition of $\alpha_v\beta_3$ expression led to

the inhibition of cell migration and invasion and an increase in apoptosis[54]. This suggests that there is a more complex interaction involved in cell binding possibly via other ECM proteins and integrins.

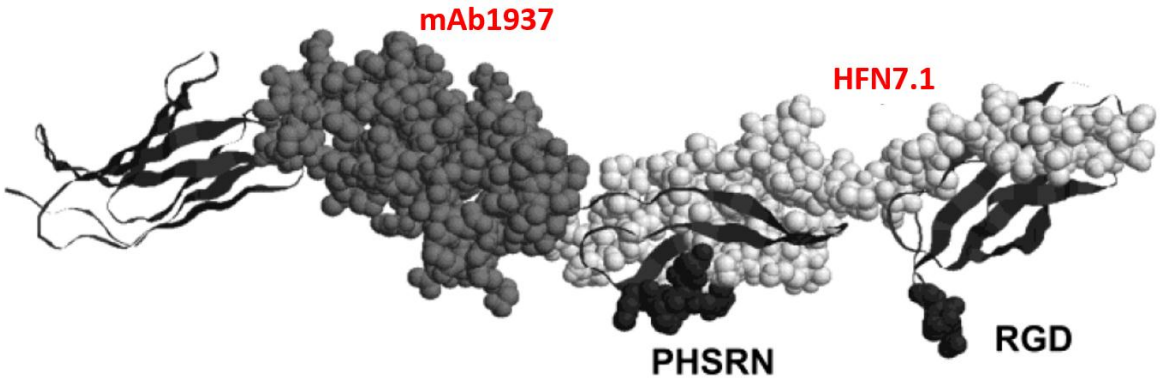

Figure 4: FN-III$_{7\text{-}10}$ model showing RGD and PHSRN binding sites and epitopes for antibodies blocking them. HFN7.1, and mAb1937 are used in this thesis to block the RGD and synergy sequences respectively. Image from Michael, K. E. *et al.*[55] (© 2003, American Chemical Society).

1.2.2 FN-integrin signalling

Integrins are transmembrane protein receptors responsible for the adhesion and communication of cells with the surrounding extracellular matrix. They form a link between ECM proteins and the actin cytoskeleton and once bound, intracellular signalling pathways are activated leading to response in cell binding, FA formation, spreading, growth and proliferation (Figure 5).

A

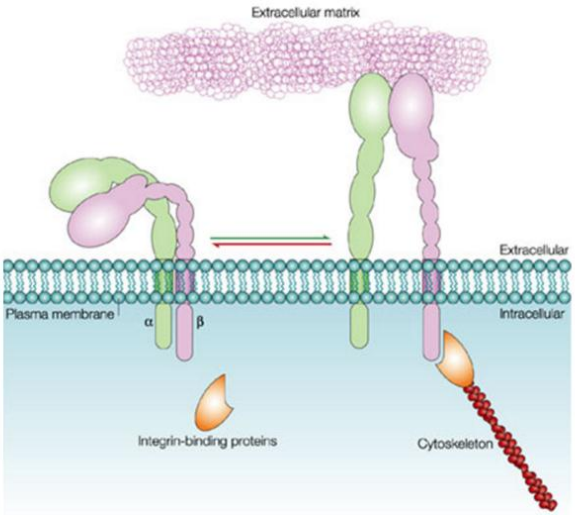

B

ECM Protein	Integrin combination
Collagen	$\alpha_1\beta_1$, $\alpha_2\beta_1$, $\alpha_{10}\beta_1$, $\alpha_{11}\beta_1$
Laminin	$\alpha_3\beta_1$, $\alpha_6\beta_1$, $\alpha_6\beta_4$, $\alpha_7\beta_1$
Fibronectin	$\alpha_5\beta_1$, $\alpha_8\beta_1$, $\alpha_{IIb}\beta_3$, $\alpha_v\beta_3$

Figure 5: Integrin and ECM interaction. (A) Schematic of integrin with ECM and intracellular proteins from Kinbara, K. *et al.*[56] (© 2003, Springer Nature). The activation of integrins depend on their interaction with the ECM and intracellular components such as FAs and the cytoskeleton. (B) Different combinations of α and β integrin subunits and their ECM ligand.

They are found in a large number of animal species and are non-covalent heterodimers composed of two main sub-units, α and β with large extracellular domains that bind to the ECM and short cytoplasmic domains that link to the cytoskeleton. There are 18 and 8 different types of α and β sub-units, respectively which combine to form at least 24 distinct integrin heterodimers[57]. The most notable heterodimers in regard to FN signalling being $\alpha_5\beta_1$, $\alpha_8\beta_1$, $\alpha_{IIb}\beta_3$, $\alpha_v\beta_3$ which are major factors in cell binding with the RGD domain and PHSRN synergy sequence on the FN-$III_{7\text{-}10}$ repeats.

The binding of FN to integrin induces the formation of adhesion complexes that are initially small in length and area with FA proteins such as talin, tensin and vinculin linked to the actin cytoskeleton, known as focal complexes. Integrins then form clusters, recruiting more FA proteins such as paxillin, α-actinin and focal adhesion kinase (FAK) forming larger FA complexes leading to the formation of actin stress fibres (*Figure 6*)[58-60].

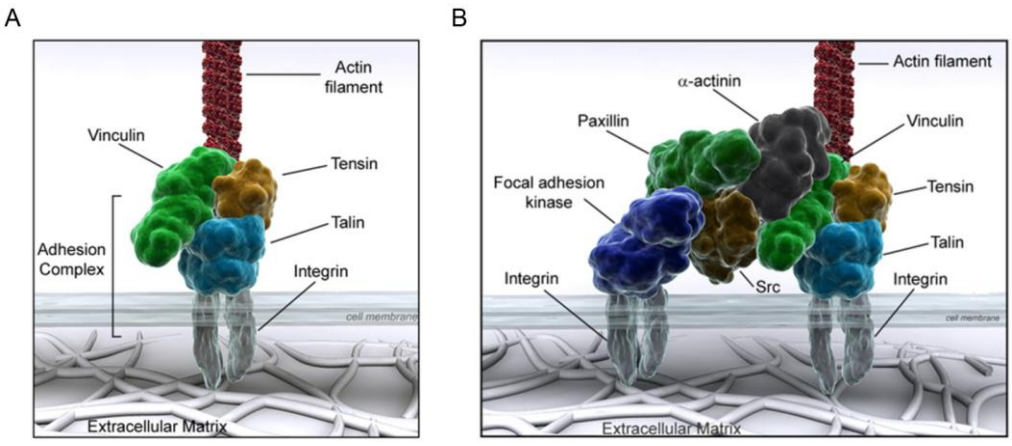

Figure 6: Schematic representation of FA components[58]. (A) Adhesion complexes are formed initially when integrins bound to the ECM recruit primary FA proteins such as talin, tensin, and vinculin. (B) Mature FAs form after time when more FA proteins are recruited such as FAK and paxillin,

binding to other integrins and making the FA stronger. Images from the University of Reading – Cell adhesion (2017)[58].

These focal adhesions are very dynamic, disassembling and reassembling within active and highly mobile cells allowing migration using the ECM as a scaffold[61-63]. Moreover, there is a distinct relationship between forces on the ECM and FA formation with stiffer surfaces leading to an increase in FA size[64-66].

1.2.3 Fibrillogenesis: cell-mediated and material-driven

Not only does FN interact with cells, it also interacts with other FN proteins, assembling into a network. FN is secreted as a soluble dimer, but then undergoes conformational changes that expose hidden sites that promote its polymerization into insoluble fibrils[67-69]. Although it is known that fibrillogenesis is mainly a cell-mediated process, the controlling factors are not fully understood. In this process, soluble FN binds to integrins. This causes FN to be coupled with the actin cytoskeleton that can exert forces on the bound proteins causing them to unfold. The unfolded FN molecules interact with each other and associate resulting in the formation of a matrix[70].

Studies suggest that fibrillogenesis is also possible in the absence of cells by applying force, shear, using denaturants as well as when FN is adsorbed on different substrates that promote the unfolding of FN[68]. Furthermore, cells can interact with these biomaterials via the FN on its surface by recognising and attaching to the adsorbed FN and in turn remodel the two-dimensional FN network. Material-driven fibrillogenesis is possible on some poly acrylates such as poly (ethyl acrylate) (PEA), whereas this is not observed on poly (methyl acrylate) (PMA), even if the two polymers are very similar chemically[71].

PEA and PMA are both hydrophobic rubber-like polymers that are very similar in structure and physico-chemical properties. The following (Table 1) depicts physico-chemical properties comparing both polymers.

Table 1: Properties of PEA and PMA

Polymer	PEA	PMA
Structure	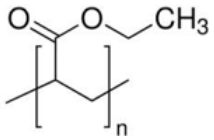	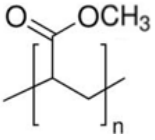
Molecular formula	C5H8O2	C4H6O2
Glass transition temperature	-21°C	9°C
Density (25°C)	1.12 g/cm^3	1.22 g/cm^3
MW of repeat unit	100.12 g/mol	86.09 g/mol

These two acrylates have very similar properties, the only structural difference being a slightly longer side chain for PEA. That leads to a noticeable difference in the glass transition temperature. Further surface chemistry studies carried out on these polymers show similar wettability and total amount of FN adsorbed[68]. However, the conformation of the adsorbed FN is drastically different. On PEA, FN is organised as an interconnected network whereas on PMA FN is dispersed in a globular form[68, 72]. This has a direct effect on cell function and more particularly on cell differentiation and formation of FAs. These differences are possibly due to conformation of FN on these surfaces. When FN is unfolded when adsorbed to PEA, more domains such as the cell binding sequence are available as opposed to folded FN on PMA[67, 73, 74]. Although the cell binding domain appears to be more available on PEA, the effects of cell binding and attachment have yet to be studied.

PEA is able to induce material-driven fibrillogenesis and serves as a biomimetic of cell-mediated fibrillogenesis as opposed to PMA. This can be used as a model to better understand fibrillogenesis in general and how cells interact with FN depending on its conformation. This is important in order to study and characterise cell function where the ECM and more particularly FN plays an important role such as in differentiation and proliferation. One potential application is understanding the role that FN has in cancer cell proliferation and metastasis.

1.3 Fibronectin and cancer

1.3.1 Cancer

Cancer is an abnormal growth of cells forming tumours, caused by several factors such as changes in gene expression that lead to dysregulation of cell proliferation and death. Although it is difficult to estimate the total number of people with cancer worldwide there were over 14 million new cases in 2012 alone with a projected increase to 24 million new cases of cancer per year by 2035[75]. The most common forms being of the lung, breast, colorectal and prostate cancer, resulting in over 8 million deaths worldwide in 2012, it has become the leading cause of mortality in the UK surpassing heart disease[76]. The need to understand the genetic and environmental causes as well as the cellular and molecular mechanisms involved have never been more relevant for the development of treatments.

Over the past few years, many advances have been made in understanding the biology and genetic mechanisms at play in cancer progression[77-79]. The main categories of cancers include carcinomas (epithelial cells), sarcomas (bone, cartilage), leukaemia (blood, bone marrow), lymphoma and myeloma (immune cells) and nervous system cancers (brain, spinal cord). Carcinomas are the most common type of cancer (85% of cases in the UK) and develop within cells that comprise epithelial tissue which line and cover the outer body (skin) as well as the organs and body cavities[75].

The process through which cancerous cells develop, mutate, form tumours, recruit other cells and blood vessels is known as tumorigenesis. This begins with a series of mutations of several genes within a cell, known as oncogenes and tumour suppressor genes, which regulate cell growth, proliferation and death. An increase in oncogenes such as ras and myc which upregulate cell proliferation and a decrease in tumour suppressor genes such as p53 and PTEN which upregulate apoptosis leads to a rise in mutated cells. Once enough cancerous cells are present, the solid tumour outgrows blood supply and the centre of the mass is deprived of oxygen. This phenomenon is thought to be a leading factor in metastasis as hypoxia upregulates the expression of metalloproteinase (MMP) enzymes that degrade ECM proteins, including FN, allowing invasion into surrounding tissue[80-82].

1.3.2 Cancer treatments

1.3.2.1 Brief history of treatments

A wide range of treatments have been and are currently being used to treat tumours, from invasive surgical procedures to cancer gene therapy. Ancient surgeons would generally perform exploratory surgeries to locate and remove tumours only to see them reform[83]. The understanding that cancer cells were able to spread from the primary tumour and invade other tissue along with the advent of ultrasound, computed thermography (CT), magnetic resonance imaging (MRI) and positron emission tomography (PET) scans in the early 1970s have drawn attention to the fact that invasive surgeries, although important in the removal of the main tumour, are limited in effectiveness.

In the early to mid-20th century radiation and surgery were predominantly used to treat cancer. The term “chemotherapy” was first described by German chemist Paul Ehrlich in 1914 to describe the use of drugs to treat infectious diseases[84]. He was also responsible for the documentation of the use of animal models to screen several chemicals to test their effectiveness against diseases. The first chemical agents tested in the early 1900s were arsenicals (based on arsenic) but had little success. In the early 1940s, nitrogen mustard was shown to kill lymphoma cancer cells that proliferated rapidely[83]. The mid-1940s to the 1960s saw the development of compounds such as thiopurines, and antitumour antibiotics, with the first talks of actually curing the disease. The field of chemotherapy has since evolved at an exponential rate with over 100 different drugs used. This was made possible thanks to the development of combination treatment (the use of several drugs), drug screening methods, and targeted therapies. In parallel, less invasive surgical techniques have recently been developed such as cryosurgery, which consists of freezing the tumour by spraying it with liquid nitrogen, or the use of miniature video cameras and endoscopy to remove certain tumours in the gastrointestinal tract or bladder[83]. Furthermore, advances in cell biology and oncology have given further insight into understanding the cancer machinery in order to develop treatments affecting specific mechanisms involved. The following Figure 7 provides a history of anticancer treatments.

A.

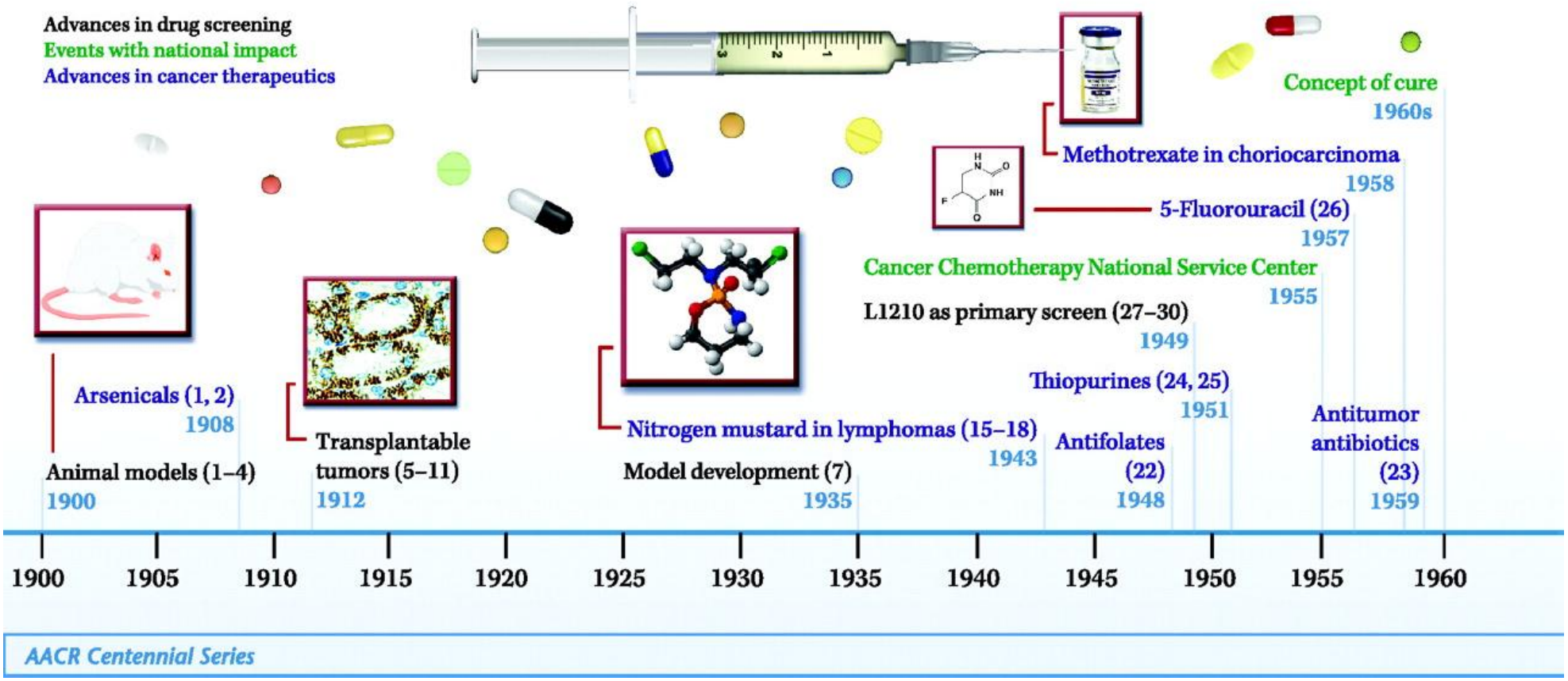
Advances in drug screening
Events with national impact
Advances in cancer therapeutics
Concept of cure
1960s
Methotrexate in choriocarcinoma
1958
5-Fluorouracil (26)
1957
Cancer Chemotherapy National Service Center
1955
L1210 as primary screen (27–30)
1949
Thiopurines (24, 25)
1951
Antitumor antibiotics (23)
1959
Antifolates (22)
1948
Nitrogen mustard in lymphomas (15–18)
1943
Model development (7)
1935
Transplantable tumors (5–11)
1912
Arsenicals (1, 2)
1908
Animal models (1–4)
1900
1900
1905
1910
1915
1920
1925
1930
1935
1940
1945
1950
1955
1960
AACR Centennial Series

B.

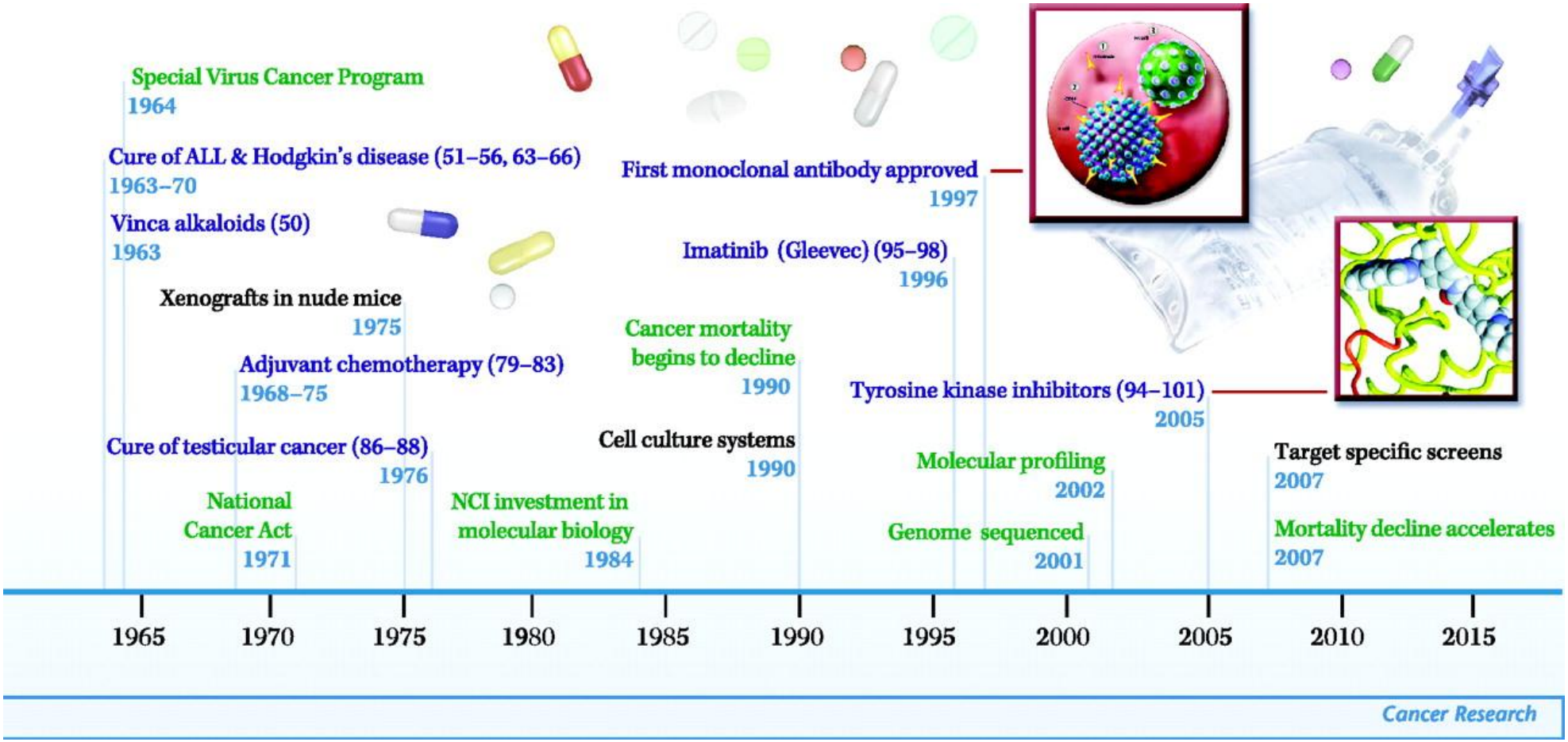

Figure 7: Key advances in the history of cancer chemotherapy. (A) The first half of the 20th century (1900 – 1960). (B) Second half of the 20th century to early 21st century (1965 – 2015). Images from DeVita V.T. and Chu E., 2008[84] (© 2008, AACR).

1.3.2.2 Chemotherapeutic drugs

The bulk of chemotherapy drugs are cytotoxic, which inhibit metabolic function and stop reproduction or kill cancer cells altogether. Other drugs affect specific parts of the cell cycle, most notable the S or M phases. The different categories of chemotherapy drugs along with their mechanism of action can be seen in the following table 2.

Table 2: Categories of chemotherapeutic drugs with their mechanism of action[85]

Chemotherapy drug category	Mechanism of action	Examples of drugs
Alkylating Agents	Damages DNA by attaching an alkyl group to guanine.	- Streptozocin (Zanosar®) - Thiotepa (Thioplex®)
Kinase Inhibitors (Small molecule inhibitors)	Blocks tyrosine kinase. Regulates cell proliferation and cell cycle.	- Imatinib (Gleevac®) - Toceranib (Palladia®) - PND-1186 (Phase I)
Vinca Alkaloids	Halt cell division by preventing the formation of tubulin.	- Vinblastine - Vinorelbine - Vincristine
Anthracyclines	Multiple factors such as intercalation with DNA and DNA binding proteins, binding of p53 to DNA inducing apoptosis.	- Daunorubicin - Doxorubicin - Epirubicin - Valrubicin
Antimetabolites	Folic acid, analogues of pyrimidine and purine. Induction of cell death at the S phase by disrupting normal nucleic acid production.	- 5-flurouracil (5-FU) - Capecitabine - 6-Mercaptopurine (6-MP) - Methotrexate
Aromatase inhibitors	Interference with aromatase enzyme which reduces oestrogen production. Slows growth of oestrogen dependent tumours.	- Exemestane (Aromasin®) - Anastrozole (Arimidex®) - Tamoxifen
Topoisomerase inhibitors	Binds topoisomerase enzymes which inhibits the rebinding of DNA after being cut.	- Camptothecin - Doxorubicin - Etoposides - Mitoxantrone

These compounds have been proven to be useful and effective in the treatment of many types of cancers, but they lack specificity to the cancerous cells and often affect healthy cells.

The characteristic of most chemotherapy drugs is that they attack rapidly dividing cells. However, many proliferating normal cells are damaged causing the well-documented side-effects association with chemotherapy[86-88]. These drugs can cause sever local tissue necrosis, cardiotoxicity and myelosuppression among other destructive responses leading to fatigue, hair loss, nausea and vomiting. Other major difficulties faced with these treatments are drug resistance, which has been well documented, and the recurrence of tumours after treatment.

Cancer cells develop drug resistance through various mechanisms such as drug inactivation, cell death inhibition, drug efflux and epithelial-mesenchymal transition (EMT)[89, 90]. The development of resistance of a few cancer cells after adjuvant and combination treatments can lead to the regrowth of the tumour, also known as recurrence[91].

These hurdles in the treatment of tumours places emphasis on the development of drugs and methods that are able to counteract the issues encountered with standard therapies.

1.3.2.3 Targeted therapies

The advancement of targeted therapies such as the use of monoclonal antibodies has had a profound impact on cancer treatment in recent years[92]. The exploitation of the immune system as a weapon against tumours has been studied since the beginning of understanding basic immune pathways. It has since displayed exceptional effectiveness in patients with various types of cancers[93-95]. This is done by recruiting the host's immune system to recognise specific tumour antigens, which has shown to be effective *in vitro*[96, 97] but represents a much more difficult challenge *in vivo* due to the tumour microenvironment (TME)[98, 99]. In order for immunotherapy to be successful the tumour antigens must be recognised in order to activate the immune system. This process is hindered by the microenvironment of surrounding accessory cells preventing the priming of lymphocytes and supresses the infiltration of effector cells[100].

1.3.2.4 FAK inhibitors - PND-1186

FAK is a potential target for anti-cancer therapy. PND-1186, also known as VS-4718 is a substituted pyridine reversible inhibitor of FAK[101]. This small molecule inhibitor is currently in phase 1 clinical trials and has shown to promote tumour cell apoptosis in 3D environments and decrease tumour growth and spontaneous breast cancer metastasis in mice[101, 102]. With a reported *in vitro* IC50 of 1.5 nM and an *in vivo* IC50 of ~100 nM[101-103] this drug show promise for treating metastasis and fighting tumour progression as it targets one of the key components of cell anchorage and motility in FAK and therefore FAs. Although 3D and *in vivo* models have been used to study the efficacy of this drug, its effects on cell migration and FA formation have yet to be elucidated.

Moreover, despite the anti-tumorigenic properties of these drugs, there are still concerns as to their non-specificity and therefore potential toxicity[104].

1.3.2.5 Matrix metalloproteinase inhibitors

Matrix metalloproteinases (MMPs) are a large contributing factor in ECM structure and remodelling[105]. These enzymes secreted by the cell degrade surrounding ECM proteins such as collagen, fibronectin and laminin. There is a total of 24 known MMPs that are generally secreted at low levels are deregulated in many cancers allowing for degradation of the ECM and beginning the process of epithelial-mesenchymal transition (EMT)[106]. This has caused MMPs to be of great interest in cancer treatment by developing MMP inhibiting drugs since the 1990s. Unfortunately, many of the drugs developed such as Batimastat, Marimastat, and Prinomastat that were all cancelled in Phase 3 of clinical trials due to poor solubility or insignificant efficacy[107, 108]. More recently, interest in MMPs as a therapeutic target has significantly diminished due to unsuccessful clinical trials.

1.3.3 The epithelial-mesenchymal transition

The ECM is a fundamental component of the TME which serves as a niche for cancer and auxiliary cells such as fibroblasts and lymphocytes. In healthy conditions it helps to maintain tissues in a state of homeostasis[109], however, within tumours it plays a pivotal role in the epithelial-mesenchymal transition (EMT).

EMT, which was first described by Elizabeth Hay, is the process through which an epithelial cell that would normally interact with the basement membrane sustains changes that cause it to take on a mesenchymal cell phenotype with those characteristics[110] (Figure 8). The newly acquired characteristics include an increase in the cell's ability to migrate and invade other tissues, an increase in the resistance to apoptosis and a rise in the secretion of ECM proteins[110-113]. The biochemical processes implicated in EMT are numerous, enabling the different steps. These include but are not limited to: the activation of transcription factors, the expression of cell-surface proteins, the restructuring of intracellular cytoskeletal proteins, an increase in the production of matrix metalloproteinases (MMPs) which are ECM-degrading enzymes[111].

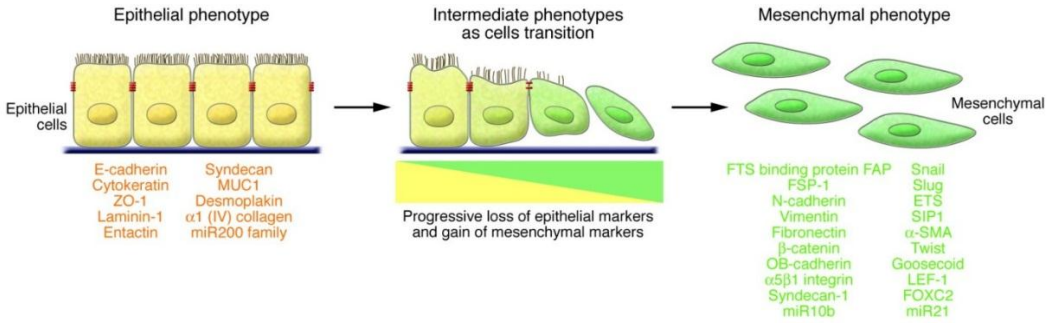

Figure 8: The Epithelial-Mesenchymal transition with epithelial and mesenchymal markers. Cells begin with an epithelial phenotype but progressively lose epithelial markers which are replaced by mesenchymal markers. Image from Kalluri *et al*., 2009[111] (© 2009, American Society for Clinical Investigation).

This natural phenomenon has long been thought to occur solely during embryogenesis with epithelial cells being relatively flexible, possessing the ability to switch back and forth between epithelial and mesenchymal states. This occurs naturally with the process of EMT as well as the reverse process of mesenchymal-epithelial transition (MET)[113]. Once embryogenesis and development is complete, cells usually lose their ability to differentiate. This, however, has been put into

question in light of observations of EMT to take place not only during the developmental stage but also into adulthood as it also plays an important role in tissue repair[114, 115].

Although the signalling pathways are not well defined or differentiated, there are 3 subtypes of EMT recognisable by functional differences[111, 116] (Figure 9). The first type of EMT being the classic case observed during morphogenesis. These cells are able to undergo EMT transformations as well as the reverse MET[117].

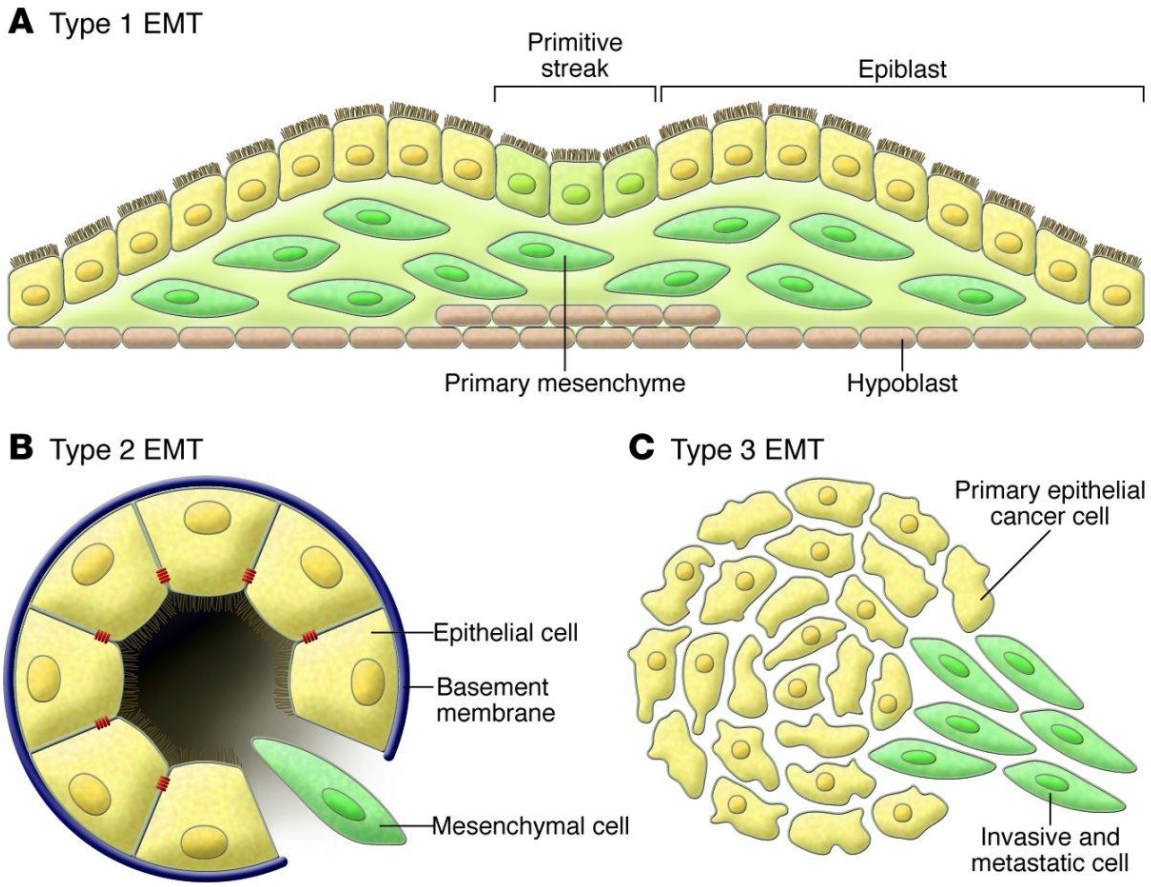

Figure 9: Different types of EMT and when they occur. (A) Type 1 EMT during embryogenesis which plays an important role in development. (B) Type 2 EMT associated with tissue regeneration, leading to tissue fibrosis and inflammation. (C) Type 3 EMT linked to cancer progression and metastasis. Image from Kalluri *et al*., 2009[111] (© 2009, American Society for Clinical Investigation).

The second type of EMT is associated with healing and tissue repair. Key characteristics of this type of EMT are the formation of fibrotic tissue and inflammation[118].

The third form of EMT is associated with metastasis and cancer progression and has been the most studied form. A main trait of epithelial cancers is the fact that cells proliferate excessively and new blood vessels form within the tumour[119]. Cells that undergo type 3 metastatic EMT begin by losing polarity and thus detaching from and infiltrating the basal membrane which also undergoes changes in ECM composition and therefore present altered cell-ECM signalling pathways. The second step in the process is the intravasation of mutated cells into the bloodstream followed by extravasation in distant tissue[120, 121]. Finally, cells adhere to the tissue forming metastatic colonies by undergoing the reverse mesenchymal-epithelial transition in some instances. The areas most frequently prone to being affected by cancer metastasis are the lungs and the liver making metastasis responsible for the largest number of cancer related deaths[122-124].

The signalling pathways implicated in metastatic EMT are not entirely clear. It is believed that the genetic alterations sustained by cancer cells in the primary tumour causing the disruption of cell-cell adherence junctions and the cell-ECM adhesions via integrins facilitates the activation of EMT programs[125-127].

It is therefore crucial to understand the interaction between cancer cells and their surrounding ECM environment at the molecular level in order to determine the mechanisms that dictate the migration of cancerous cells from the main tumour to other tissues.

1.3.4 The importance of fibronectin in cancer

As previously stated, one of the key aspects of EMT is the acquired ability of the mutated cells to increase their production of extracellular matrix proteins such as FN. Furthermore, cancer cells interact differently with their surrounding ECM proteins compared to normal cells. Their ability to disrupt the cell-ECM bond due to an increased production of matrix metalloproteinase (MMP) facilitates the process of EMT and therefore metastasis. Fibronectin, which is a main ECM component, plays a key role in this process and is a reasonable protein candidate to study these interactions at a closer level. The ECM and FN more specifically is essential in cancer cell adhesion and migration by serving both as a scaffold that cells can migrate on within the tumour towards blood vessels and as an anchoring point for cells seeking to attach to a host tissue away from the main tumour[128]. FN is known

to play an important role at several stages of tumour development[129, 130]. It has been shown to have a protective role against tumour necrosis factor-α-induced apoptosis by activating the AKT/Survivin pathway via β_1 integrins in PC3 and LNCaP-LN3 prostate cancer cells[131]. In ovarian cancer fibronectin activates the secretion of MMP-9 using the MEK1-MAPK and PI3K-Akt pathways which contributes to metastasis[132]. A study by Pontiggia *et al*. showed that fibronectin promoted tamoxifen resistance in human and mouse breast tumour via β1 integrins and subsequent activation of survival pathways[21].

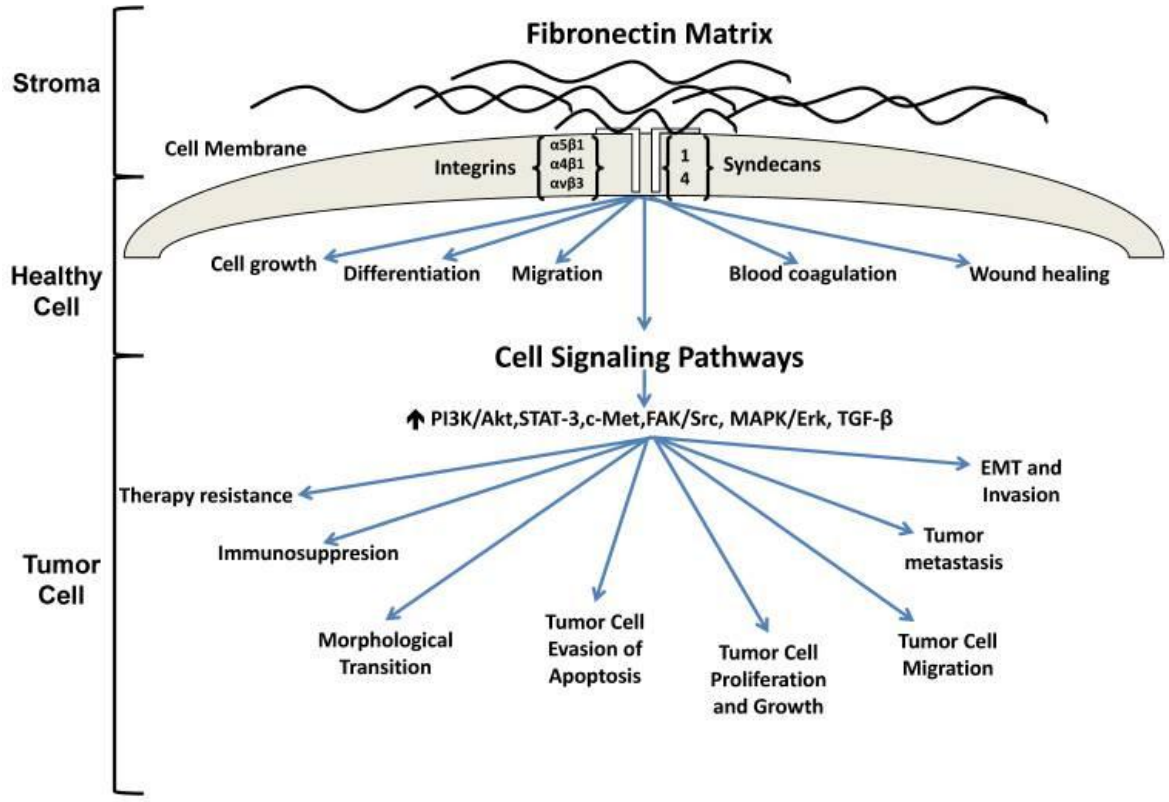

Figure 10: Fibronectin signalling in healthy and tumorigenic cells. Fibronectin is responsible for many processes in healthy cells such as cell growth, differentiation, migration and wound healing. In tumorigenic cells, there is an upregulation of signalling pathways leading to abnormal growth, drug resistance, epithelial-mesenchymal transition and ultimately metastasis. Image from Wang J.P. *et al*. 2017[133].

Given the vast array of fibronectin's implication in tumour progression (e.g. increased expression, cell migration/metastasis, therapy resistance), it is a focal point of cancer research with the potential to serve as a potent tool in therapeutic

targeting, but also as a means to understand the elusive interactions between cancer cells and their microenvironment. PHSCN, a competitive inhibitor of the activity of the PHSRN synergy sequence, has been shown to have antitumorigenic and antimetastatic properties[49]. Moreover, KAI1/CD82 which is a metastatic suppressor was shown to inhibit cell adhesion to ECM by suppressing the expression of FN[134]. These examples highlight the promising avenues in the research of fibronectin in cancer.

1.4 Overall Aims of the Thesis

This thesis aims to answer key questions and shed light on the role of fibronectin in cancer using innovative platforms. In particular, we are interested in investigated the role of fibronectin conformation (fibrillar vs globular) in cancer cell behaviour. The key goals of this project are:

- Understanding and characterising the material-protein and protein-cell interfaces using fibroblasts (Chapter 2)

Fibroblasts are well-studied cell types with known interactions with FN via integrins of interest for this project ($\alpha_5\beta_1$ and $\alpha_v\beta_3$)

- Studying the effect of fibronectin conformation on FA formation and cell migration in cancer cells (Chapter 3)

Once methods have been refined with fibroblasts, a relevant cancer cell line will be used to assess FA formation and motility.

- Directing the attachment and adhesion of L929 mouse fibroblasts and DU145 human prostate cells by using FN-coated poly(alkyl) acrylates (Chapters 2 and 3)

Cells will be seeded onto poly(ethyl) acrylate and poly(methyl) acrylate substrates coated with FN. Upon adsorption unto these polymers, FN undergoes

conformational changes which can have an impact on the cell-protein interaction and therefore cell behaviour.

- Clarifying the underlying mechanisms involved in the cell's interaction with its environment (Chapter 3)

The cell-protein interaction is key in determining cell behaviour but also ECM protein reorganisation via bi-directional integrin signalling. Gaining deeper insight in the intracellular pathways implicated in these processes is key in understanding the role of FN in cancer.

- Developing novel methods for analysis of cell traction on polymers (Chapter 3)

A major component of cell motility is analysing the cells ability to modify and exert forces on its surroundings in order to migrate. Cell traction force microscopy is a known method for this purpose which uses polyacrylamide hydrogels or nanopillars. In order to take into account the material properties (stiffness) as well as protein conformation (FN on PEA and PMA), a novel computational technique is used to assess traction forces.

- Studying cell behaviour in a simplified 3D model (Chapter 4)

Having a 3D model is essential for studying cancer. They offer the advantage of mimicking *in vivo* conditions more faithfully but are often more expensive and are made up of complex components. Here we use a simplified and tuneable 3D model that could help understanding specific cell-protein interactions with the benefit of having a more natural structure as opposed to cells on tissue culture plastic.

2 Modulation of fibronectin activity and focal adhesion assembly with L929 fibroblasts

2.1 Introduction

2.1.1 The use of fibronectin as a tool to direct cell response

The need for a reliable cellular microenvironment that can be easily fine-tuned is important for cancer research and general biological research. *In vitro* cells are known to adhere to synthetic surfaces via an intermediate layer of protein. However, there is little to no control of the protein layer in traditional cell culture systems on tissue culture plastic, whereas the cell-protein interaction directly determines cell fate[135, 136]. Traditionally soluble ECM proteins such as FN, vitronectin and fibrinogen found in biological fluids like foetal bovine serum are intentionally deposited and adsorbed onto the synthetic surface[135-139]. The initial interaction between cells and this layer of protein is adhesion via integrins, which then determines cell fate through spreading, growth, differentiation, and viability. Being able to direct cellular response through controlling the protein layer using a reliable material-based system is useful for many applications in biomedical research such as regenerative medicines, tissue engineering and cancer research.

FN, a fundamental ECM glycoprotein of high molecular weight found in extracellular fluids and connective tissue in its soluble and insoluble forms respectively, is a feasible protein choice to modulate in order to direct cell fate via integrins [44, 140-142]. Cell binding via FN leads to the formation of FAs and the initiation of adhesive and migratory processes, which are fundamental characteristics in cell behaviour.

2.1.2 FN-material interactions

A large number of studies have shown that the amount and conformation of adsorbed FN can be altered by surface chemistry[143-146]. García *et al.* determined with the use of differently terminated self-assembled monolayers (SAMs) that hydrophilic surfaces induced little conformational changes to FN whereas hydrophobic surfaces lead to more significant structural changes[55, 147]. This shows that surface chemistry has a direct effect on protein conformation upon adsorption and can therefore influence its activity. It has been previously shown that PEA surfaces induce the organisation of FN protein into a fibrillar (nano) network conformation, comparable to their physiological state, upon adsorption on the polymer. Interestingly the use of PMA, whose monomer has one less methyl group

in the side chain, has a completely different effect, with a globular conformation of FN upon adsorption[71, 148].

2.1.3 Hypothesis and experimental aims

We hypothesise that the differences in conformation of FN upon adsorption to PEA and PMA leads to differences in cell behaviour which suggests that it is possible to use these materials to modulate cell response via FN. In this study, the state of FN upon adsorption on PEA and PMA was characterised using various protein concentrations. L929 mouse fibroblasts were seeded on FN-coated PEA and PMA to determine cellular response in relation to the conformation of FN presented on the polymeric surface. The overall goal being the development of a tissue culture system that is both simple and reliable with which it is possible to fine-tune and control cellular behaviour via the modulation of activity of adsorbed protein, thus controlling the microenvironment that cells are exposed to.

2.2 Materials and methods

2.2.1 PEA and PMA sample preparation and FN coating

Bulk polymers of PEA and PMA were prepared and supplied by the Universidad Politècnica de València. There, polymers were synthesised by radical polymerisation of ethyl and methyl acrylate (Sigma, St Louis MO).

PEA and PMA were then prepared respectively at 2.5% and 6% (w/v) in toluene. These concentrations were used to have similar solution viscosities between PEA an PMA, making the spin coating process more uniform between polymers.

Next, polymer solutions were spin coated onto 12 mm cover glasses. The parameters of the spin coating process for each polymer are listed in Table 3 below:

Table 3: Spin coating parameters

	Velocity	Acceleration	Time
PEA 2.5%	2000 rpm	3000 rpm/s	30 s
PMA 6%	3000 rpm	3000 rpm/s	30 s

After spin coating excess solvent is removed by placing samples in a desiccator under vacuum for 60 minutes at 60°C. Samples are then stored under vacuum in a desiccator with silica beads in order to minimize humidity until ready to use.

Human plasma FN (Sigma) was used in order to carry out experiments. FN was diluted in Dulbecco's phosphate buffered saline with magnesium and calcium (DPBS++) and 200µl of FN at different concentrations (2, 5, 10 and 20 µg/ml) were then placed on the samples for 10 minutes or 1 hour. The solution was then removed and samples were rinsed twice using DPBS++. A further rinse using milliQ water followed by drying with a nitrogen flow was performed for WCA and AFM measurements.

2.2.2 Water contact angle

Water contact angle analysis was carried out on PEA or PMA surfaces alone and on FN coated surfaces. For each condition the static (SCA), advancing (ACA) and receding (RCA) contact angles were determined (n=9). Contact angles are determined by measuring the angle between the baseline and the drop as is shown in the following Figure 11.

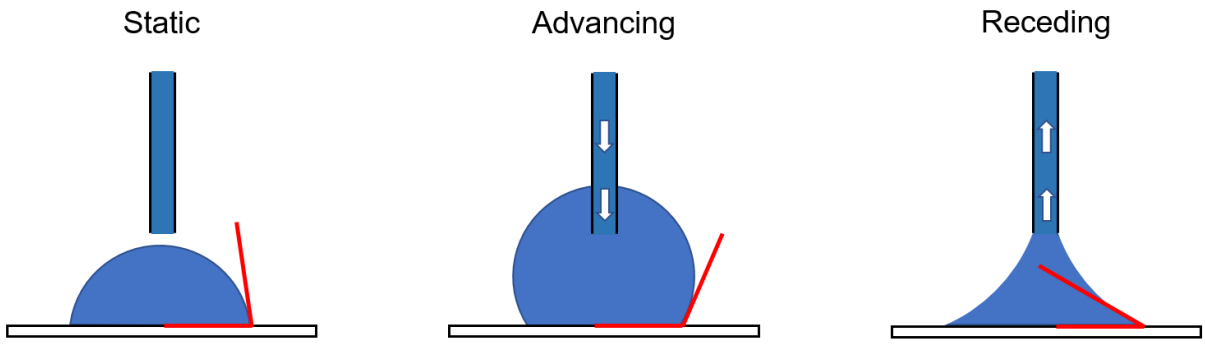

Figure 11: Schematic representation of static, advancing and receding water contact angle measurements. Static WCA assesses the angle formed when the drop of water is in contact with the surface. Advancing and receding WCA respectively assess the maximum and minimum angles of the water droplet right before it advances or recedes.

SCA was determined by placing a drop of 3 µl of water on the surface using a needle and recording the images at 12 frames per second for 30 seconds while measuring the angle of the drop with the polymer surface.

ACA was determined by placing the needle in the previously deposited drop and progressively adding water in order to observe an increase in the length of the baseline. The ACA is the angle at which the baseline increases.

RCA was determined by progressively removing the water with the needle until the drop has been removed. The receding contact angle is the angle at which the baseline starts decreasing.

Hysteresis is defined as the difference between advancing and receding contact angles and is an indicator of the roughness and wettability of the surface.

Measurements were carried out using a Theta optical tensiometer (Biolin Scientific).

2.2.3 FN immunostaining

Immunostaining was done with polyclonal anti-FN (Sigma) primary antibody directed against FN. PEA and PMA samples were coated with FN at different concentrations for 1 hour and 10 minutes.

Freshly prepared samples were fixed with formaldehyde 4% for 30 minutes at 4°C and then washed three times with DPBS. Samples were then incubated with anti-FN (1:400 dilution in DPBS/BSA 1%) for 1 hour at room temperature and then washed twice with DPBS/Tween20 0.5%. Samples were then incubated with Cy3 anti-mouse (1:200 in DPBS++/BSA 1%) for 1 hour at room temperature in the dark. Samples were washed twice and mounted with mounting medium (Vectashield – Vector Laboratories, Inc. Burlingame, CA) and observed using an inverted

epifluorescent microscope (Zeiss AXIO Observer Z1, Jena, Germany). Images were taken at 5, 10, 20, 40, and, 63x magnification.

2.2.4 Atomic force microscopy (AFM)

In order to observe the protein conformation upon adsorption, samples were coated with FN for 10 minutes or 1 hour and rinsed twice with DPBS before being gently dried using a nitrogen flow. Surface height, lock-in phase, and lock-in amplitude were scanned using the Nanowizard 3 AFM from JPK in tapping mode. The cantilever used had a force constant of 3 N/m, a resonance frequency of 75 kHz and a pyramidal tip (MPP-21220, Bruker, Billerica, MA) with a radius curvature inferior to 8 nm. Several areas of each surface were scanned at the following area sizes and line rates: 5x5µm (0.5Hz); 2x2µm (0.7Hz); 1x1µm (1Hz); 0.5µm (1Hz).

2.2.5 Micro bicinchoninic acid (BCA) protein quantification assay

BCA protein quantification is a method that utilizes bicinchoninic acid (BCA) as the detection reagent for Cu^{+}, which is formed when Cu^{2+} is reduced by protein in an alkaline environment. A purple-coloured reaction product is formed by the chelation of two molecules of BCA with one cuprous ion (Cu^{+}). This water-soluble complex exhibits a strong absorbance at 562 nm that is linear with increasing protein concentrations[149].

PEA, PMA and glass cover slips were coated with FN for one hour at different concentrations. The coating was carried out by placing 200 µl of the different FN solutions on the cover slips for one hour. This was done in triplicates.

During this time an albumin stock solution provided with the Micro BCA Protein Assay Kit (Thermo Scientific, Lot# OH189757) was diluted by serial dilution at 40, 20, 10, 5, 2.5, 1.25, 0.625 and 0 µg/ml in order to obtain a standard curve. A stock solution of FN was also diluted at 20, 10, 5 and 2 µg/ml in order to determine the exact concentration of the stock FN solution and to be able to determine the actual amount of FN deposited onto the cover slips.

After coating for one hour the FN solution is collected (about 200 µl) and placed into Eppendorf® protein LoBIND tubes (Sigma). The cover slips are rinsed with 200 µl of DPBS and the resulting solution is placed in the same tubes.

The albumin and FN standards as well as FN solutions were transferred to a 96-well plate (150 µl per well in triplicates for albumin and FN standards and duplicates for each cover slip). 150 µl of BCA working reagent (a mixture of 25 parts BCA reagent A, 24 parts BCA reagent B and 1 part BCA reagent C) was added to each well. The plate was then shaken for 30 seconds, covered and placed in an incubator for 2 hours at 37°C. The plate was left to cool and absorbance was read using a Tecan NanoQuant Infinite M200 Pro plate reader at 562 nm.

To obtain graphs from absorbance values, the blank of the albumin standard is removed from each well and the blank of each surface (FN0 – no fibronectin coating on PEA, PMA or glass) is removed from the respective wells. The results are therefore normalized according to the surface. The amount of protein adsorbed on each surface is then calculated via depletion. Knowing the total amount of protein on the coverslips (200 µl of 20 or 1 µg/ml of FN) and the concentration of FN remaining in the solution after coating, the amount of FN left on the surface was determined using the following equation.

Equation 1:

$$\boldsymbol{Adsorbed\ FN\ =\ Total\ FN - Measured\ FN}$$

Total FN: the amount of FN used to coat coverslips (200 µl x 20 µg/ml = 4 µg FN or 200 µl x 1 µg/ml = 0.2 µg FN)

Measured FN: 200 µl x BCA measured results

2.2.6 Enzyme-linked immunosorbent assay (ELISA)

The availability of the cell binding domain and synergy sequence of FN was measured by ELISA using HFN7.1 (DSHB, Iowa City, IA) and mAb1937 (Millipore) primary antibodies respectively. A horseradish peroxidase (HRP) coupled secondary antibody was used for absorbance reading. HRP is an enzyme which oxidises a substrate using hydrogen peroxide, resulting in a change of colour detectable by spectrophotometry at 450 nm (with a background reading at 550 nm).

Tests were first carried out using different dilution combinations of primary and secondary antibodies in order to optimize results for the actual experiments. HFN7.1 was diluted at 1:32 and 1:128 combined with HRP-Goat Anti-Mouse (Invitrogen) at 1:5000 and 1:10,000. mAb1937 and HRP-Goat Anti-Mouse were both diluted at 1:10,000 and 1:20,000. For the test experiments, FN was adsorbed at 20 µg/ml and 2 µg/ml on glass as well as a control without protein for 1 hour. Samples were washed with DPBS, transferred to 24-well plates and then blocked with DPBS/BSA 1% for 30 minutes at room temperature. Next, samples were incubated with the primary antibodies at different dilutions (1:32 and 1:128 for HFN7.1 and 1:10,000 and 1:20,000 for mAb1937) for 1 hour at room temperature and then washed twice with DPBS/Tween20 0.5%. The secondary antibody (HRP-Goat Anti-Mouse) was then added at different dilutions (1:5000 and 1:10,000 for HFN7.1; 1:10,000 and 1:20,000 for mAb1937) for 1 hour at room temperature in the dark and then washed with DPBS/Tween20 0.5%. The substrate (colour reagents A and B from R&D systems) cv solution (R&D Systems) and transferred to a 96-well plate in order to read the absorbance. Absorbance was read using a Tecan NanoQuant Infinite M200 Pro plate reader at 450 nm and 550 nm.

In the case of the actual experiments, FN was adsorbed at 0, 2, 5 10 and 20 µg/ml on PEA and PMA. The same procedure was carried out for the actual experiments using HFN7.1, mAb1937 and HRP-Goat anti-mouse antibodies at 1:128, 1:20000 and 1:10000 dilutions respectively which were the optimal combinations for the best results.

2.2.7 Cell culture

L929 mouse fibroblasts (ECACC-85011425, London, UK) were thawed and resuspended in Dulbecco's modified Eagle's medium (DMEM) supplemented with 4.5 g/L glucose and L-glutamine, 1% penicillin/streptomycin and 10% foetal bovine serum (FBS; Life Technologies, Carlsbad, CA). Cells were grown using standard cell culture conditions (37°C, 5% CO_2), harvested by trypsinisation and centrifuged at 1000 rpm before being resuspended in growth media (supplemented DMEM) for passaging or use at 90% confluence.

2.2.8 Cell attachment assay

This protocol is adapted from Methods in Molecular Biology - Methods and Protocols - Extracellular Matrix Protocols Second Edition[150]. The attachment assay is modified for use on 12 mm cover slips in a 24-well plate. Instead of using Crystal Violet as a marker to determine the percentage of attached cells, samples are fixed and stained with DAPI in order to count the number of cells attached in each condition. The same cell density, incubation times and buffers are used as described in the protocol.

All cell-related experiments were carried out in sterile conditions (with the use of sterile FN) in a laminar flow cabinet suitable for cell culture. PEA, PMA and glass coverslips were sterilised in UV for 20 minutes, coated with sterile supplied FN (20 µg/ml) for 1 hour, and, washed twice with PBS. Samples were then blocked with heat-denatured 1% BSA (Roche) in DPBS for 30 minutes at room temperature. During this period, cells were harvested, trypsinised and resuspended in complete growth medium (containing 10% FBS). The cell suspension was then transferred to a tube and incubated for 10 minutes at 37°C, 5% CO_2.

Cells were then seeded onto the surfaces at a seeding density of $8.5x10^4$ cells/cm² ($3.4x10^5$ cells/ml) for 20 minutes at 37°C, 5% CO_2. Surfaces were then rinsed twice with DPBS to remove cells that were not firmly attached, fixed with formaldehyde 4% for 20 minutes at 4°C and rinsed three times with DPBS.

Samples were then permeabilised using the triton X-100 based permeabilisation buffer in the following Table 4 and mounted with Vectashield® containing DAPI to stain the nuclei.

Table 4: Permeabilisation buffer composition

Reagent	Amount (for 100 ml)
Saccharose	10.3 g
NaCl	0.292 g
$MgCl_2$	0.06 g
Hepes	0.476 g
Triton X-100	0.5 ml
pH adjusted to 7.2 and filtered (0.22 µm filter)	

Images were taken using an inverted epifluorescent microscope and the number of cells attached was determined using CellC, a program that was developed to count cells (in this case their nuclei)[151].

This experiment was also carried out with an extra blocking step in which the RGD cell binding and the PHSRN synergy sequence domains of FN were blocked. This was done using HFN7.1 (DHSB) and mAb1937 (Millipore) antibodies respectively. Samples coated with 20 µg/ml FN were further incubated for 1 hour with HFN7.1 and/or mAb1937 at 14.6 µg/ml for a 1:1 antibody-FN ratio. Cell seeding, incubation, fixing and staining were all done in the same way.

2.2.9 Early adhesion assay

Samples (PEA, PMA and glass cover slips) were sterilized for 20 minutes using a UV lamp and then coated with FN at 2, 5, 10 and 20 µg/ml for 1 hour. Samples were then rinsed twice with DPBS and cells were seeded at $5x10^3$ cells/cm^2 ($2xss^4$ cells/ml) and cultured for 3 hours (37°C, 5% CO_2). Triplicates were used for each condition.

After washing, samples were fixed with formaldehyde 4% for 20 minutes at 4°C and rinsed three times before being stored in DPBS at 4°C until ready to be stained.

Samples were then permeabilised using the same permeabilisation buffer previously described in Table 4, blocked for 30 minutes with 1% BSA (in DPBS), and, incubated for one hour using an antibody against vinculin hVIN-1 (in mouse; 1:400 dilution; Sigma) to visualise FAs. Samples were then rinsed twice with 0.5% Tween20 (in DPBS) and incubated with a Cy3-conjugated anti-mouse secondary antibody (Cy3 anti-mouse; 1:200 dilution) for 1 hour in the dark. The secondary antibody was coupled with Phallacidin (1:100 dilution) which stains the actin cytoskeleton.

Samples were then rinsed twice with 0.5% Tween20 (in DPBS) and mounted with Vectashield® (Vector laboratories, Inc.) with DAPI which stains the nuclei.

Staining was then observed using an inverted epifluorescence microscope at different magnifications. Images were taken and merged using ImageJ in order to have cells with stained nuclei, actin and FAs.

2.2.10 Early adhesion with blocking

In the case of cell adhesion after blocking specific FN domains, samples coated with 20 µg/ml FN were further incubated for 1 hour with HFN7.1 and/or mAb1937 at 14.6 µg/ml for a 1:1 antibody-FN ratio, to block the RGD and the synergy domains respectively. Antibodies were diluted in 1% BSA. Samples were coated with 20 µg/ml of FN only.

Cells were then seeded onto surfaces and samples were fixed and permeabilised just as described in the standard early adhesion assay.

Due to the fact that the antibodies directed against the cell binding domain and synergy sequence (HFN7.1 and mAb1937 respectively) were produced in mouse just as the antibody used to stain vinculin (hVIN-1), the Zenon® labelling technology kit was used.

The Zenon® technologies kit (Life technologies) is able to label small quantities of primary antibody with an incubation time of 10 minutes. They consist of labelled Fab fragments that bind to the Fc domain of the primary antibody thus eliminating the need for the secondary antibody.

The following Figure 12 shows the principle of the Zenon® labelling technology.

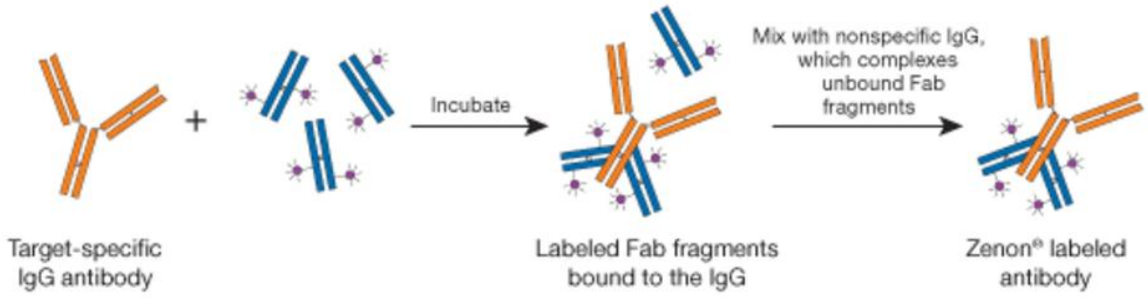

Figure 12: How Zenon® Labelling Technology works. Noncovalent labelling with Zenon® antibody labelling[152]. Labelled Fab fragments were incubated with the primary antibody of interest (in this case hVIN-1) and excess Fab fragments were bound to a nonspecific IgG provided with the kit. The Zenon® labelled antibody was then ready to be used with the samples. From Thermo Fisher Scientific[152].

In this instance, the Zenon® kit was used to bind labelled Fab fragments to hVIN-1 before incubating the antibody with the cells. 1 µl of hVIN-1 (1mg/ml) was diluted in 190 µl of 1% BSA in DPBS. 5 µl of Alexa Fluor® 555 labelled Fab fragments (reagent ZA) was then added and incubated (5 minutes, RT) after which 5 µl of nonspecific IgG1 (reagent ZB) was added to complex unbound Fab fragments (5 minutes, RT). 2 µl of Phallacidin was then added to stain the actin cytoskeleton. Samples were then incubated with this mixture for 1h at room temperature before being rinsed three times with 0.5% Tween20 in DPBS and mounted with Vectashield® containing DAPI.

Staining was then observed using an inverted epifluorescent microscope at different magnifications (5x, 10x, 20x and 40x in dry conditions and 63x using immersion oil). Images were taken and merged using ImageJ in order to have cells with stained nuclei, actin and FAs.

2.2.11 Focal adhesion quantification – focal adhesion analysis server

In the case of the early adhesion assay (with and without blocking), images of vinculin staining taken at 63x magnification were analysed using the Focal Adhesion Analysis Server (FAAS) web tool[153] (Figure 13). This webserver, hosted from the University of North Carolina at Chapel Hill, has been previously described in literature and is commonly used to analyse labelled FAs proteins in cells by measuring the number, size, area, intensity, and, distribution of FAs among other parameters[154].

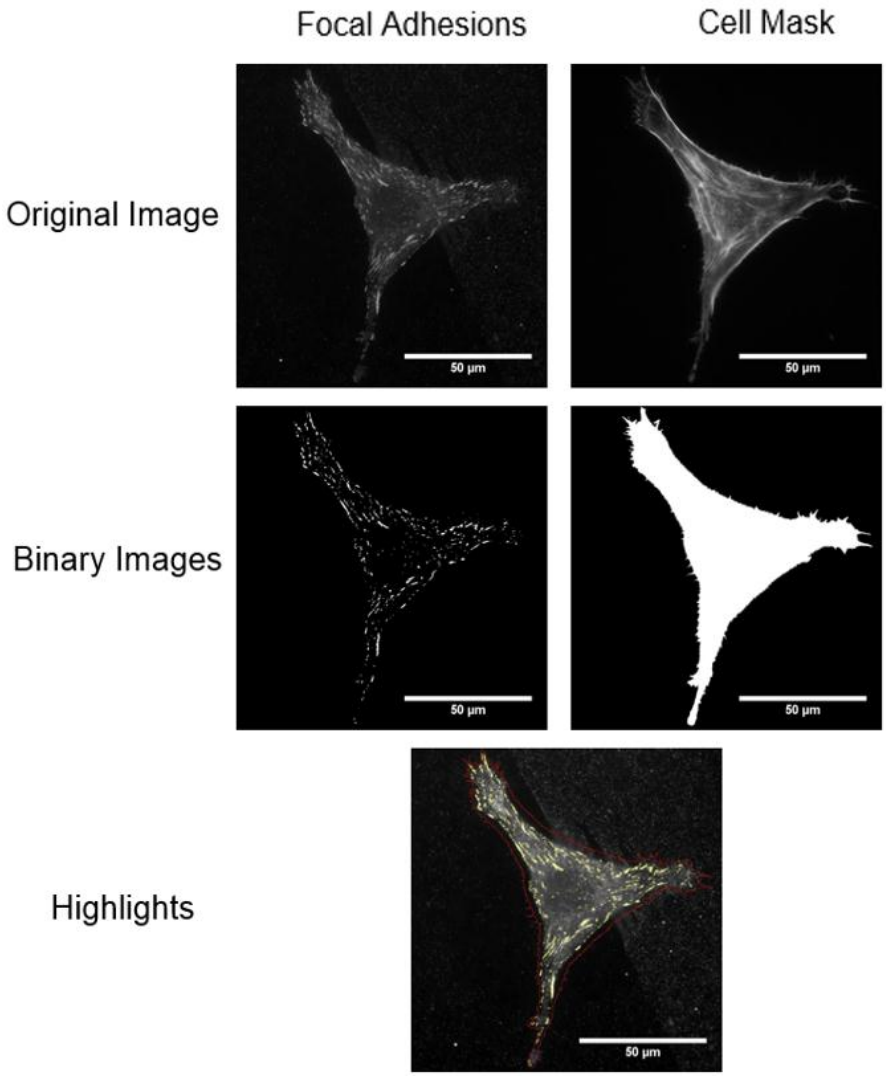

Figure 13: Focal Adhesion Analysis Server. Example of the different steps to identify and quantify FAs (in green). Images of the FAs and cell mask were uploaded to the server which converts them to binary images. FAs detected within the cell mask were then characterised (number, area, length… *etc.*). Scale bar: 50 µm.

In order to determine if the FAAS produced reliable results a validation test was set up (Figure 14). Samples which represent cells and their FAs were created with known parameters such as ‘cell’ size, ‘FA’ size and ‘FA’ distance from the centre and from the edge of the ‘cell mask’.

Several shapes of cells were used such as circles, triangles and squares of different sizes along with different sizes of FAs that are consistent with natural FA sizes.

The following figure represents different images submitted and analysed by the FAAS with known parameters.

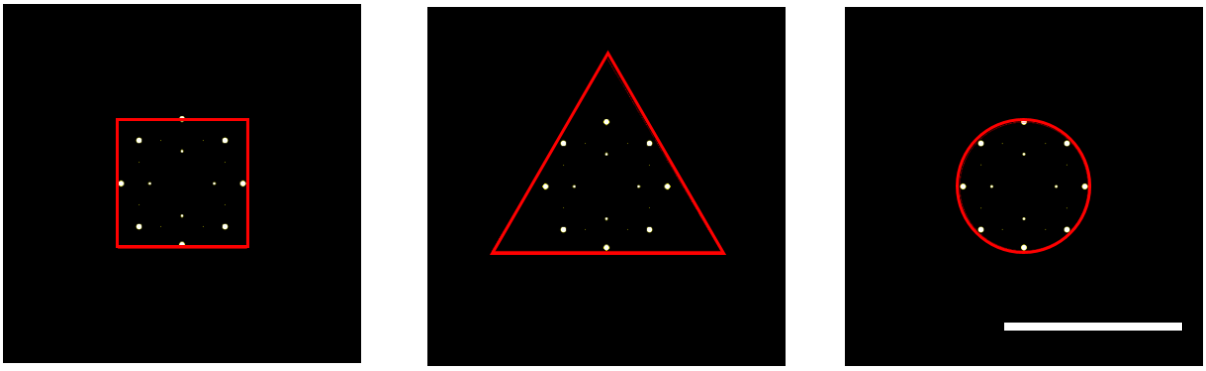

Figure 14: FAAS tool validation. From left to right: square, triangle and circle images submitted with “FAs” of different sizes and distances from the centre and edges of the shapes. With known values for size and distance we were able to assess to ability of the server to accurately characterise FAs. Scale bar: 50 µm.

Once the tool was validated, images of vinculin and the corresponding actin cytoskeleton (mask) staining of cells for each condition were uploaded to the server and analysed.

This data was used to establish the size distribution of the FAs and the ‘geometric moment of inertia’ for each condition. The geometric moment of inertia (*I*) is calculated based on FA size within the cell and the distance from the centre of the cell.

Equation 2:

$$I = \sum_{i=1}^{N} a_i . r_i^2$$

I: moment of inertia of each cell

a: Area of focal adhesion (µm^2)

r: Distance of focal adhesion from centre (µm)

Five cells per condition were used for these experiments. Only FAs larger than 1 µm in length were taken into account in order to exclude focal complexes[60, 155].

2.2.12 Statistical analysis

Two-way ANOVA was used for the comparison of the different groups using a Bonferroni post-test to compare all columns. Data is represented as mean ± SD and the differences between groups were considered significant for $P<0.05$.

2.3 Results

2.3.1 FN adsorption

Once PEA and PMA were spun onto glass coverslips and coated with FN surface wettability was characterised by water contact angle (Figure 15), FN adsorption was characterised by AFM, immunostaining and micro BCA, and, domain availability was characterised by ELISA.

Static, advancing and receding WCA were measured on polymers and on glass with different amounts of FN adsorbed on each surface.

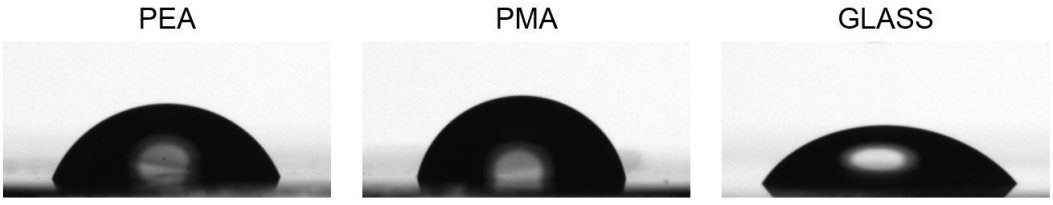

Figure 15: Comparison of water droplets on PEA, PMA and glass surfaces with no FN coating. Visible differences were noted between droplets on different surfaces. Water droplets on PMA were the most rounded compared to droplets on PEA and glass, which was the flattest, indicating varying degrees of hydrophobicity.

Depending on the hydrophobicity of the surface, the contact angle of the droplet differs. Angles are larger on polymers which are more hydrophobic surfaces compared to glass.

The following Figure 16 shows static, advancing and receding contact angles along with hysteresis of PEA and PMA coated with FN.

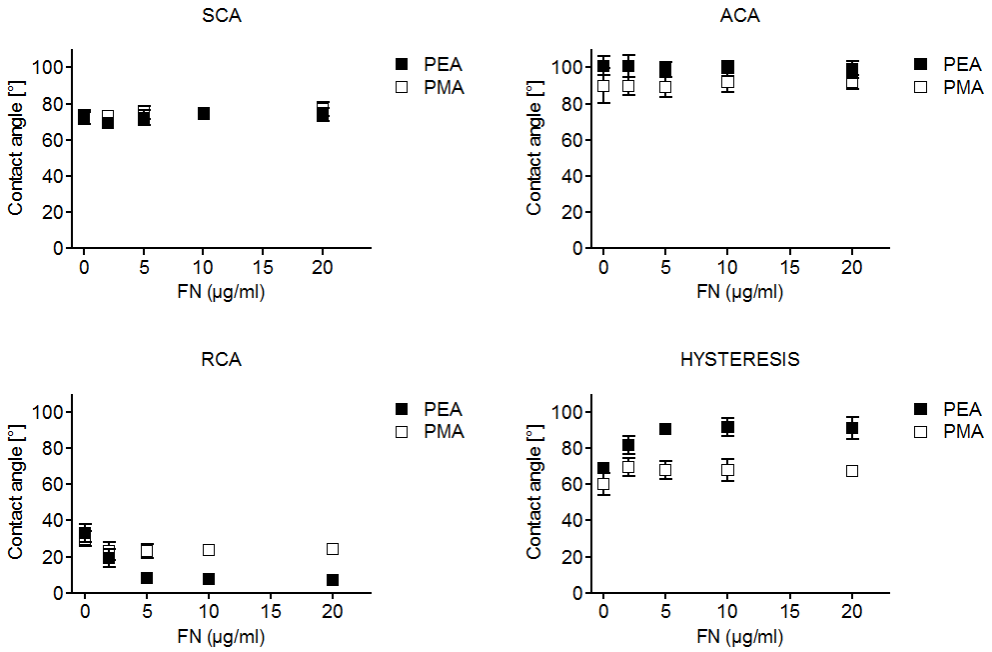

Figure 16: Water contact angle of PEA and PMA with 0, 2, 5, 10 and 20 µg/ml of FN. Static WCA was similar on both FN-coated polymers. Differences were observed in dynamic contact angles (advancing and receding) leading to differences in hysteresis. N = 9.

The similar chemical composition of PEA and PMA is highlighted in the similarities in hydrophobicity with a SCA of approximately 75° on bare polymers and when coated with increasing amounts of FN. A similar trend is observed with the ACA with contact angles between 90-100° on both surfaces. A noticeable difference in receding contact angles was observed with a larger decrease in contact angle on PEA compared to PMA with increasing concentrations of FN. With no FN on surfaces, the RCA on both surfaces is ~30°. However, when FN is coated on the surface the RCA decreases to 7° on PEA as opposed to 24° on PMA. This translates to increased hysteresis on PEA compared to PMA.

AFM (Figure 17) and immunostaining (Figure 18) were used to observe the conformation of FN upon adsorption unto polymers.

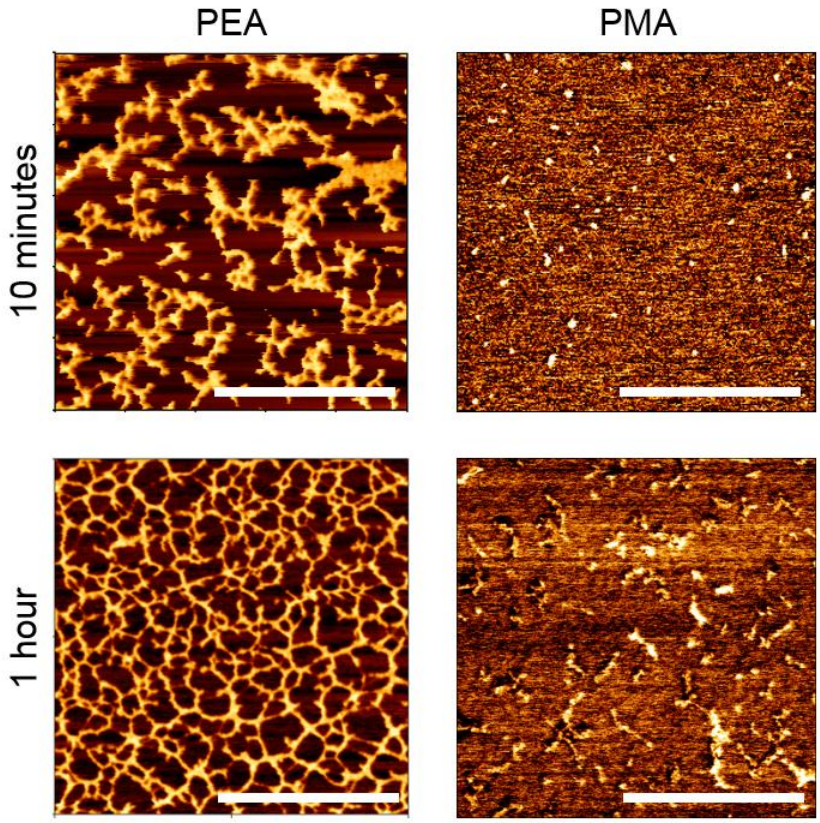

Figure 17: AFM representation of PEA and PMA coated with 20 µg/ml of FN for 10 minutes and 1 hour. The beginning of a FN network was seen after 10 minutes on PEA with a fully formed network observed after 1 hour. On PMA, FN remains globular after 1 hour. Scale bar: 0.5 µm.

Upon adsorption on PEA, FN has a network conformation that develops with time, as observed with AFM. After 10 minutes the protein absorbed begins forming networks and after 1 hour those networks are fully formed across the surface (Figure 18). This is in contrast to PMA where FN remains in a globular conformation even after being adsorbed for 1 hour.

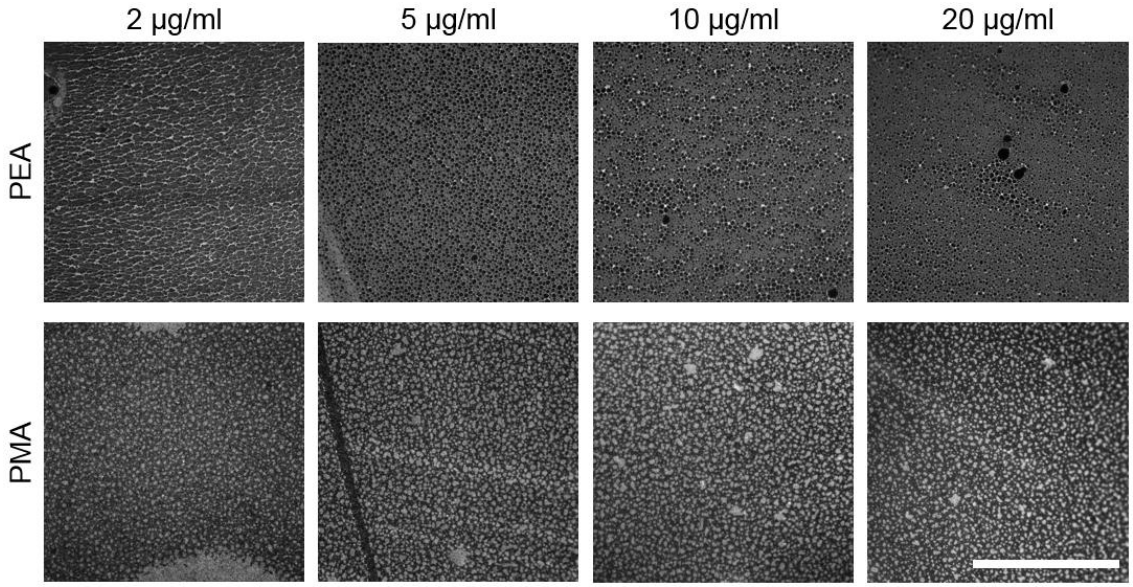

Figure 18: Immunostaining of FN on PEA (top) and PMA (bottom) at 2, 5, 10 and 20 µg/ml after 1-hour coating. FN on PEA formed a network after 1 hour regardless of the concentration. Likewise, FN on PMA formed globules after 1 hour for all concentrations used. Scale bar: 50 µm.

Immunostaining confirmed that FN has a network conformation on PEA whereas it forms aggregates on PMA for all concentrations of FN on the surface.

FN adsorbs more onto PEA compared to PMA for a small amount of coating (i.e. 1 µg/ml) with protein surface densities of 200 and 30 ng/cm^2 respectively (Figure 19 A). However, for the standard coating concentration of 20 µg/ml, no significant differences are visible with protein surface densities of 550 – 750 ng/cm^2.

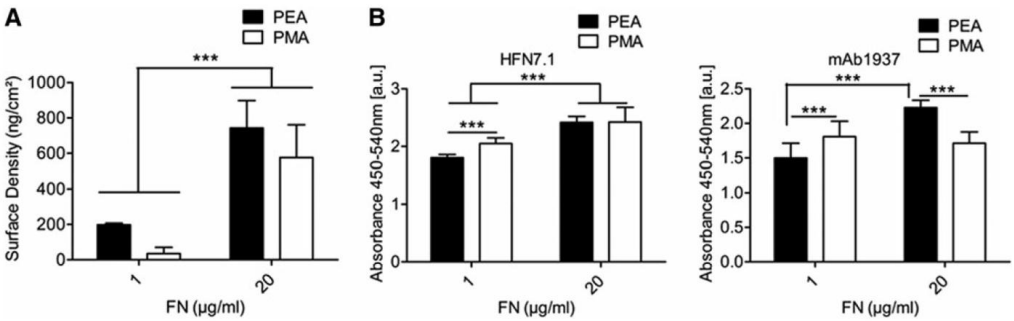

Figure 19: FN adsorption and domain availability on PEA and PMA coated with 1 and 20 µg/ml of FN for 1 hour. (A) Surface density of FN on PEA and

PMA. (B) Availability of RGD and PHSRN domains of FN. N = 9, ***p<0.001. From Vanterpool, F. *et al*. 2014[5].

In order to analyse the exposure and availability of integrin binding domains after adsorption of FN onto polymers, an ELISA using monoclonal antibodies directed against the HFN7.1 cell binding domain and the PHSRN synergy sequence was carried out (Figure 19 B). At a low concentration (1 µg/ml) of FN, the binding of both antibodies is higher on PMA indicating a higher biological activity of the protein. However, an increase in the concentration to its standard 20 µg/ml results in similar availability of the RGD domain on both polymers whereas there is significantly higher availability of the PHSRN synergy sequence on PEA compared to PMA.

2.3.2 Cell attachment and adhesion

Cell culture experiments with L929 mouse fibroblasts were carried out to assess short-term attachment and adhesion on FN coated polymers. This was done using a standard 20-minute attachment protocol and 3-hour early adhesion protocol.

When cells attach for 20 minutes to surfaces coated with 20 µg/ml of FN solution (Figure 20 A), over 90% of cells initially seeded remain attached after several washes with PBS, which is the same amount as FN coated surfaces that were washed. When surfaces were not coated with FN however cells did not attach to the surface, highlighting the importance of FN for early cell attachment.

In order to study cellular response to FN-coated polymers, 3-hour adhesion experiments were carried out with FN at 2, 5, 10 and 20 µg/ml in serum-free conditions. A low seeding density was used (5000 cells/cm^2) in order to avoid any cell-cell interactions and focus solely on cell-FN-material interactions. L929 fibroblasts spread on all surfaces with FN and remained rounded on surfaces with no FN (Figure 20 C). Cells maintained a consistent size on both surfaces of 1000-1500 µm^2 when coated with 2, 5 and 10 µg/ml of FN whereas for 20 µg/ml cells were significantly larger on PEA, ~ 2000 µm^2, compared to PMA, ~ 1400 µm^2 (Figure 20 B). Moreover, for the minimum concentration (2 µg/ml), the actin cytoskeleton was not as developed with stress fibres only visible at the periphery. This is in contrast with 20 µg/ml where stress fibres are visible across the cells, more notably on PEA.

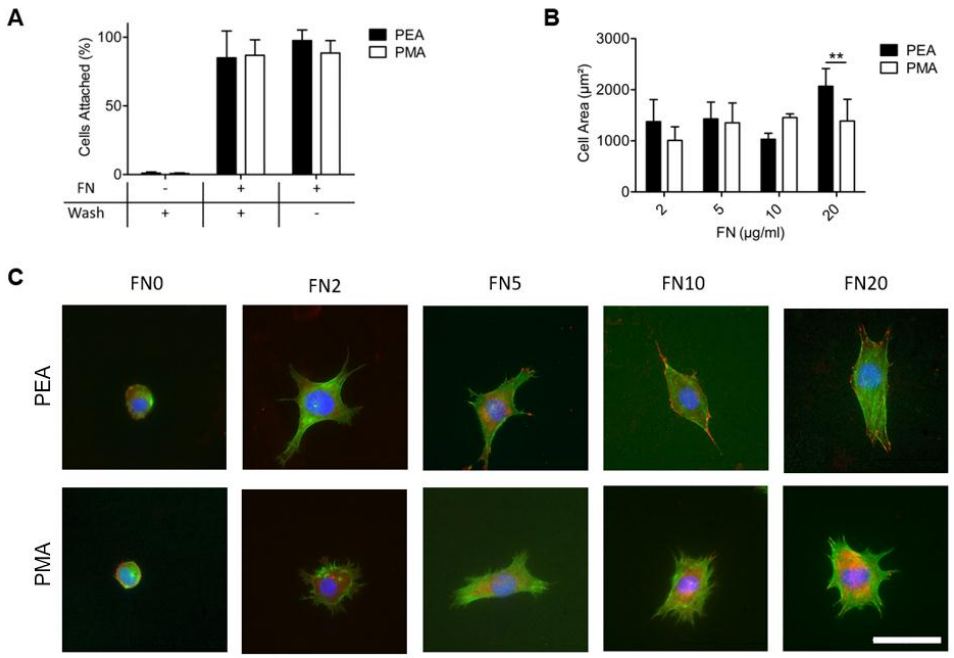

Figure 20: Attachment and spreading on L929 mouse fibroblasts on PEA and PMA coated with various concentrations of FN. (A) Attachment for 20 minutes of L929 on PEA and PMA coated with 20 µg/ml of FN. Cells attach firmly to both PEA and PMA after 20 minutes once FN in present on the surface whereas cells don't attach to the bare polymers without FN. (B) Cell area after 3 h adhesion on PEA and PMA coated with 2, 5, 10 and 20 µg/ml FN solution for 1 h. Cell area remains constant for cells on PEA and PMA coated with lower concentrations of FN (2 – 10 µg/ml) whereas cells are significantly larger on PEA compared to PMA when coated with 20 µg/ml of FN.(C) Representative images of L929 cells on PEA (top) and PMA (bottom) coated with 0, 2, 5, 10 and 20 µg/ml of FN (noted: FN0, FN2, FN5, FN10 and FN20). Samples are stained for actin (green), vinculin (red) and nucleus (blue). **p<0.01. Scale bar: 50 µm. (A and B from Vanterpool, F. *et al*. 2014[5]).

FAs were more developed with increasing FN concentrations on both polymers, located at the end of stress fibres (*Figure 21 A*). To assess FA maturity, the length of the major axis of focal plaques were quantified. Vinculin images were used and processed as previously described (Figure 13) and focal complexes inferior to 1 µm in length also known as focal points were discarded from analysis.

Cells on PMA presented a higher percentage of shorter FAs(35-40%) compared to cells on PMA (25-30%). Furthermore, the percentage of larger FA (≥ 3 µm) was slightly higher on PEA compared to PMA (*Figure 21 B*).

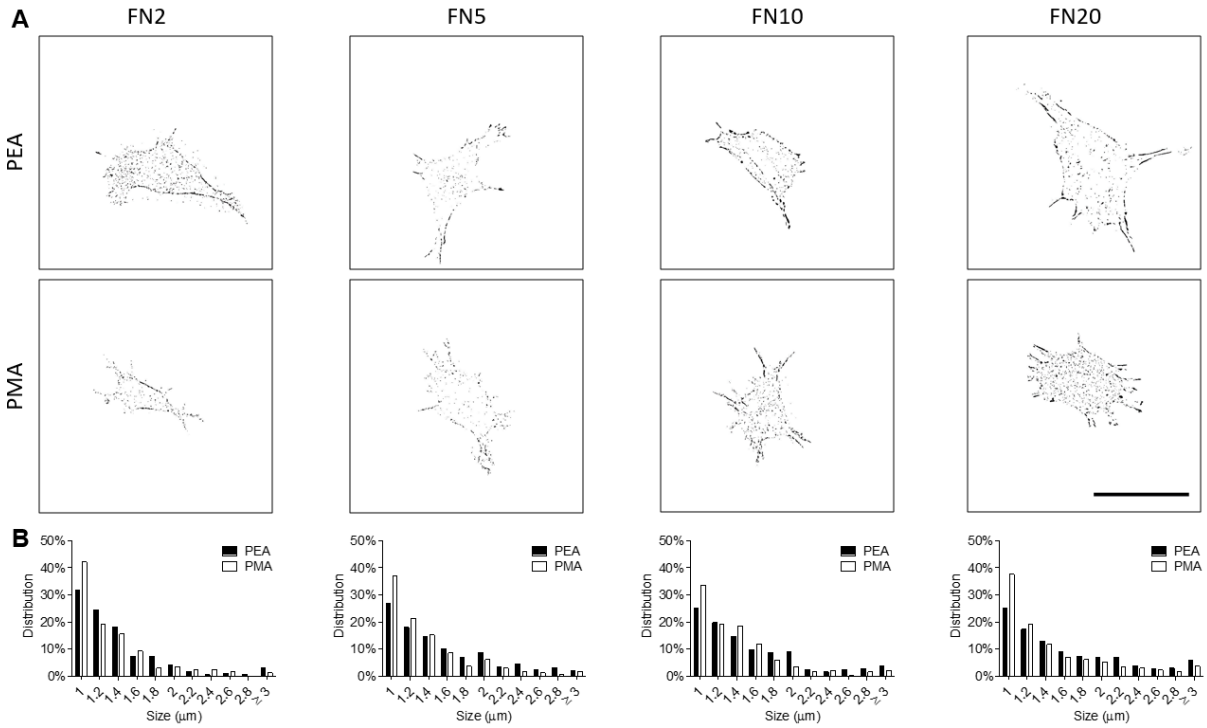

Figure 21: FA organisation on PEA and PMA coated with 2, 5, 10 and 20 µg/ml of FN solution. (A) Representative inverted binary representation of FAs. (B) Size distribution of FAs quantified with the FA analysis server. n = 5, scale bar: 50 µm. From Vanterpool, F. *et al*. 2014[5].

The median of FA size (Figure 22 *A*) increased significantly with increasing amounts of FN for cells on PEA whereas they remained constant for cells on PMA. Essentially, the slope for PEA (0.0101x + 0.00203) is statistically different from 0 ($p<0.05$) whereas the slope for PMA was not.

The area moment of inertia (*Equation 2*) which assess the distribution of points (in this case FAs) around a central axis (in this case the central axis of the cell) was used to analyse FAs on PEA and PMA with varying concentrations of FN (Figure 22 *B*). PEA presented a significantly higher moment of inertia ($4x10^4$ µm^2) compared to PMA ($2x10^4$ µm^2). This being the result of increased cell size, thus increasing the

distance from the centre of the cell to the edges (where FAs are most present), as well as FAs being larger on PEA.

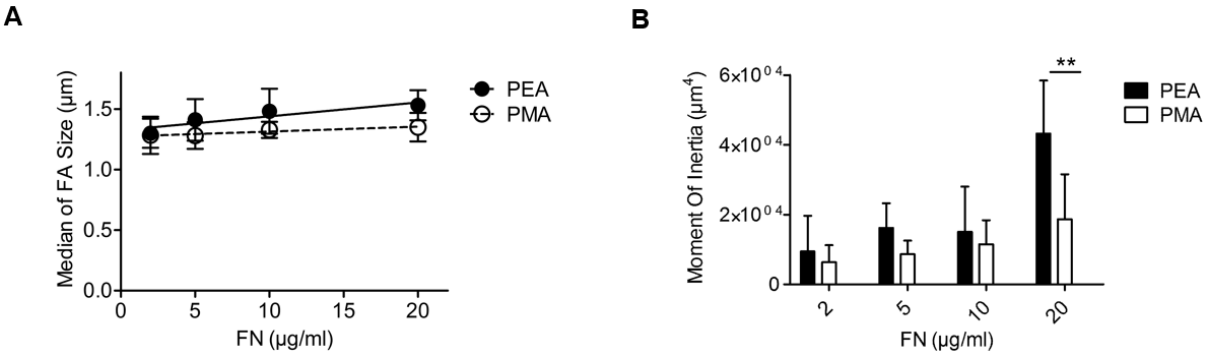

Figure 22: Assessment of FAs. (A) Median of FA size on PEA and PMA coated with 2, 5, 10 and 20 µg/ml of FN solution. (B) Moment of inertia for the distribution of FAs. **p<0.01.

2.3.3 Cell adhesion after blocking RGD and/or synergy domains of FN

Early adhesion (3 hours) as well as attachment (20 minutes) experiments were carried out with an extra step during which the RGD cell binding domain and/or the PHSRN synergy sequence of FN was blocked using HFN7.1 and mAb1937 antibodies respectively.

Though cells attached the same on polymers in normal conditions (Figure 23 A), FAs were larger in both average area and number on PEA (Figure 23 B and C). Cell attachment is inhibited on both polymers when the RGD domain is blocked (H). This blocking also results in decrease in the number of FAs and FA area, especially for cells on PMA. Blocking the synergy sequence (m) has no effect on cell attachment, however, the number of FAs as well as their size is significantly decreased on PEA with no detectable FA on PMA. The use of both HFN7.1 and mAb1937 antibodies drastically reduced the number and size of FAs on PEA and therefore the moment of inertia. No FAs were detected on PMA in this instance.

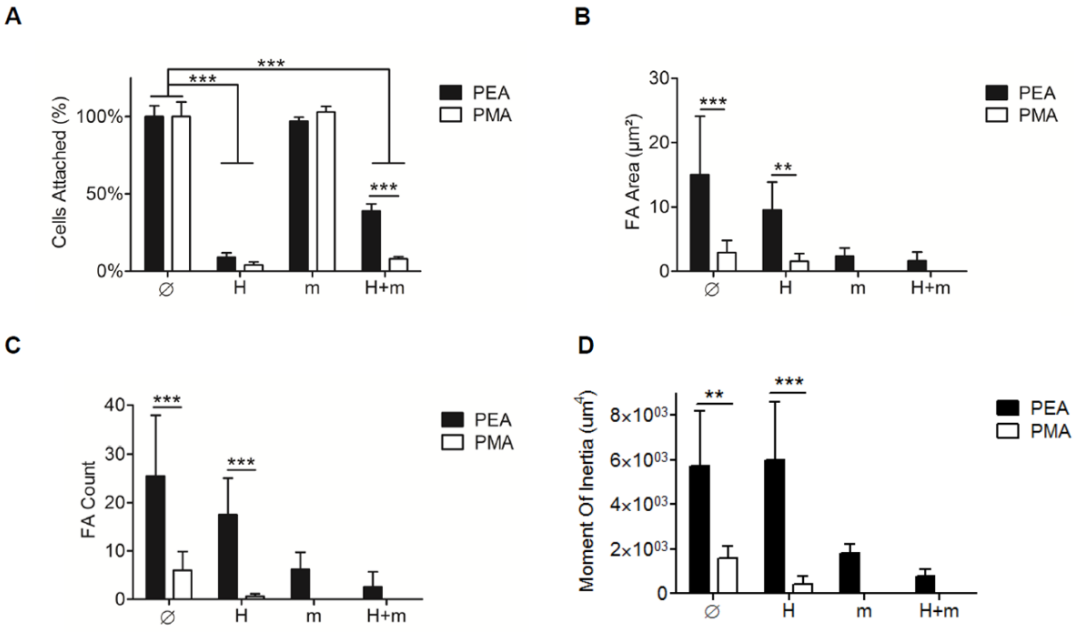

Figure 23: Cell attachment and FA quantification after blocking RGD or synergy domains of FN with HFN7.1 and mAb1937. (Ø denotes no antibodies; H denotes the use of HFN7.1; m denotes the use of mAb197; H+m denotes the use of both HFN7.1 and mAb1937). (A) Cell attachment shows that cells that bind equally on PEA and PMA when no antibodies are used attach to the polymer surfaces differently especially when antibodies are used together (H+m). (B) and (C) FA area and size shows that cells on PEA have more and larger FAs in standard conditions whereas adding antibodies significantly diminishes the size and amount of FA. (D) Moment of inertia reflects the results of FA area and count. **p<0.01, ***p<0.001. From Vanterpool, F. *et al*. 2014[5].

2.4 Discussion

2.4.1 Surface chemistry and FN adsorption

It is well known that surface chemistry influences the adsorption of FN in terms of the amount of protein and its conformation on the polymeric surface. García *et al.* showed that using hydrophilic OH-SAM lead to very little changes to the conformation of FN or the recombinant FN-III$_{7\text{-}10}$ fragment upon adsorption whereas the use of hydrophobic CH_3-SAM lead to significant changes[55, 147]. This surface

modulation resulted in modified biological activity of FN leading to changes in integrin binding, FA organisation and intracellular signalling pathways which in turn dictated various degrees of cell differentiation[147, 156, 157].

PEA and PMA polymers are hydrophobic surfaces with similar static and receding water contact angles of approximately 75° and 35° respectively. The advancing contact angle, slightly higher on PEA compared to PMA (100° on PEA versus 90° on PMA), leads to increased hysteresis indicating higher surface mobility.

2.4.2 FN conformation and integrin binding domain availability

These results confirm that the conformation as well as the distribution of FN can be controlled using surfaces with very comparable physico-chemical properties. The differences in protein conformation on PEA and PMA has far reaching implications at a molecular scale and is translated to differences in the availability of the $FNIII_{9-10}$ integrin binding domain. With the same amount of FN adsorbed after coating with the standard 20 µg/ml (600-700 ng/cm^2 measured on the surface), the RGD domain was equally available on both polymers. However, the same could not be said for the PHSRN synergy sequence located on the $FNIII_9$ domain which was more exposed on PEA compared to PMA *(Figure 19B)*. This has significant consequences in relation to integrin binding. Previous studies have shown that both the RGD domain ($FNIII_{10}$) and synergy sequence ($FNIII_9$) are needed in order to bind integrin $\alpha_5\beta_1$[50, 158]. Furthermore, blocking both RGD and PHSRN sequences lead to complete inhibition of attachment on PMA versus partial attachment of cells on PEA (Figure 23 A). This indicates that cell attachment on FN-coated PEA was mediated preferably via PHSRN/$\alpha_5\beta_1$ as opposed to cells that attached onto PMA via the RGD/$\alpha_v\beta_3$ FN domain/integrin combination.

2.4.3 Biological response – focal adhesion formation

The biological response observed by cell attachment and FAformation are direct responses to cells being presented to FN which itself is modulated by the underlying material surfaces[68]. Vinculin was used as a marker of FA as it is one of the main proteins recruited at the site of adhesions (Figure 6) mediated by $\alpha_5\beta_1$ and $\alpha_v\beta_3$ integrins[159]. Furthermore, vinculin is necessary for myosin contractility-dependent

adhesion strength as well as the coupling of cell area with traction force[160]. A direct relationship exists between the formation (as well as size) of FAs and the mechanical properties of the external microenvironment of the cell. It has been well documented that stiff substrates, along with the application of certain stresses and strains, contribute to the development of large FAs. Contrarily, soft substrates with little strain and stress favour the formation of much smaller FAs known as focal complexes[66, 161].

As a side-note, nanotopography (such as nanopillars, nanopits and nanogrooves) has also been shown to have an effect on the size and direction of FAs with integrin clustering and cytoskeleton organisation[162, 163].

This study shows that the conformation and distribution of FN on surface materials with similar properties can be used as a tool to dictate FA organisation. The globular FN on PMA allowed for the formation of smaller FAs (focal complexes) whereas the fibrillar conformation of FN on PEA allowed for longer and more developed adhesions (Figure 21A). This was shown to be independent of the amount of FN used to coat the surfaces as the trend was observed when coating with low amounts of FN (2 µg/ml) all the way to 20 µg/ml FN. Moreover, the size distribution of FAs remained constant on PMA with increasing amounts of FN. The same could not be said of the FA distribution in cells on PEA where the fraction of large FAs increased with increasing concentrations of FN. Although it is a crude representation, this can be observed by looking at the median size of FAs on PEA and PMA with increasing amounts of FN (Figure 22A).

These larger FAs on PEA resulted in cells being more spread compared to PMA (Figure 20B). FA size as well as cell size both contributed to higher values of moment of inertia of cells on PEA compared to PMA. Previous studies have shown that cells apply an approximate stress of ~5.5 nN/µm on substrates[65]. This suggests that cells are able exert larger forces on FN when in a fibrillar conformation on PEA than on FN in a globular conformation on PMA, surfaces which are both sensed as stiff by the cell due to their Young's moduli (Table 8) which are much higher than physiologically 'soft' tissue such as fat and muscle[164].

2.4.4 Biological response – blocking integrin binding domains

When $FNIII_9$ and $FNIII_{10}$ domains of FN were blocked with mAb1937 and HFN7.1 monoclonal antibodies respectively, results corroborated the idea that PEA and PMA can influence biological response. When $FNIII_{10}$ was blocked, thus inhibiting the RGD domain availability, a drastic reduction in cell attachment was observed on both surfaces. When $FNIII_9$ was blocked, inhibiting the availability of the PHSRN synergy sequence, cell attachment was not affected (Figure 23A). This shows that when the synergy sequence is unavailable, cells are still capable of adhering to the FN irrespective of conformation using the equally available RGD domain via the $\alpha v\beta_3$ and not the $\alpha_5\beta_1$ integrin. Blocking also had a clear effect on FA formation with a significantly lower amount of FAs on PMA after blocking with either antibody compared to PEA where FAs, albeit smaller than normal, were found. Cells were still able to adhere to fibrillar FN on PEA via other biding domains on the extended proteins but not on PMA due to the fact that the protein remains in a globular conformation, with no other available binding domains.

The following (Figure 24) is a summary of this model in which an underlying material surface can influence the conformation of FN, thus the availability of integrin binding domains that in turn directs cell behaviour.

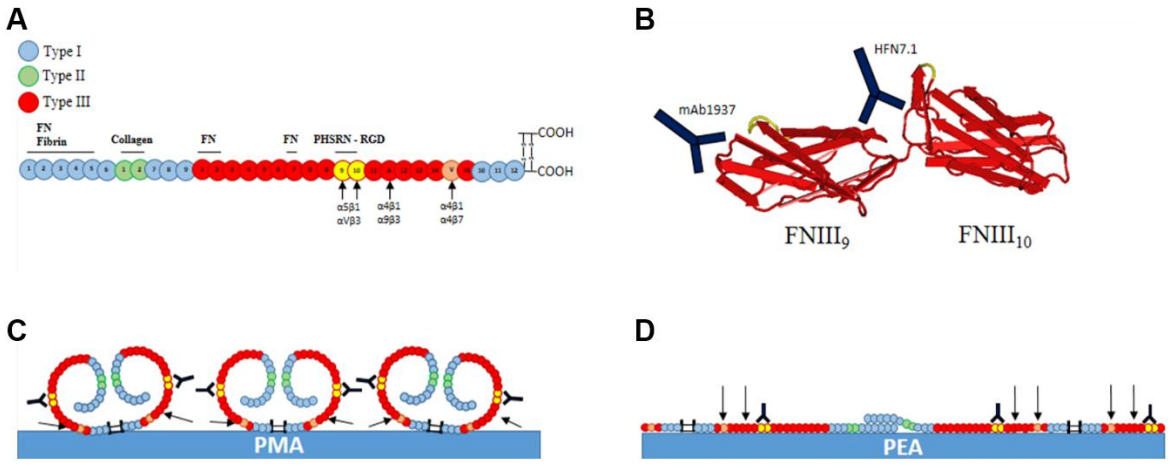

Figure 24: Mechanistic model for the material-based modulation of FN conformation. (A) FN monomer with binding domains of integrins and other ECM proteins. The main integrin binding domain of FN (FNIII9-10) highlighting the RGD and PHSRN sequences in yellow. (B) $FNII_{9-10}$ fragment of FN with binding sited of HFN7.1 and mAb1937 antibodies which block the RGD domain on $FNIII_9$ and the PHSRN synergy sequence on $FNIII_{10}$ respectively. (C) FN takes on a globular conformation on PMA, therefore hiding the integrin binding sites which is accentuated by blocking the RGD and PHSRN sequences. (D) When on PEA FN extends and takes on a fibrillar conformation, exposing more integrin binding sites even when the RGD and PHSRN sequences are blocked leading to more possibilities for cell interactions. Adapted from Vanterpool, F. *et al*. 2014[5].

2.5 Conclusions

It's been demonstrated that it is possible to modulate FN conformation via material surfaces that have similar physico-chemical properties. The difference between PEA and PMA being only one methyl group in the side chain with both having comparable wettability characteristics. This however translates to noticeable differences in the organisation of FN upon adsorption with nanonetwork structures forms on PEA whereas globules form on PMA. Consequently, the extended conformation of FN on PEA led to an increase in the availability of integrin binding domains, more notably the PHSRN synergy sequence located on the FN-III_9 repeat.

This specific difference on FN-coated PEA led to a higher distribution of larger FAs compared to smaller focal points noticed on PMA. The differences in FN conformation were confirmed by blocking the FN-III9-10 domain with monoclonal antibodies which showed that FAs were maintained on PEA but not on PMA. These results show that cells are susceptible to FN organisation and domain availability on polymeric surfaces independent of the underlying physico-chemical properties of the materials.

3 Focal adhesion formation and cell migration in DU145 human prostate cancer cells

3.1 Introduction

3.1.1 Prostate cancer

Once considered a very rare disease in the 19th century, prostate cancer has become the most common form of cancer in men. In the US and Europe respectively, it is the second and third most common cause of death [165, 166]. It consists in the formation of tumorous cells in the prostate, with various types of prostate cancer existing depending on the tissue and cell type where it originated. The most common type being acinar adenocarcinomas which develops in the gland cells that line the prostate. Other forms of prostate cancer include ductal adenocarcinomas (cells that line the tubes of the prostate gland), and urothelial cancer (cells within the urethra)[167].

3.1.2 Current and potential treatments of prostate cancer

One of the most common treatments for prostate cancer is hormone therapy. Male hormones known as androgens are needed for the growth and function of the healthy prostate gland[168]. However, these hormones also promote the growth of cancerous prostate cells via their androgen receptors (AR). This is the main therapeutic target in prostate cancer treatment due to the fact that studies have shown that AR is necessary for cell viability, proliferation and invasion[169-171]. Hormone therapy, also known as androgen suppression/deprivation therapy consists of inhibiting the production and utilisation of androgens[172]. This is done by inhibiting production of androgens by the testicles (medical or surgical castration), blocking the action of androgens (antiandrogens that competitively bind AR), or, blocking the production of androgens throughout the body (blocking production in adrenal glands and cancer cells). These treatments are carried out in parallel with standard chemotherapy and radiation and it has been shown to be more effective than simply removing the prostate or testicles surgically[173].

Prostate cancers, however, tend to develop resistance to this form of treatment and become less sensitive to androgen depletion causing a relapse in cancer progression[174, 175]. Although many drugs such as Enzalutamide, Cabaitaxel and Radium-223 have recently been developed to treat castration resistant treatments, they fail to effectively halt cancer progression and metastasis.

3.1.3 Choice of DU145 cell line

DU145 is a classical epithelial prostate cancer cell line and is derived from a metastatic site in the brain of a 69 year old Caucasian male [176]. It is considered to have moderate metastatic potential compared to PC3 which has a high metastatic potential. Many studies have been done using this cell line due to the fact that it is reportedly not hormone sensitive but has shown to interact with ECM protein including FN, more notably via the $\alpha_5\beta_1$ and $\alpha_v\beta_3$ integrins. Several studies have used the PHSCN, a competitive inhibitor of the PHSRN sequence, in order to supress metastasis in this cell line[48, 49, 177, 178]. Interestingly, a study by Livant *et al.* suggested that the PHSRN synergy sequence without the RGD sequence is sufficient to induce invasion of DU145 cells whereas the same could not be said of the opposite scenario[49].

Our studies have shown that upon adsorption to PEA and PMA, FN takes on fibrillar and globular conformations respectively where the extended fibrillar form on PEA confers higher availability of the PHSRN sequence compared to PMA[5] (Figure 19B). Seeing that the DU145 is particularly sensitive to PHSRN, using material-based platforms that can affect that sequence's availability could prove useful to study its importance in cancer cell motility.

3.1.4 Hypothesis and experimental aims

We hypothesise that differences in FN conformation on PEA and PMA have an impact on human prostate cancer cell attachment, traction and migration via the differential expressions of intracellular proteins involved in FA formation such as FAK. The aims of this study are therefore to use well-defined and characterised polymer systems with known effects on FN upon adsorption to characterise cancer cell proliferation, migration, traction, and drug resistance and to elucidate the underlying mechanisms involved in these processes.

3.2 Materials and methods

3.2.1 Cell culture

DU145 human prostate cancer cells (ATCC – HTB81) were thawed and resuspended in Minimum Essential Media Alpha growth medium (MEM Alpha) supplemented with GlutaMAX^{TM}, 1% P/S, and, 10% FBS. Cells were grown using standard cell culture conditions (37°C, 5% CO_2), harvested by trypsinisation and centrifuged at 1000 rpm before being resuspended in growth media (supplemented MEM Alpha) for passaging or use at 90% confluence.

In order to better characterize the DU145 human prostate cancer cell line (ATCC – HTB81), a growth assay was carried out. This was done using MTT (3-(4,5-dimethylthiazol-2-yl)-2,5-diphenyltetrazolium bromide) and alamarBlue® assays, both of which assess cell viability by measuring colorimetric changes proportional to cell activity.

3.2.2 DU145 growth

3.2.2.1 MTT assay

Cells use the NAD(P)H-dependent oxidoreductase enzymes to reduce MTT, a tetrazolium dye, to formazan, a water-insoluble purple product[179].

In this experiment, cells were seeded into 96-well plates at 500 and 5,000 cells/well ($1.6x10^3$ and $1.6x10^4$ cells/cm^2 respectively). Every day for 7 days, 20 µl of MTT was added to a row in the 96-well plate and incubated at 37ºC for 5 hours. The medium with MTT was then carefully removed without removing the formed crystals and replaced with 110 µl of DMSO in order to dissolve the formazan crystals for 15 minutes at 37ºC. The solution was then transferred to a new plate and absorbance was read at 570 nm using a Multiskan Ascent, model no. 354 plate reader (Thermo Labsystems).

3.2.2.2 AlamarBlue® assay

Similarly to MTT cells reduce Resazurin, a blue non-toxic active ingredient in alamarBlue®, to resofurin, a fluorescent red compound[180].

This experiment was carried out on tissue culture plastic (TCP) as well as on PEA, PMA and glass. Coverslips were sterilised by UV and coated with FN or just DPBS for 1 hour before being rinsed twice and transferred to a 24-well plate.

In the case of TCP, cells were seeded in a 96-well plate at different seeding densities ranging from $1.5x10^3$ to $6x10^5$ cells/cm^2 in order to determine an optimal seeding density for growth on polymers. Cells were subsequently seeded onto PEA, PMA, and, glass at $1.5x10^3$ and $1.5x10^4$ cells/cm^2. In both instances cells were seeded and incubated in media without FBS for the first 3 hours, after which, the media was replaced with fresh media containing 10% FBS and incubated overnight. AlamarBlue® was then added (10% of the total volume per well) and samples were incubated for 4h at 37°C, 5% CO_2. The media was then transferred to a black, flat-bottom 96-well plate and fluorescence was measured using the Tecan® M200 pro plate reader, with an excitation wavelength at 560 nm and an emission wavelength at 590 nm. This was done over the course of one week. Fluorescence was measured using constant gain at 60 throughout.

3.2.3 Cytotoxicity (docetaxel and PND-1186)

For both drugs, cytotoxic studies were first carried out in a 96-well to determine the IC_{50} from a wide range of concentrations. Cells were seeded at $5x10^3$ cells per well ($1.5x10^4$ cells/cm^2) and incubated overnight. Media was then removed and replaced with media containing 10^{-4}, to 10^3 nM of docetaxel[181] or PND-1186. After 72h, the viability of cells was measured using alamarBlue®.

Cytotoxicity of docetaxel alone was measured on PEA, PMA and glass coated with FN using the same seeding density ($1.5x10^4$ cells/cm^2) and viability was also measured using alamarBlue®.

Fluorescence was measured using the Tecan® M200 pro plate reader, with an excitation wavelength at 560 nm and an emission wavelength at 590 nm.

3.2.4 Cell attachment assay

PEA, PMA and glass coverslips were sterilised in UV for 20 minutes, coated with FN (20 µg/ml) for 1 hour, and, washed twice with PBS. Samples were then blocked with heat-denatured 1% BSA (Roche) in DPBS for 30 minutes at room temperature.

During this period, cells were harvested, trypsinised and resuspended in complete growth medium (containing 10% FBS). The cell suspension was then transferred to a tube and incubated for 10 minutes at 37°C, 5% CO_2.

Cells were then seeded onto the surfaces at a seeding density of $8.5x10^4$ cells/cm^2 ($3.4x10^5$ cells/ml) for 20 minutes at 37°C, 5% CO_2. Surfaces were then rinsed twice with DPBS to remove cells that were not firmly attached, fixed with formaldehyde 4% for 20 minutes at 4°C and rinsed three times with DPBS.

Samples were then permeabilised using the triton X-100 based permeabilisation buffer in the following table and mounted with Vectashield® containing DAPI to stain the nuclei.

This was also carried out with an extra blocking step with the use of HFN7.1 and mAb1937 as previously described.

3.2.5 Cell attachment assay with PND-1186

For experiments in which FAK phosphorylation was inhibited, PND-1186, a potent FAK inhibitor currently in phase 1 clinical trials for metastatic cancer, was used. This drug reported to have a cellular IC50 of ~100 nM in breast carcinoma cells as determined by anti-phospho-specific immunoblotting to FAK Tyr-397[101] and has shown to supress cell migration.

Samples were prepared in the same way as in the standard attachment assay (Chapter 2). However, cells were harvested and resuspended in growth media with 0, 150 or 1500 nM of PND-1186 and were incubated in tubes with gentle agitation for 1 hour. Concentrations of 0, 150 and 1500 nM of PND-1186 were chosen to have cells in normal conditions with no drug, cells with the approximate reported IC_{50} value and cells with a 10-fold increase of drug concentration. Cells were then seeded onto surfaces, incubated, rinsed, fixed and imaged in the same way.

3.2.6 Early adhesion assay

Samples (PEA, PMA and glass cover slips) were sterilized for 20 minutes using a UV lamp and then coated with FN at 2, 5, 10 and 20 µg/ml for 1 hour. Samples were then rinsed twice with DPBS and cells were seeded at $5x10^3$ cells/cm^2 ($2x10^4$ cells/ml) and cultured for 3 hours (37°C, 5% CO_2). Triplicates were used for each condition.

After washing, samples were fixed with formaldehyde 4% for 20 minutes at 4°C and rinsed three times before being stored in DPBS at 4°C until ready to be stained.

Samples were then permeabilised, blocked for 30 minutes with 1% BSA (in DPBS), and, incubated for one hour using an antibody against vinculin hVIN-1 (in mouse; 1:400 dilution; Sigma). Samples were then rinsed twice with 0.5% Tween20 (in DPBS) and incubated with a Cy3-conjugated anti-mouse secondary antibody (Cy3 anti-mouse; 1:200 dilution) for 1 hour in the dark. The secondary antibody was coupled with Phallacidin (1:100 dilution) which stains the actin cytoskeleton.

Samples were then rinsed twice with 0.5% Tween20 (in DPBS) and mounted with Vectashield® (Vector laboratories, Inc.) with DAPI which stains the nuclei.

Staining was then observed using a Zeiss Z1 Observer inverted epifluorescence microscope at different magnifications. Images were taken and merged using ImageJ to have cells with stained nuclei, actin and FAs.

In the case of early adhesion with blocking, an extra step was added after FN coating during which the RGD and PHSRN domains were blocked with HFN7.1 and mAb1937 antibodies respectively at 14.6 µg/ml for a 1:1 antibody-FN ratio for 1h at room temperature. Cell seeding, rinsing and fixing were done in the same way as the standard early adhesion assay. The Zenon® kit was used as described in Figure 12 to label hVIN-1 anti-vinculin antibody before incubating with cells. Staining was observed with an inverted epifluorescent microscope. Images were taken at 63x magnification with immersion oil and FAswere analysed using the FA analysis server.

3.2.7 Focal adhesion quantification

Images of vinculin and actin staining were analysed using the FA analysis server web tool as previously described in Figure 13. A total of 30-45 cells per condition

were analysed. An R script was therefore developed with the help of Ross Gurden of the Centre for Cell Engineering (CCE), part of the Institute of Molecular, Cells and Systems Biology of Glasgow University to process the output data of the FAAS. This script was used to collect data on cell size, and FA parameters for FAs larger than 1 µm in length (anything less than 1 µm is characterised as a focal complex or focal point[182]) such as: FA count, size, area, distance from centre, distance from the edge of the cell and calculate the area moment of inertia (Equation 2) of each cell and output the mean, standard deviation and median of FA parameters per condition.

3.2.8 Wound healing assay

PEA, PMA and glass coverslips were coated with 20 µg/ml of FN for 1h, rinsed with PBS and left to dry. Ibidi® inserts were then placed on coverslips. DU145 cells were harvested, resuspended in media containing no FBS and seeded in insert wells at $70x10^3$ cells/ml for a confluent layer of cells. After 2h of seeding, the media in each well was replaced with media containing PND-1186 for an extra hour.

After 1h, inserts were removed and wells were filled with media containing 2% FBS with no drug, 100 nM or 1000 nM of PND-1186. Images were then taken with the EVOS FL Auto automated epifluorescent microscope (Life Technologies) every 15 minutes for 20 hours.

3.2.9 FAK phosphorylation inhibition with PND-1186

Wound healing assay was carried out with in the same way as previously described with 0 nM, 150 nM and 1500 nM of PND-1186.

3.2.10 Single cell traction force microscopy (CTFM)

The use of a polyacrylamide hydrogel containing fluorescent beads is a common method used in CTFM. Due to the inert properties of PAA, the hydrogel must be treated to allow cell adhesion and traction. This is usually done by functionalising the hydrogel using reagents such as sulfo-SANPAH to bind ECM proteins[183] or by

coating the surface with maleic anhydride copolymers that can bind ECM proteins[184]. Here we engineer a system of PEA and PMA coated hydrogels in order to study the effect of FN conformation on cell traction.

3.2.10.1 Passivation of coverslips with Sigmacote®

Glass coverslips (32mm ø) were placed in an ultrasonic bath for 30 min and rinsed twice with water. Coverslips were then placed in an ultrasonic bath for 30 min with 99% ethanol and rinsed twice with water.

Coverslips were then cleaned for 10 min using an RCA solution (H_2O : H_2O_2 medical grade 35% : NH_3 p.a. 28%; 5 : 1 : 1) heated to 60°C before being rinsed twice with water and dried with a nitrogen flow (N_2).

Coverslips were then individually submerged in Sigmacote® (Sigma-Aldrich, Lot# SLBF4357V) solution (<5 sec) and left to dry at room temperature. In order to remove impurities, coverslips were then placed in an ultrasonic bath with 99% ethanol for 15 min and then dried with N_2. Coverslips are then rinsed and stored in water at 4°C until ready to use.

3.2.10.2 Acrylsilinisation

Glass coverslips (22mm ø) were cleaned using the ultrasonic bath and RCA solution in the same way as described above.

Acrylsilane solution was prepared with 94.8% EtOH p.a., 4.74% H_2O and 0.44% acrylsilane. Coverslips were submerged in acrylsilane solution for 2 h, rinsed with ethanol and dried with N_2. Samples were then tempered for 1h at 120°C and stored at 4°C until ready to use.

3.2.10.3 Gel preparation

PAA gels were prepared at 9 kPa stiffness with a mixture of acrylamide (AAm – monomer), bis-acrylamide (BisAAm – cross-linker), tetramethylethylendiamin (TEMED - accelerator), ammonium persulfate (APS – initiator) and Fluoresbrite

Microspheres (0.5 µm). The following Table 5 shows the amount of each ingredient added for the gels.

Table 5: Gel preparation in order of addition

Reagent	Concentration (w/w)	Quantity (µl)
AAm	30%	60
BisAAm	2%	60
H_2O (degassed)	-	256
Microspheres	-	20
TEMED	1.5%	20
APS	5%	4

The APS (initiator) was added last and the solution was vortexed briefly to mix everything together before pipetting 20 µl of the gel solution onto sigmacote coverslips. Acrylsilanised coverslips were then placed on top and left for 20 minutes until gels were polymerised. The following Figure 25 represents this process.

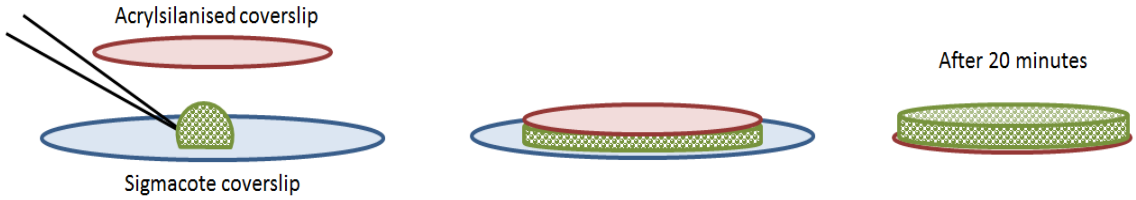

Figure 25: PAA gel preparation. Gels were prepared systematically on acrylsilanised coverslips with the use of a hydrophobic coverslip coated with Sigmacote® to maintain a flat surface.

After polymerisation, gels were left in H_2O for half an hour to allow them to swell. Gels were then either left in H_2O and stored at 4°C until ready to use (wet conditions) or vacuum dried at room temperature for 45 mins (dry conditions) to be used immediately.

3.2.10.4 PEA and PMA polymer preparation

Polymers were prepared just as described in previous reports. For this experiment, however, PEA and PMA were prepared at 1% w/v in order to have a layer of polymer as thin as possible to spin coat on top of the PAA hydrogel.

The thickness of the polymer layer was measured by spin coating onto glass coverslips and after drying, a scratch was made with a needle on the surface of the polymer and measured by AFM (tapping mode). This was done for different spin coating speeds in order to determine an optimal speed for polymer layers as thin and as homogeneous as possible.

3.2.10.5 Polymer-coating of PAA hydrogels

Polymers were coated onto hydrogels with the optimised spin coating conditions listed in the table below:

Table 6: Traction force microscopy spin coating parameters

Time	30 seconds
Speed	4000 rpm
Acceleration	200 rpm/sec

This was done in both dry and wet conditions. For wet conditions, hydrogels were spun at 500 rpm for 7.5 seconds (with an acceleration of 750 rpm/sec) to remove any drops of water on the surface of the hydrogel before adding the polymer solution.

Excess toluene was extracted by placing samples at 40ºC under vacuum for at least 4 hours. In the case of wet conditions, toluene was extracted in a humid environment (wet paper towels were placed alongside samples to prevent drying while extracting toluene).

After extraction of toluene, polymer coated hydrogels were sterilized for 30 min using a UV lamp, covered with MilliQ water, and stored at 4°C until ready to use (no longer than 24h).

3.2.10.6 Force spectroscopy

Mechanical properties of polymers and PAA hydrogel as well as PAA coated with poly(styrene-alt-maleic anhydride) (PSMA), PEA and PMA was measured by force spectroscopy. PSMA is a commonly used maleic anhydride copolymer and was used in this study as a control. Force spectroscopy measurements were carried out using the Nanowizard 3 AFM from JPK in immersed conditions.

Parameters of the cantilevers and tips used are listed in the table below.

Table 7: Force spectroscopy parameters

	PEA	PMA	PAA	PAA+ PEA	PAA+ PMA	PAA+ PSMA
Spring constant [N/m]	3	3	0.1 – 0.3	0.15 – 0.35	0.11 – 0.37	0.11 – 0.2
Sensitivity [nm/V]	26.88	26.88	25 – 41	25 – 38	27 – 34	25 – 40
Bead radius [µm]	10	10	5	5	5	5
Setpoint [nN]	150	150	7.813	7.954	8.58	9.889
Indentation Depth for fitting [µm]	0.1	0.1	0.2	0.2	0.2	0.2
Velocity [µm/s]	2.5	2.5	1	1	1	1

3.2.10.7 Bead displacement and traction force measurements

Polymer-coated hydrogels were rinsed with PBS, coated with 20 µg/ml of FN for 30 min at 37°C, and rinsed twice with PBS.

DU145 human prostate cancer cells (grown in MEM-alpha media containing 10% FBS, 1% P/S and 1% glutamine), were harvested by trypsinisation, counted and

seeded onto hydrogels at a seeding density of 2000 cells/cm^2 (in order to observe individual cells) for 2 hours.

Cells were then observed using the Axio Observer Z1 epifluorescent microscope at 40x magnification using phase contrast (to observe cells) and GFP fluorescent channel to observe microbeads (Figure 26).

Images of individual cells were taken as well as the underlying fluorescent microbeads structure. This was identified as the "*contracted*" form of the gel. Once images were taken, growth media was removed and cells were detached using trypsin. PBS was then added to keep gels completely hydrated. Images of fluorescent microbeads in the same areas, where cells once were, were taken in order to obtain a reference or "*relaxed*" form of the gel to compare.

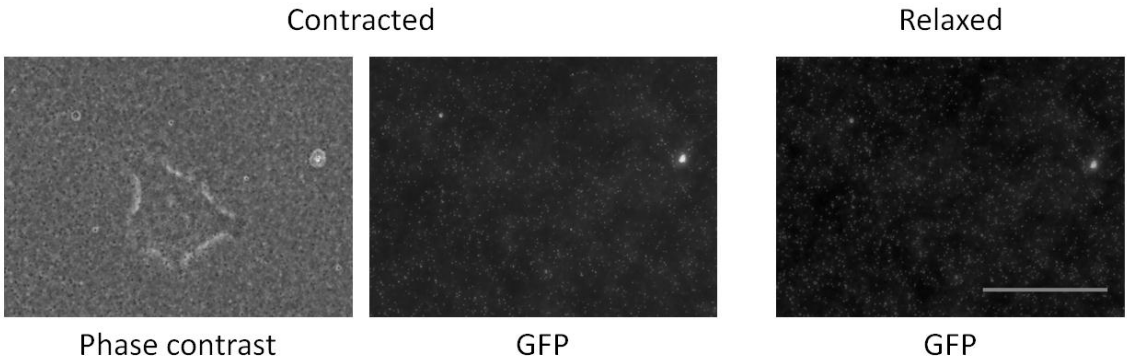

Figure 26: Obtaining images. Images of cells were taken using phase contrast and the underlying microbeads structure was taken using GFP fluorescent channel before and after removing cells (contracted and relaxed states respectively). Scale bar: 50 µm.

Images were then processed using Fiji (ImageJ v. 1.51k) in order to combine the compressed and relaxed state of the gel into a stack and correct for any slight x-y shift that could have occurred during the removal of cells. Bead displacement is then determined using a script in MATLAB able to identify small changes in the microbeads' positions and determine a displacement field (displacement of beads)[184-186]. Knowing the mechanical properties of the gel (Young's modulus and Poisson ratio), this is then converted into a traction field (forces exerted by the cell

on the gel) by the Fourier Transform Cell Traction Force Microscopy (FT-CTFM)[187, 188] or via in-house finite element modelling (Figure 27).

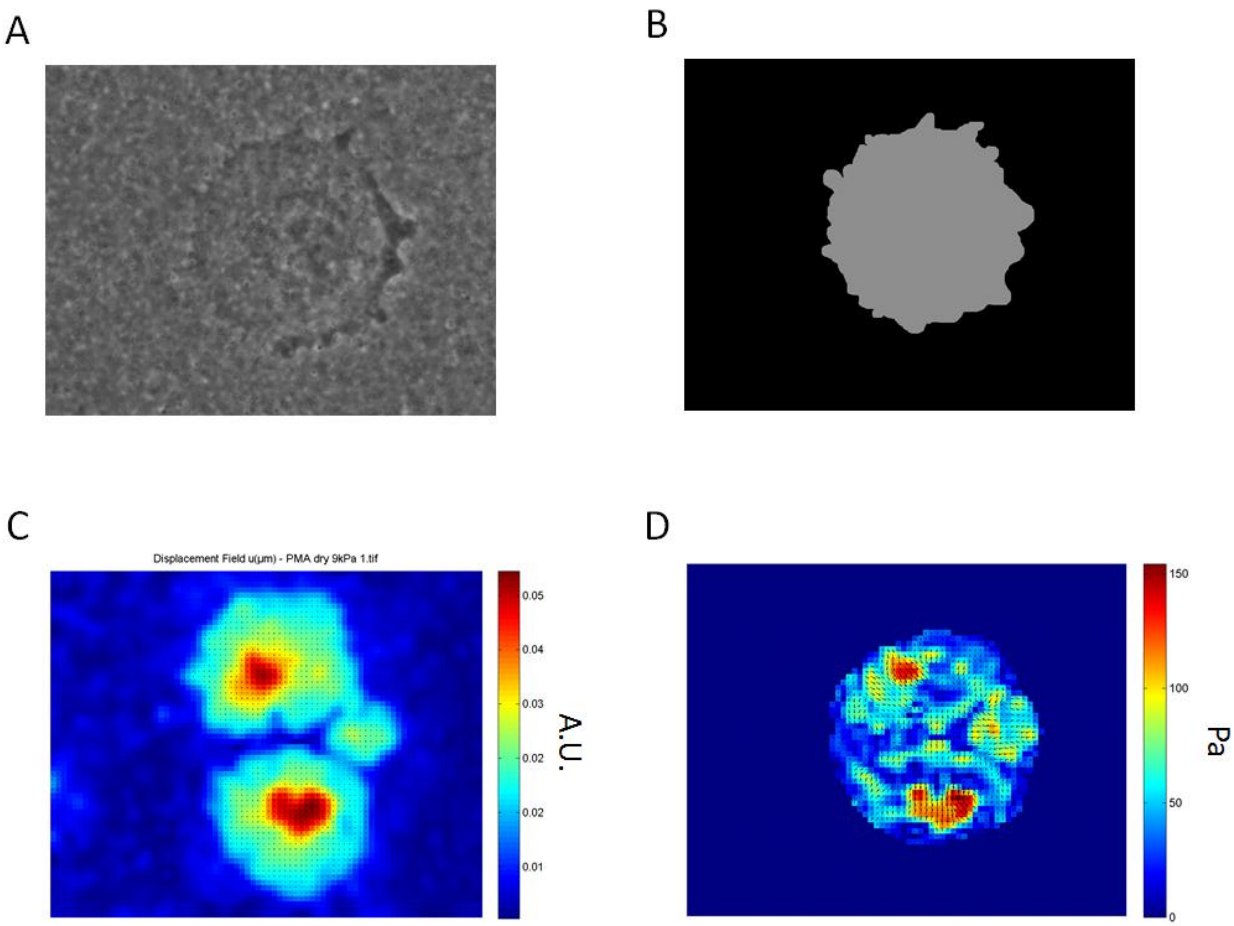

Figure 27: Traction force analysis. (A) Phase contrast image of the cell converted to (B) a cell mask. Fluorescent channels of beads were used to determine the (C) displacement field of microbeads and converted it to (D) traction field within the cell.

For these measurements, a total on 15 cells were taken per condition and the resulting traction fields were obtained. Three independent experiments were carried out.

3.2.11 Fourier transform traction cytometry (FTTC)

This model is based on the theory that the underlying gel is a semi-infinite solid in which the lateral movements (bead displacements) are small compared to the

thickness of the system. Once this is established any displacement $\vec{d}(\vec{u})$ is correlated to a point of traction on the surface $\overrightarrow{d'}(\vec{T})$ using the Green's function (K) with the following equation[187].

Equation 3:

$$(\vec{u}) = K\vec{T}$$

In which the Green's function K is represented by the following equation.

Equation 4:

$$K = \frac{2(1+\nu)}{Ek^3}\begin{pmatrix}(1-\nu)k^2+\nu k_y^2 & -\nu k_x k_y \\ -\nu k_x k_y & (1-\nu)k^2+\nu k_x^2\end{pmatrix}$$

In which ν is the Poisson ration, E is the Young's modulus and k is the displacement.

3.2.12 Finite element modelling cell traction force microscopy (FEM-CTFM)

Fourier transform traction cytometry is a well-used method that is limited by the fact that in order to be implemented, some assumptions need to be made such as the homogeneity of the substrate measured as well as its isotropicity[187]. This allows for understanding the transmission of force within a relatively simple system. Studying a bi-layered system with a relatively soft hydrogel base coated with a thin but stiff layer of polymer can therefore not be carried out using this method. Finite element model was therefore developed in order to study this complex system.

Bead displacement data obtained on the hydrogel surface with the MATLAB algorithm was also used for finite element analysis in order to determine forces exerted by cells on the polymer surface by modelling force transmission between the hydrogel-polymer interface.

This bi-layered system was modelled, thanks to Dr. Lukasz Kaczmarczyk and Karol Lewandowski of the Infrastructure & Environment research division, using the Cubit geometry and mesh generation toolkit with the thickness and mechanical properties

of each polymer layer. A fine mesh factor was chosen to have higher resolution of displacement and traction stresses. Below is a table of parameters used for these models.

Table 8: Mesh parameters for PEA, PMA and PSMA coated polyacrylamide

		Polymer		
		PEA	PMA	PSMA
Block 1 (Polymer)	Dimensions (µm)	200 x 230 x 0.07	200 x 230 x 0.1	200 x 230 x 0.01
	Young's modulus (MPa)	0.379	0.790	$3.6.10^{-3}$
	Poisson ratio	0.49	0.49	0.48
	Mesh Factor	1	1	1
Block 2 (Hydrogel)	Dimensions (µm)	200 x 230 x 50		
	Young's modulus (MPa)	0.48		
	Poisson ratio	$3.6.10^{-3}$		

Traction stresses on the surface of the polymer layer were then calculated using up to 8 processors thanks to the university servers. Results were processed with the Paraview data analysis and visualisation program. Results were then compared with results obtained using the MATLAB algorithm.

3.2.13 FAK and pFAK signalling

3.2.13.1 In-cell western

Cells were seeded into a 24-well tissue culture treated plate and left to adhere for 2h after which culture media was removed, cells were rinsed with PBS, and, fixed with 4% formaldehyde.

Seeding was done in different conditions (Figure 28). Cells were seeded using media with no FBS, however a positive control was used for each condition with

media containing 10% FBS which would in theory increase the expression of FAK. Furthermore, 2 seeding densities were used: $20x10^3$ cells/cm^2 and $40x10^3$ cells/cm^2.

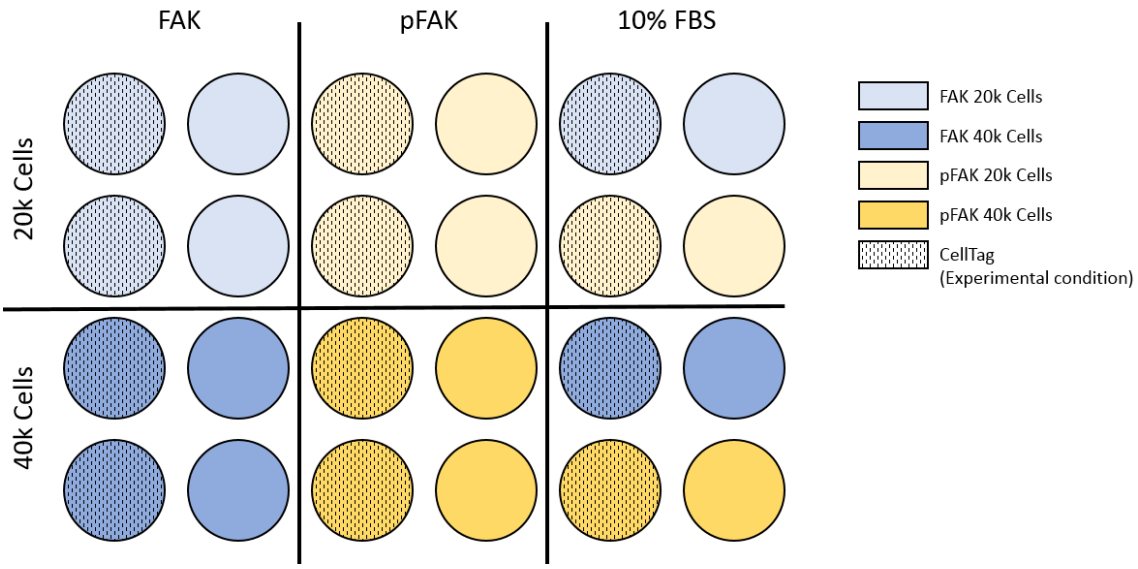

Figure 28: In Cell Western experiment setup. In cell western was carried out in several conditions: lower or higher seeding density ($2x10^4$ and $4x10^4$ cells/cm^2 respectively), incubated with CellTag or the antibody of interest (FAK/pFAK) and with or without 10% FBS.

After fixing, samples were permeabilised using 0.1% Triton X-100 in PBS for 5 minutes and rinsed 3 times with PBS before being blocked with Odyssey® blocking buffer (provided with the kit) for 1.5 h. Anti-FAK and anti-pFAK (Millipore, 06-543 and 05-1140 respectively) were then added to their respective wells (1:100 each in Odyssey® blocking buffer) and incubated with samples for 2.5 h. Samples were then rinsed 5 times with 0.1% DPBS/Tween20 for 5 minutes each and then incubated with the secondary antibodies (IRDye® anti-mouse for FAK and IRDye® anti-rabbit for pFAK, 1:800 in Odyssey® blocking buffer) for 2.5 h. CellTag 700 stain was added to wells with cells in order to normalise values by the amount of cells. Only the secondary antibody was added to control wells in order to calculate the background. Samples were then washed in the same way as previously described and dried for imaging and fluorescent quantification.

3.2.13.2 Western blot

Testing cells with PND-1186

In order to see if PND-1186 would have an effect on their ability to adhere to the surface, cells were pre-treated with the drug before seeding them onto surfaces. DU145 cells were harvested, centrifuged and resuspended in media with no FBS containing 0 nM, 150 nM or 1500 nM of PND-1186. Cells were kept suspended by gentle agitation for 1h at 37ºC. Cells were then seeded in a 24 well plate and left to attach for 2h. Wells were rinsed and the nuclei of cells were stained with NucBlue live staining and cells were observed and images taken with the EVOS epifluorescent microscope in order to see if cells were able to adhere to the surface.

Cell preparation and lysis

Cells were harvested and pre-treated with PND-1186 in the same manner as the test. Suspended cells were incubated with 0, 150 nM or 1500 nM of PND-1186 under agitation at 37ºC for 1h and then seeded onto 32 mm ø round coverslips coated with PEA, PMA, or bare glass at $2x10^4$ cells/cm^2 (in 6-well plates) for 2h at 37ºC. Wells were then rinsed with TBS and cells were lysed on ice and scraped with RIPA buffer containing protease and phosphatase inhibitors. Lysates were collected in protein low binding Eppendorf tubes and stored at -80ºC until ready to use to prevent protein degradation.

Cell lysate protein concentration

Protein concentration of the cell lysate was determined using micro BCA (bicinchoninic acid) assay. Due to the fact that this assay has a detection threshold between 2-40 µg/ml, the lysate was diluted 1:10 and 1:60.

Protein concentration

Cell lysate was thawed on ice and 100 µg of protein for each lysate was placed into Microcon® 30 K protein columns. Tubes were then centrifuged at $1.8x10^4$ rcf for 10 minutes at 4ºC to remove lysis buffer. 25 µl of RIPA buffer was then added to resuspend the protein and the sample was placed in a collection tube to collect the concentration protein and centrifuged at $13x10^3$ rpm for 1 minute at 4ºC. This was done in order to be able to successfully load 10 µg of protein in each gel.

Gel electrophoresis and transfer

Loading buffer (4x Laemmli with 20% β-mercaptoethanol) was added to the concentrated lysate. The sample was then heated at 95ºC for 5 minutes to further denature the protein and then put on ice. The sample was then loaded into a TGX 7.5% precast gel (BioRad 4561024). The gel was run at 70 V for about 2h and then transferred onto a nitrocellulose Western blot membrane for 45 minutes at 25 V.

Antibody incubation

The membrane was then cut in several pieces for the different antibodies and blocked with TBS with 5% BSA for 30 minutes at RT. Membrane pieces were then incubated with anti-FAK, anti-pFAK and α-Tubulin in TBS with 5% BSA overnight at 4ºC.

Samples were then washed 3 short times followed by 3 washes of 5 minutes each with TBS/Tween20 0.1%. Membranes were then incubated with their respective secondary antibodies (1h at RT with 5% BSA in TBS) and then washed in the same manner as the previous step.

Membranes were then dried and ECL was put onto membranes for 5 minutes in the dark. Excess ECL was then removed and placed onto a digital reader in order to visualise the blots.

3.2.13.3 FAK/pFAK staining and fluorescent quantification

Cell culture and fixing

DU145 cells were harvested by trypsinisation and incubated in suspension with agitation for 1h with 0 nM, 150 nM or 1500 nM of PND-1186 at 37°C, 5% CO_2. Cells were then seeded onto PEA, PMA and glass coverslips coated with 20 µg/ml of FN for 3 hours. Media was removed and cells were rinsed with warm PBS before fixing with paraformaldehyde 4% for 20 min at 4°C.

Cell staining and imaging

Coverslips were then permeabilised with 0.5% triton-100X for 5 min and then blocked with 1% BSA for 30 min. Samples were then incubated with anti-FAK produced in rabbit (Millipore, Ref. 06-543) at 1:100 dilution and anti-pFAK produced in mouse (Millipore, Ref. 05-1140) at 1:200 dilution for 1h at RT. Samples were then rinsed twice with 0.5% Tween20 and incubated with goat anti-rabbit Cy3 (Jackson Immuno Research, Ref. 111-165-003, 1:200 dilution), donkey anti-mouse Alexa 488 (Life technologies, Ref. A21202, 1:2000 dilution) and Alexa 660 Phalloidin (Life Technologies, Ref. A22285, 1:200 dilution) secondary antibodies for 1h at RT, protected from light. Samples were then rinsed twice and mounted using Vectashield® with DAPI. Fluorescent images of samples were taken for 20 cells per condition using the ZEISS Z1 inverted auto fluorescent microscope.

Fluorescent intensity measurements

Total fluorescent intensity was measured with ImageJ using a method described by McCloy, R. A. *et al.*[189]. For each image, the contour of the cell was selected and the area, integrated density (product of the area and mean grey value), and mean grey value were measured using the analyse menu. The fluorescent intensity of the background was also measured by averaging at least 3 different areas outside of the cell. From this the corrected total cell fluorescence (CTCF) was calculated using the following formula:

CTCF = Integrated Density – (Area of selected cell x Mean fluorescence of background readings).

pFAK image analysis and quantification (FAAS)

The number, area and size of pFAK aggregates observed were measured using the FA analysis server. This was done due to the fact that although they are not the same, pFAK aggregates had a similar layout to FAs.

3.2.14 Statistical analysis

Two-way ANOVA was used for the comparison of the different groups using a Bonferroni post-test to compare all columns. Data is represented as mean ± SD and the differences between groups were considered significant for $P<0.05$.

3.3 Results

3.3.1 DU145 growth and cytotoxicity

The proliferation of DU145 human prostate cancer cells was measured using MTT and alamarBlue® assays.Growth by measuring absorbance using the MTT assay and fluorescence using alamarBlue® showed similar evolutions for both seeding densities. For the MTT assay, a sigmoidal shaped curve is observed for the lower seeding density of 1500 cells/cm^2 (Figure 29 A) whereas cells seeded at 15000 cells/cm^2 grew quicker at the beginning before stabilising after 3 to 4 days. For the growth using alamarBlue®, cells grow quickly for the first 3 days but grow more slowly up to the 7th day (Figure 29 B).

Growth on polymers with and without FN was observed using alamarBlue®. For the lower seeding density (Figure 29 C), cells do not proliferate on PEA and PMA without FN. If FN is added cells start growing after 4 days and appear to grow much faster on PMA than on PEA.

For the higher seeding density (Figure 29 D), cells seem to grow on PEA and PMA with and without FN. However, there are initially less cells on non-coated surfaces. This can be due to the fact that although the same number of cells were initially seeded, because there is no pre-existing FN some cells detach more easily. Cells grow immediately but at a slower pace than or the lower seeding density possible because of the number of cells and confluence inhibiting growth.

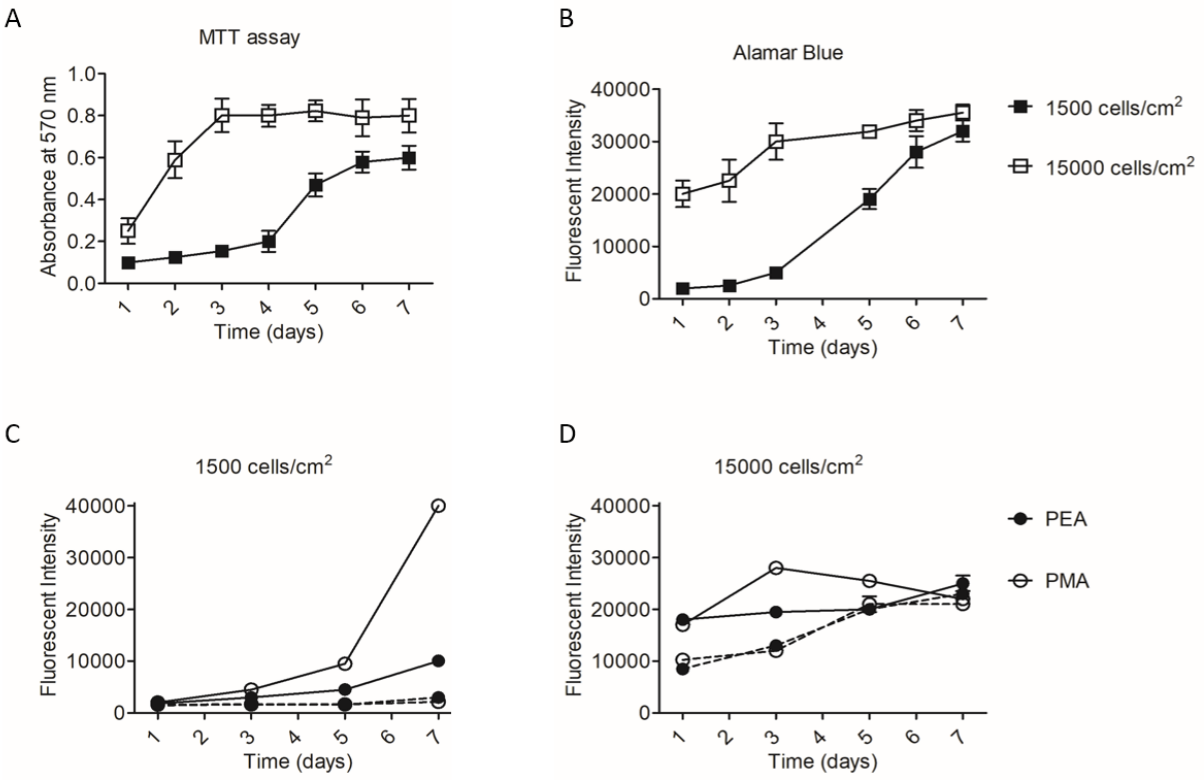

Figure 29: DU145 human prostate cancer growth over 7 days with MTT and alamarBlue® assays. (A) MTT assay on 96-well plate. (B) Alamar blue on 24-well TCP. (C) and (D) AlamarBlue® on PEA and PMA with (straight lines) and without (dotted lines) FN. Error bars for (C) and (D) are hidden in the plot symbols. A total of 3 independent experiments were carried out with triplicates per condition.

Cytotoxic studies were carried out using docetaxel (DOC), a potent chemotherapeutic cytotoxic drug used to bind microtubules and leading to cell death and PND-1186, a cytostatic drug that inhibits FAK currently in phase I of clinical trials (Figure 30).

Cell viability with DOC followed a standard sigmoidal pattern with a maximum percentage of cells alive (100% viability) for lower concentrations of drug and all cells dead (0% viability) for the highest concentrations of drug. The IC_{50}, which is the concentration at which there is 50% cell viability was determined for cells on TCP, as well as FN-coated PEA, PMA and glass coverslips. The IC_{50} of cells on TCP and FN-coated glass were 6.9 nM and 8.06 nM respectively (Figure 30 A), comparable with values described by the Wellcome trust Sanger Institute's genomics of drug sensitivity in cancer project.[190] Cells on PEA and PMA however

presented higher IC_{50} values of 28.6 nM and 20.21 nM respectively, indicating polymer-related resistance independent of FN conformation.

Table 9: Cell viability with docetaxel and PND-1186 on PEA, PMA, glass and TCP.

Drug	Docetaxel				PND-1186
Surface	PEA	PMA	GLASS	TCP	TCP
Max	85%	97%	100%	100%	95%
Min	11%	10%	10%	0%	40%
IC_{50}	28.6 nM	20.21 nM	8.06 nM	6.9 nM	N/A

Cell viability with PND-1186 showed no sigmoidal pattern (*Figure 30 B*) with maximum viability at up to 1 µM and a minimum viability at approximately 40% with 0.5 nM. It has been previously reported that PND-1186 has a cellular IC_{50} of 100-150 nM, determined by anti-phospho-specific immunoblotting to FAK Tyr-397[101, 102] and resulted in restricted movement. Cell apoptosis using this drug has only been reported in non-adherent conditions.

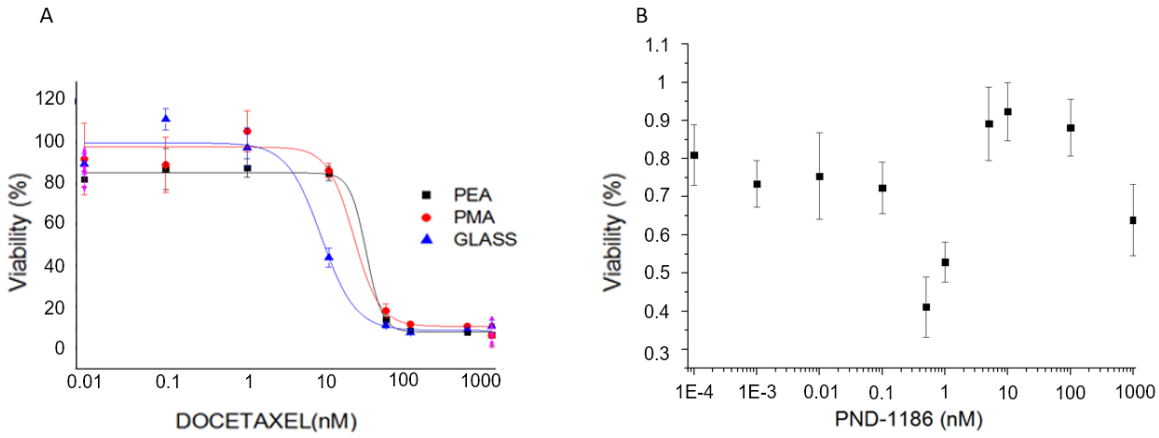

Figure 30: DU145 cytotoxicity assays with (A) Docetaxel (DOC) and (B) PND-1186 (PND). Docetaxel studies were carried out on TCP as well as PEA, PMA and glass coverslips coated with 20 µg/ml of FN. PND-1186 studies were carried out solely on tissue culture plastic.

3.3.2 Cell attachment and focal adhesion formation

Short term cell attachment assays were carried out with DU145 cells on PEA, PMA and glass coverslips coated with FN. This was done in standard conditions and after blocking the RGD domain and PHSRN synergy sequence with HFN7.1 and mAb1937 antibodies respectively.

Polymers coated with FN showed 100% attachment even after washes (Figure 31). When the RGD cell binding domain was blocked with HFN7.1 (H) 7-8% percent of cells remain attached. When the PHSRN synergy sequence was blocked with mAb1937 (m) there was partial inhibition of cell attachment on PEA with no effect on attachment on PMA, highlighting the difference in domain availability of PHSRN on FN adsorbed to PEA and PMA. When both domains were blocked together less than 10% of cells remained attached on both surfaces.

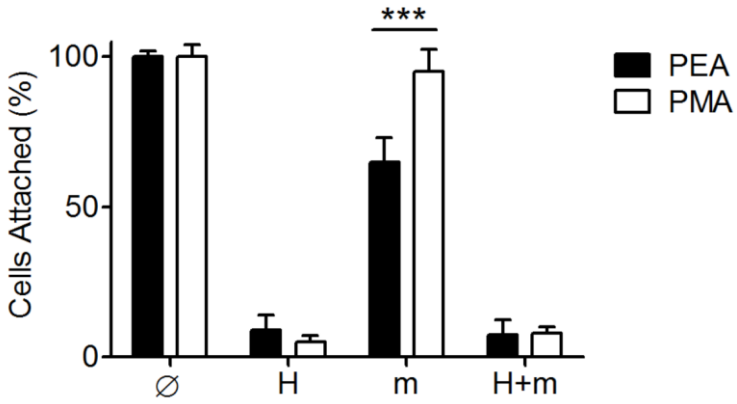

Figure 31: 20-minute attachment assay of DU145 cells on FN-coated PEA and PMA, blocked with HFN7.1 and/or mAb1937 antibodies. DU145 cells were seeded onto PEA and PMA coated with 20 µg/ml of FN after blocking the RGD and PHSRN sequences using HFN7.1 (H) and mAb1937 (m) respectively at a 1:1 FN:antibody molar ratio. N = 3; n = 3, ***p<0.001.

Early adhesion assays of 3 hours were carried out on PEA and PMA with 2, 5, 10 and 20 µg/ml of FN in standard conditions and blocking RGD and/or PHSRN sequences. Cell size and FAs were quantified for all conditions.

Cells were of similar size on both polymers for lower concentrations of FN (~1000 μm^2), however, for 20 µg/ml of FN cells were more spread on PEA compared to PMA with sizes of roughly 1800 μm^2 and 1500 μm^2 respectively (Figure 32 A). Although FAs were the same size in all conditions (Figure 32 C), there were more of them on PEA than on PMA with 2 and 20 µg/ml of FN (Figure 32 B). This resulted in significantly higher moment of inertia on PEA with those concentrations of FN.

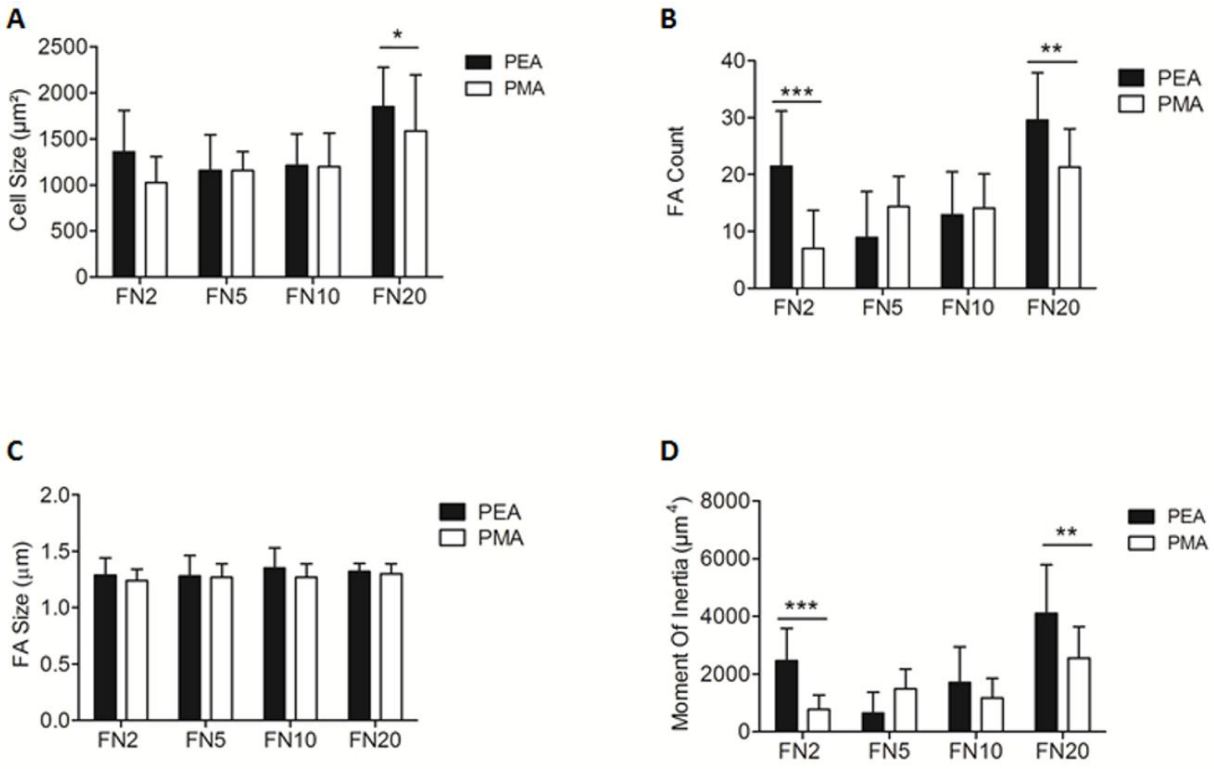

Figure 32: Cell spread and FA analysis of cell on PEA and PMA coated with 2, 5, 10 and 20 µg/ml of FN (denoted FN2, FN5, FN 10 and FN20 respectively) for 3 hours. (A) Cell size. (B) FA count. (C) FA size. (D) Moment of Inertia. n = 30, *p<0.05, **p<0.01, ***p<0.001.

A detailed analysis of FA size distributions (Figure 33) on polymers with different concentrations of FN revealed that although there was a higher proportion of small FAs of 1 µm on PMA, no differences in overall size was observed.

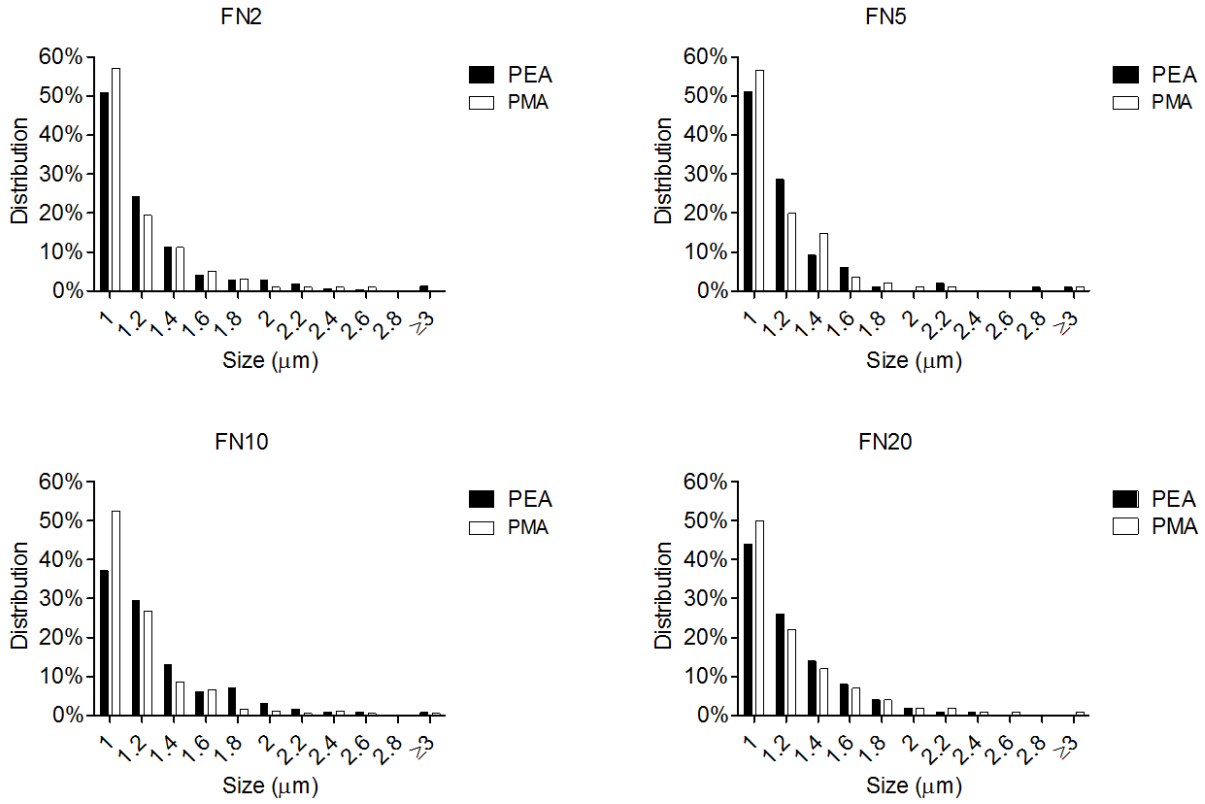

Figure 33: FA size distribution on PEA and PMA coated with 2, 5, 10 and 20 µg/ml of FN (denoted FN2, FN5, FN 10 and FN20 respectively). Size distribution of FAs were assessed on FAs equal to or larger than 1 µm in length and were binned at every 0.2 µm interval up until 3 µm. N=10.

The RGD cell binding domain and PHSRN synergy sequences were blocked on samples coated with 20 µg/ml of FN (Figure 34). In standard conditions with no blocking, cells were well spread on all surfaces with actin stress fibres and vinculin well defined.

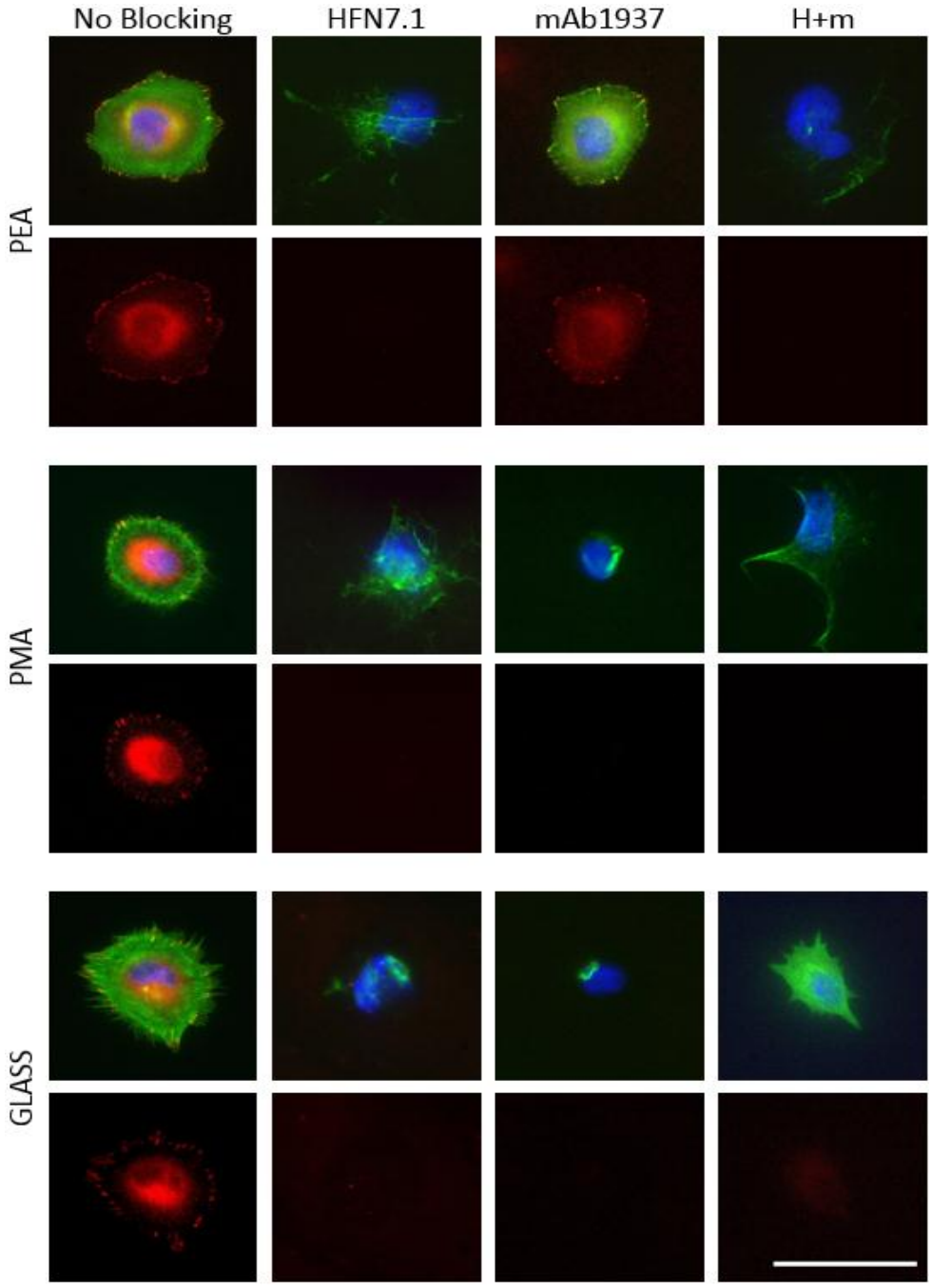

Figure 34: Representative images of DU145 cells on PEA, PMA and glass coated with 20 µg/ml of FN after 3-hour early adhesion with HFN7.1 (H) and/or mAb1937 (m) antibodies. Composite images (above) and their respective vinculin images (below) are shown. Cells on surfaces that weren't blocked were well spread with prominent FAs. Blocking the RGD domain and/or the PHSRN synergy sequence with HFN7.1 and mAb1937 respectively led to cells with poorly defined cytoskeleton structures and lack of FA formation. This is with the exception of cells on the fibrillar FN on PEA where cells were spread with well-defined FAs even when the synergy sequence is blocked. Scale bar: 50 µm

When the RGD cell binding domain was blocked with HFN7.1, no FAs formed and although the cells were spread the actin cytoskeleton appeared very disorganised with no visible stress fibres. When the PHSRN synergy sequence was blocked with mAb1937, cells on PEA behaved normally with cells spread out and a normal FA distribution. This is opposed to cells on PMA and glass where there were no FAs and cells were rounded. When both sequences were blocked cells were spread out on all surfaces with no FAs.

The difference observed when blocking the synergy sequence is in some way linked to the differences in conformation of FN and availability of this sequence on PEA and PMA. Due to the fact that the PHSRN sequence of FN is less exposed on FN-coated PMA compared to PEA (Figure 19 B) we can hypothesise that when this sequence is blocked using mAb1937, the antibody can more easily block the fewer synergy sites presented on PMA as opposed to the higher amount of available PHSRN sequences present on FN-coated PEA.

3.3.3 Cell migration

Cells were seeded onto polymers coated with 20 µg/ml FN and incubated with PND-1186, a cytostatic drug, at different concentrations: the cellular IC50 (~150 nM) and an excessive amount (1500 nM). Cells were then imaged and gap closure was measured (Figure 35, Figure 36).

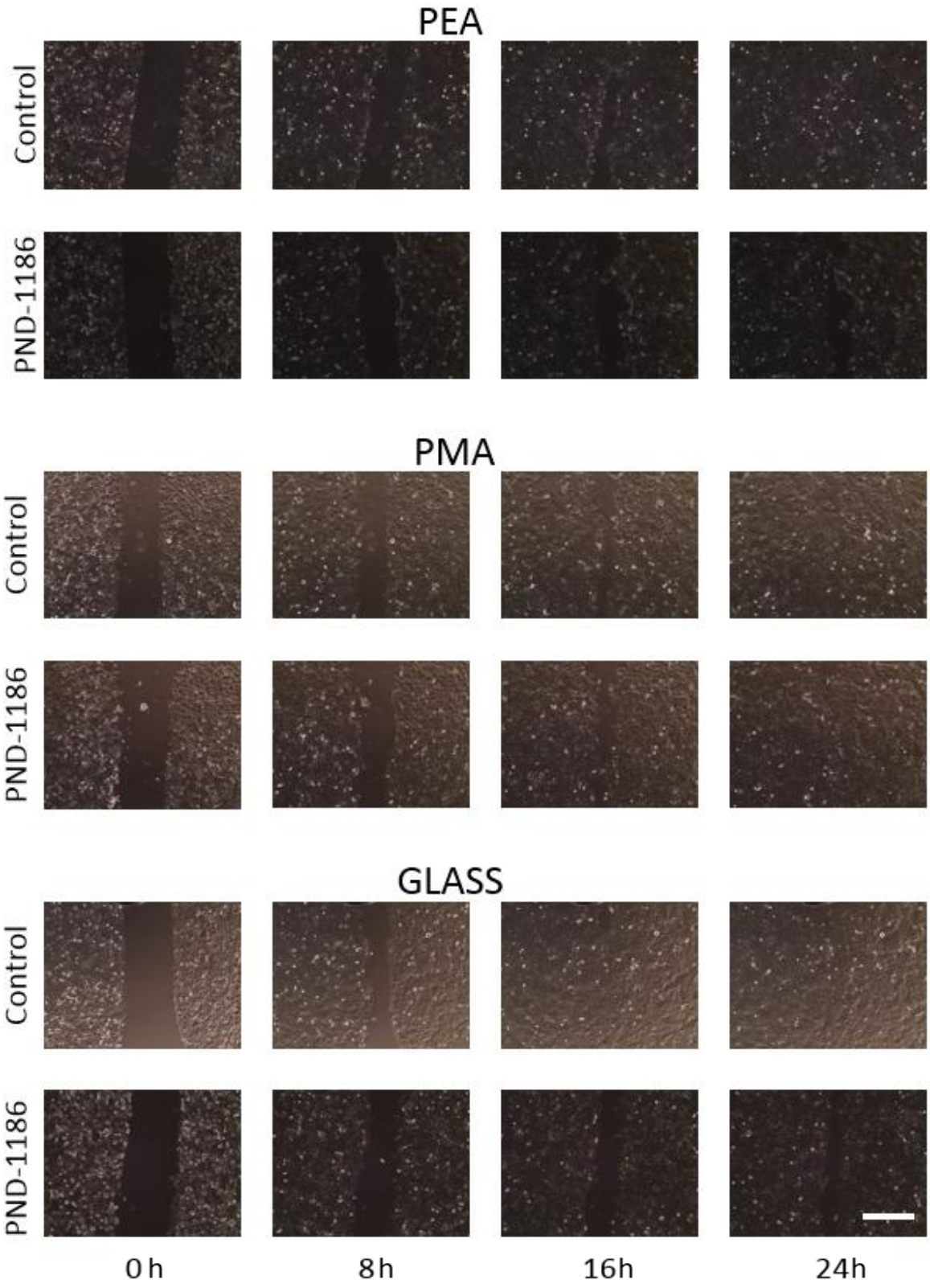

Figure 35: Wound healing assay time-lapse representative images at 0, 8, 16 and 24 hours with 150 nM and without PND-1186. In normal conditions without PND-1186, cells were able to close the 500 µm gap within 16-24 hours. Adding the drug at a concentration close to its cellular IC_{50} led to cells migrating slower, not closing the gap in many cases after 24 hours. Scale bar: 500 µm.

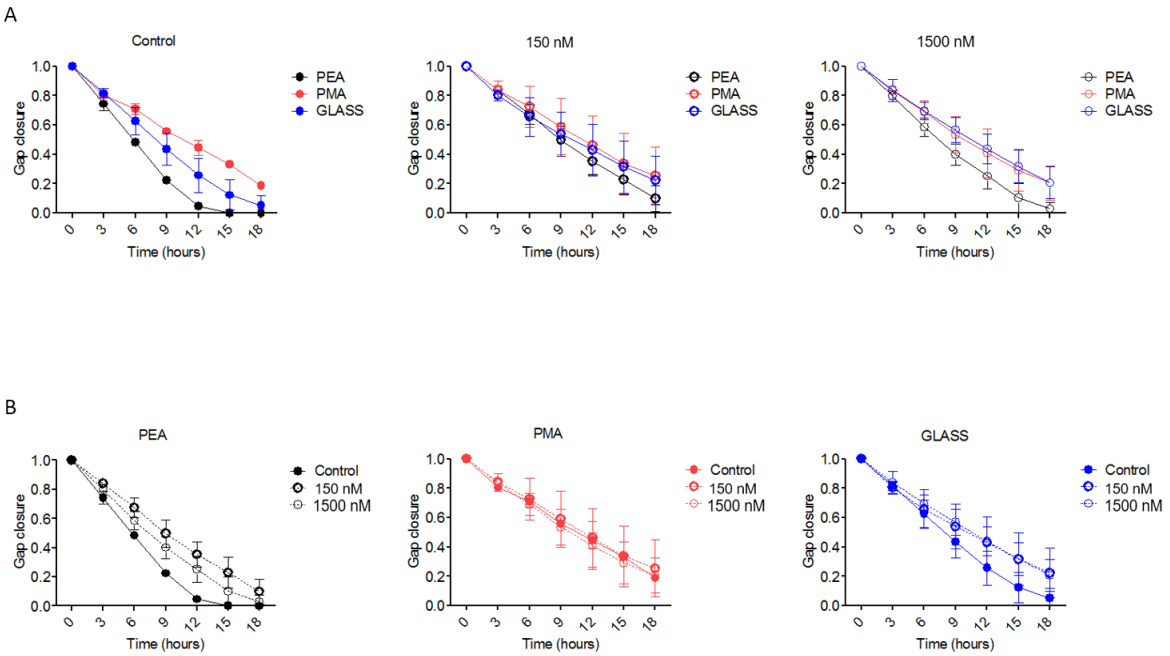

Figure 36: Wound healing assay gap closure analysis of cells on PEA, PMA and glass in standard conditions and with 150 and 1500 nM of PND-1186 over the course of 18 hours. (A) Comparison of polymers per concentration. (B) Comparison of concentrations per polymer. The area of the gaps was measured to determine gap closure. n = 12.

In standard conditions with no drug, cells close the 500 µm gap within 15 hours on PEA whereas only 80% of the gap was closed on PMA surfaces after 18 hours. Cells could close the gap on glass after 18 hours. A noticeable decrease in cell migration was observed when incubated with PND-1186, notably on PEA and glass whereas the effect was minimal on PMA. Cells migrate faster on PEA compared to other surfaces in normal conditions as well as in the presence of a cytostatic drug, highlighting the importance of FN conformation and domain availability in cell migration. This allows to infer that fibrillary FN, as it is found in the ECM enhances cell migration.

3.3.4 Cell traction force microscopy – finite element analysis

3.3.4.1 Traditional CTFM

A total of 3 independent experiments were carried out, looking at 15-20 cells per condition for each experiment. The following results are the combined results of these experiments (Figure 37).

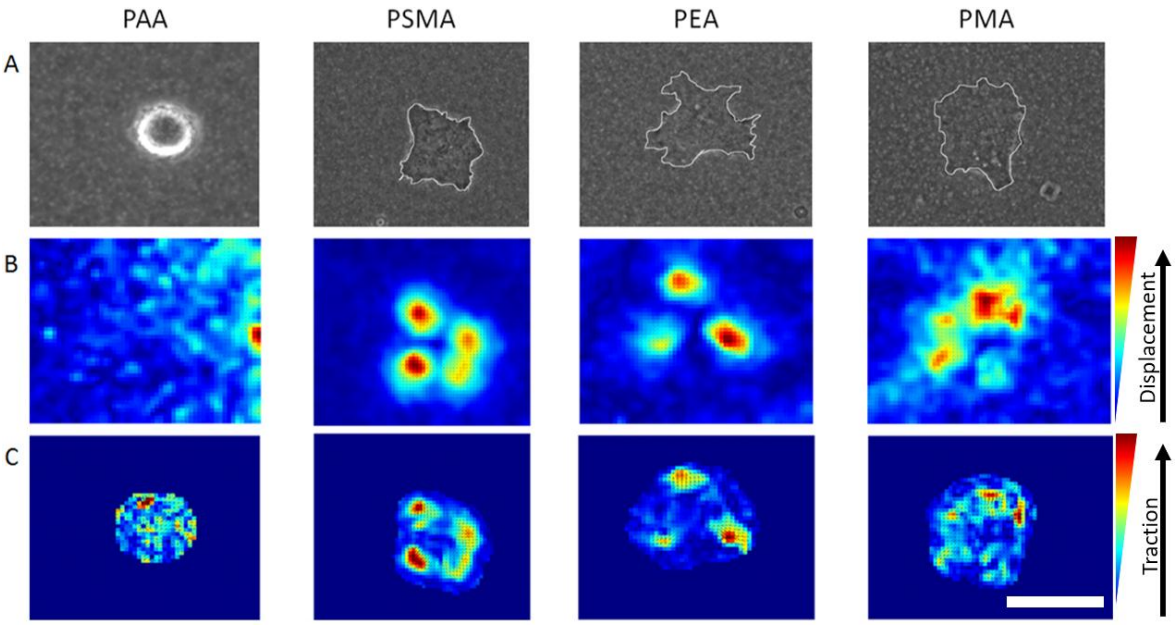

Figure 37: Representative images of CTFM analysis on different surfaces. (A) DU145 cells on PAA, PSMA, PEA and PMA with an outline delimiting the cell contour. (B) Displacement field: highlighting the movement of the microbeads. (C) Traction field: obtained by equating the displacement of the beads to the stress exerted by cells on the substrates. Displacement and traction field scales are arbitrary from low displacement/traction (dark blue) to high displacement/traction (dark red). Scale bar: 50 µm.

In the case of the displacement and tractions fields, it is important to note that colour intensity scales are different for each cell. What is also immediately noticeable is the fact that cells on PAA alone are rounded indicating that FN does not adsorb to PAA alone therefore preventing cells from adhering properly.

The CTFM results are from 3 independent experiments analysing a total of 30-45 cells per condition (Figure 38). Large error bars are due to high variability between cells.

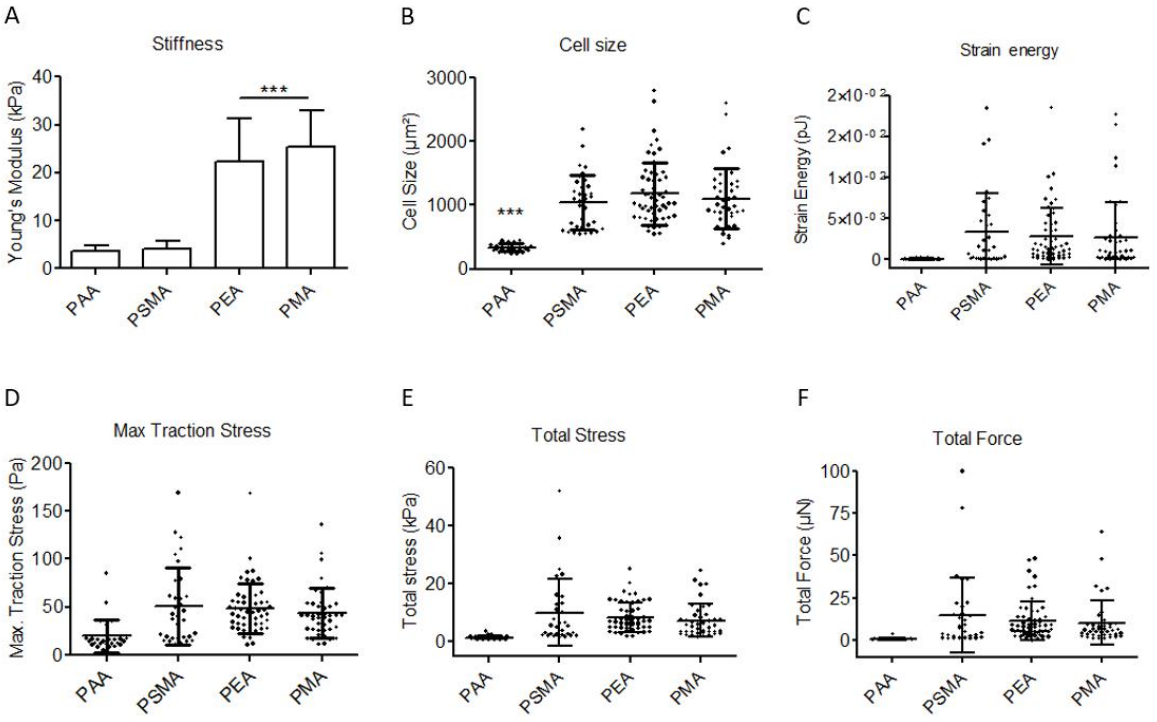

Figure 38: Characterisation of PAA hydrogels coated with PSMA, PEA and PMA polymers and CTFM analysis using MATLAB script of DU145 cells seeded onto PAA alone or PAA coated with PSMA, PEA or PMA for 3 h. (A) Force spectroscopy measurements of PAA alone, and PAA coated with PSMA, PEA or PMA. (B) DU145 cell size after 3 hours adhesion on each substrate coated with 20 µg/ml FN. (C) Strain energy which is the energy stored in the gels undergoing deformation. (D) Maximum and (E) total traction stress which is the stress on the surface exerted by the cell. (F) Total force (product of stress and surface area). Traction stresses were directly proportional to the stiffness values measured by force spectroscopy, bringing into question the methods used to assess stiffness of the hydrogel-polymer system. N = 3; n = 15, ***p<0.001.

In order to determine the forces cells were exerting on each system, the stiffness of substrates was measured by force spectroscopy. PAA substrates had a stiffness of 3.5 kPa which was similar to PSMA coated PAA (4 kPa). This confirms that PSMA coating has no significant effect on the stiffness of the hydrogel, most likely due to the fact that the PSMA coating is very thin (10-20 nm). Upon measuring PEA and PMA coated hydrogels, a 6 to 7-fold increase in stiffness is observed (22 and 25 kPa

respectively). Just as with PSMA, this is in large part due to the polymer thickness (100 nm for PEA and 70 nm for PMA). This difference in stiffness is then taken into account in measuring the mechanical properties of the system such as strain energy, traction stress and force.

Cell size on polymer coated PAA is similar (around 1000 µm²) whereas cells are significantly smaller on PAA alone (around 400 µm²) indicating that cells do not attach or spread very well on the bare hydrogel.

Strain energy is inexistent on PAA but is similar on polymer coated PAA with an increase in strain energy from PSMA to PMA. This value varies most between cells which causes high error bars.

Values of the maximum traction stress, total stress and total force are similar between PAA and PSMA whereas a significant increase for these values is observed for PEA and PMA. These results directly reflect the differences in surface stiffness.

3.3.4.2 Finite element modelling CTFM

FEM-CTFM was done in order to have a more correct depiction of force transmission within the polymer-hydrogel bi-layered system.

A total of 10 cells per condition (PSMA, PEA and PMA) were used as representatives in order to compare results obtained through standard CTFM and finite element analysis. Maximum stress and total force were calculated (Figure 39).

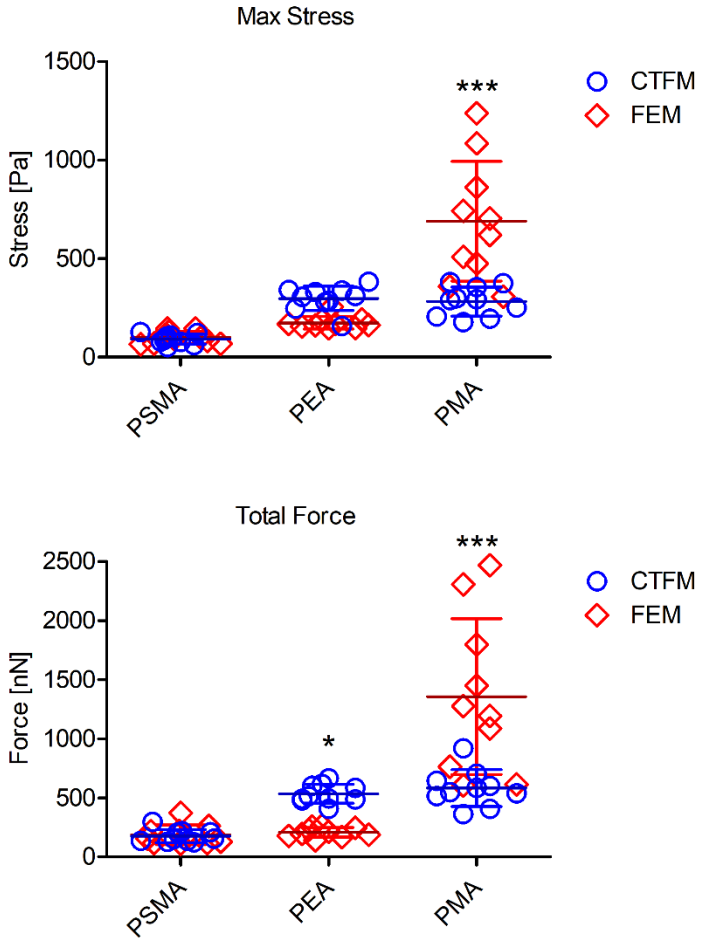

Figure 39: Maximum stress (top) and total force (bottom) of cells on PSMA, PEA, and, PMA determined by standard CTFM and finite element modelling. n = 10, *p<0.05, ***p<0.001.

Cells on PSMA-coated polyacrylamide exerted very little stress on the surface. Both analysis methods have similar values with a maximum stress of 90 – 100 Pa and total force of 175 – 185 nN. The layer of PSMA was very thin (~10-20 nm) and therefore is considered negligible. Furthermore, the stiffness (~4 kPa) was very close to bare PAA (~3.5 kPa) while still allowing FN and therefore cell binding.

The maximum stress of cells on PEA-coated PAA was measured to be ~300 Pa with standard CTFM using a MATLAB script compared to ~175 Pa obtained by finite element modelling. Discrepancies between CTFM and FEM were also observed in total force with ~535 nN and ~210 nN respectively.

Similarly to cells on PEA, differences were observed between CTFM and FEM methods for PMA, with high variability using the latter. The maximum stress was recorded at ~280 Pa by CTFM and ~790 Pa by FEM whereas the total force was recorded at ~580 nN by CTFM and ~1350 nN by FEM.

The differences between both methods are especially pronounced in cells on PEA and PMA coated polyacrylamide.

3.3.5 Expression of FAK and pFAK

3.3.5.1 In-cell western

The following Figure 40 and Figure 41 show the results of the in-cell western.

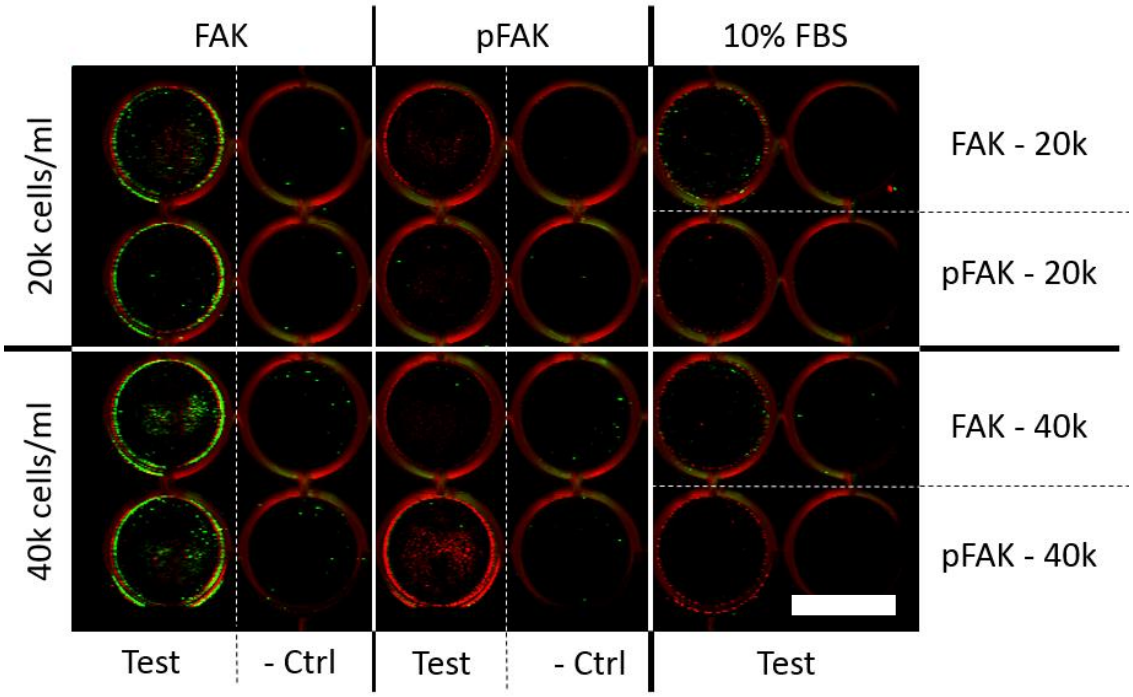

Figure 40: Merged image of fluorescent scanning of plate stained with FAK/pFAK antibodies (green) and CellTag 700 (red). FAK was detected at high (40k - 40.10^3 cells/ml) and low (20k - 20.10^3 cell/ml seeding densities with the appearance of a ring of cells at the edges due to pipetting errors. pFAK was not detected in this instance highlighting the inefficacy of this method (or the antibody) for detecting pFAK expression. Scale bar: 15 mm.

The wells stained with anti-FAK have a high fluorescent signal whereas wells stained with anti-pFAK have very little green signal compared to the CellTag total

cell staining. The traces of pFAK staining are similar to the background noise observed in the negative control which indicates that the pFAK antibody was not effective in staining. This in reinforced by the fact that in the positive control wells with 10% FBS where it is expected to have a higher expression of FAK/pFAK there is no sign of pFAK staining.

It is also worth noting that there is a 'coffee ring' effect on the edges of the wells where a lot of cells are aggregated. This is due to the way in which cells were seeded in the wells by pipetting quickly in the centre of the well resulting in most cells going to the edges.

The fluorescent intensities of this image were also analysed. Values were obtained by subtracting the background noise of each condition from the values.

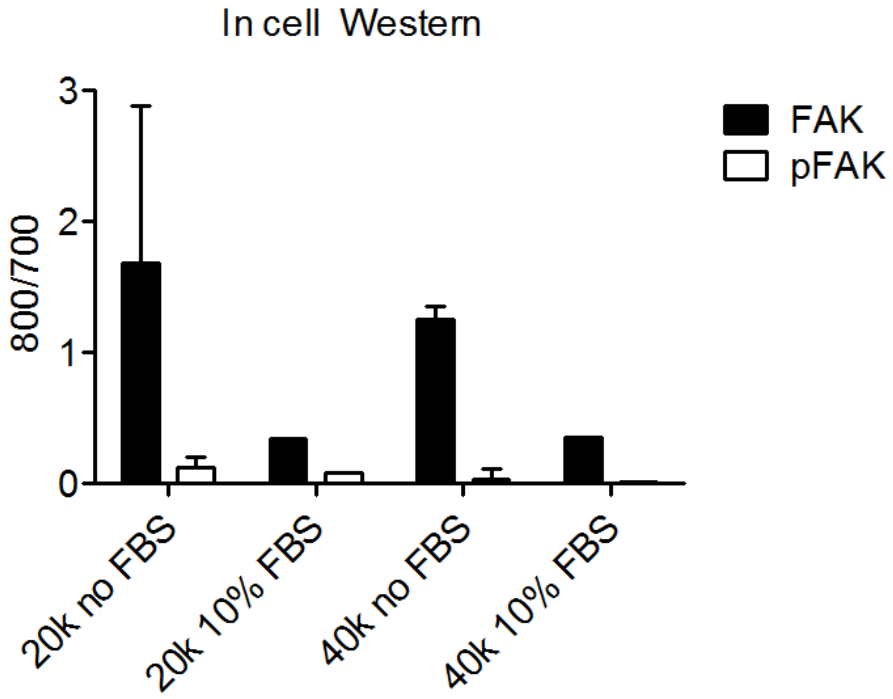

Figure 41: Fluorescent intensities of FAK and pFAK in DU145 cells (800) normalised by total cell amount (CellTag 700) after seeding 2.10^4 (20k) and 4.10^4 (40k) cells/cm^2 with and without 10% FBS for 2 h. FAK is detectable in all conditions whereas pFAK in not detected even in the optimal conditions (high seeding density of 4.10^4 cells/cm^2 with 10% FBS) highlighting the inefficacy of this method and/or the questionable quality of the pFAK antibody.

These results show that FAK can be detected using this system with both seeding densities. Interestingly, there appears to be a decrease in FAK expression when cells are seeded with 10% FBS. Furthermore, pFAK does not seem to be detected in any conditions, as the little amount of fluorescence is most likely due to background noise by unspecific binding of the secondary antibody.

The in-cell western method does not appear to be sensitive enough to detect the small quantities of pFAK expressed by the cells. Ultimately, this method is not effective for detecting the phosphorylation of FAK in cells due to the lack of sensitivity of the system or the quality of the antibody used.

3.3.5.2 Western blot

Western blot was also used in order to quantify FAK/pFAK expression in DU145 cells that were incubated with 150 nM and 1500 nM of PND-1186. Cells were first harvested, and the protein concentration was measured by micro BCA in order to load the same amount of protein in each well (Figure 42).

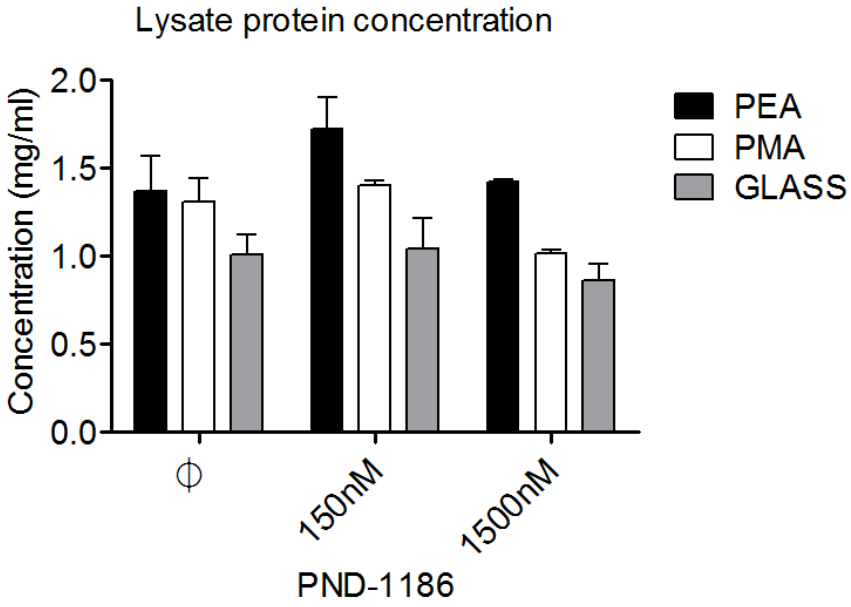

Figure 42: Lysate protein concentration of cells seeded onto PEA, PMA and glass coated with 20 µg/ml of FN after PND-1186 treatment.

The protein concentration of cell lysates for each condition was measured. Concentrations were between 0.8-1.7 mg/ml, which was enough to load gels without the need to use protein columns for concentration. These lysates allow loading of 10 µg of protein in wells using a small volume (5-10 µl of lysate).

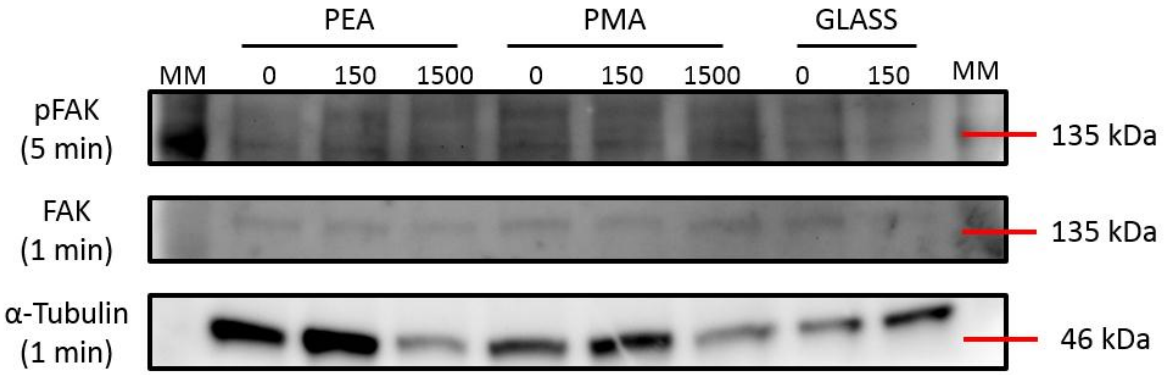

Figure 43: Expression of pFAK, FAK and α-Tubulin in DU145 on PEA, PMA and glass after treatment with PND-1186. pFAK and FAK bands are very weak with the appearance of double bands in the case of pFAK whereas α-tubulin bands are clear but don't show consistent amounts of protein. These results can therefore not be used to assess FAK/pFAK expression.

Bands were visible for each protein (pFAK, FAK, α-Tubulin). Although they are very clear for α-tubulin, there appears to be more background for FAK and pFAK. In the case of pFAK there appears to be double bands which was not due to protein degradation seeing as tubulin bands are intact.

Several attempts were made to quantify FAK/pFAK expression using this technique but to no avail. Cells were therefore stained in order to quantify fluorescent intensity.

3.3.5.3 Immunofluorescent quantification

The following images (Figure 44) represent cells on PEA, PMA and glass coated with FN after incubation with PND-1186.

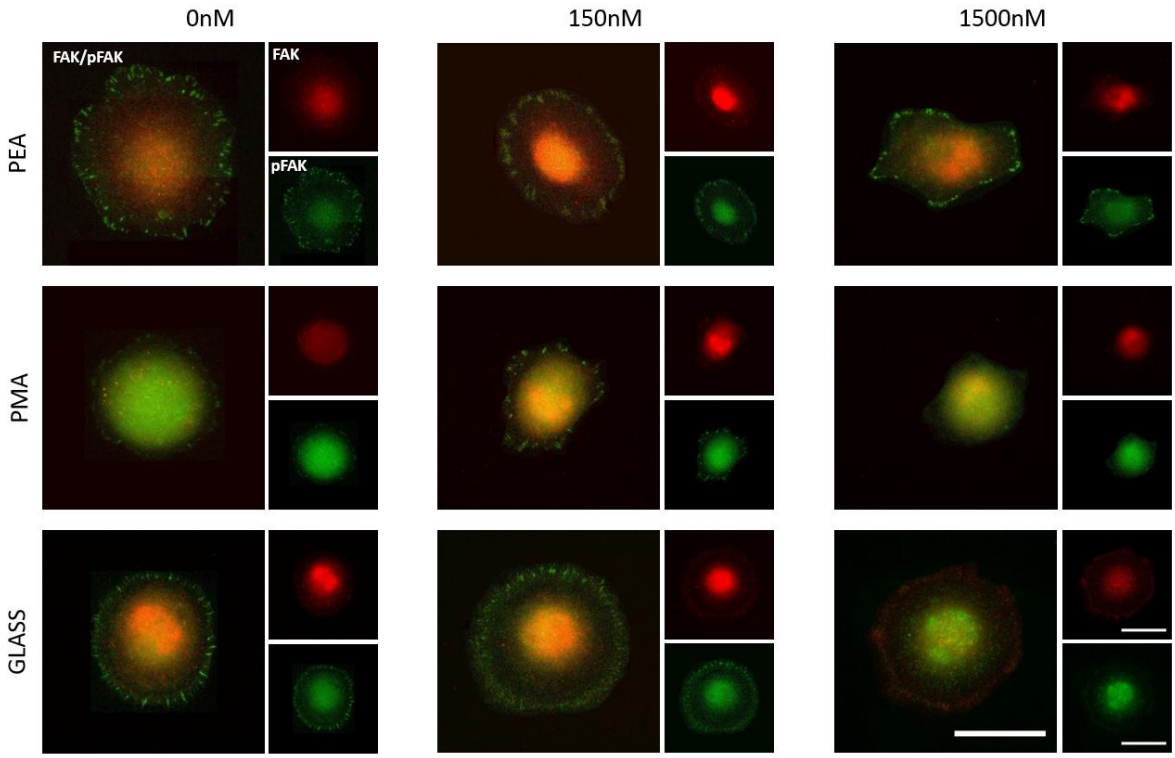

Figure 44: FAK and pFAK staining of DU145 cells on FN coated PEA, PMA and glass after a 1h incubation with 0 nM, 150 nM and 1500 nM PND-1189. pFAK appears to be at the edge of the cell where FAs are expected to be whereas FAK staining only appears within the cytoplasm with no distinct organisation. This might indicate that the FAK antibody has not been effective. Scale bar: 50 µm.

With no drug, cells appear to be well spread on all surfaces with pFAK organised in a similar fashion to FAs. Interestingly, there appears to be no co-localisation between FAK and pFAK (Figure 44) suggesting that the FAK antibody might not have been effective.

With increasing amounts of PND-1186, cells on PEA and PMA appear smaller with less organised pFAK especially in the case of cells on PMA. A similar effect can be observed on glass although the size appears to be more consistent.

The organised pFAK was measured (using only 5 cells per condition) along with the cell size (20 cells per condition).

It has already been established that in normal conditions with no drugs, cells are larger on PEA compared to PMA and the same is observed in this instance. Furthermore, cell size decreases significantly in the presence of PND-1186 on both

polymers (Figure 45 A). This is observed with cells on PEA and PMA between 0 nM and 150 nM and 150 nM and 1500 nM of PND-1186 respectively. A similar trend is observed with cells on glass.

Moreover, the amount of organised pFAK is higher in cells on PEA compared to PMA in normal conditions (Figure 45 B). This reinforces previous results which showed that there are more FAs in cells on PEA compared to PMA. In the presence of PND-1186, the amount of pFAK decreases significantly on PEA as opposed to PMA where the amount of pFAK remains consistently low. At the highest concentration of drug, no pFAK aggregates were measured on PMA. Although not significant, a similar trend of decrease in pFAK was observed in cells on glass.

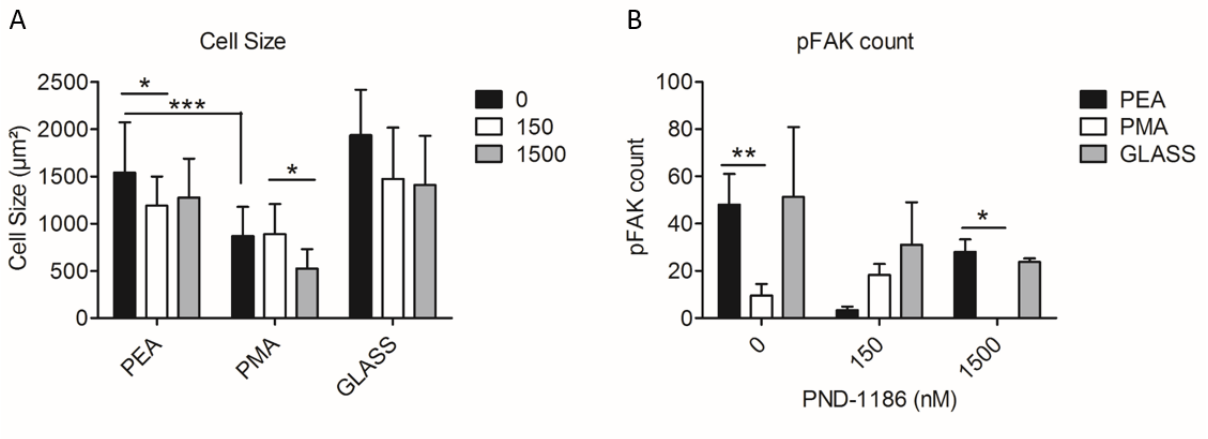

Figure 45: (A) Cell size and (B) organised pFAK count of cells on PEA, PMA and glass with 0 nM, 150 nM and 1500 nM of PND-1186. pFAK count was determined using the FAAS. N = 20 for cell size, N = 5 for organised pFAK count. * $P < 0.1$, ** $P < 0.01$, *** $P < 0.001$.

The size and area of organised pFAK was measured with the same tool used for FA analysis in order to see if there were any relation between the concentration of PND-1886 and the expression and organisation pFAK in cells on PEA and PMA (Figure 46).

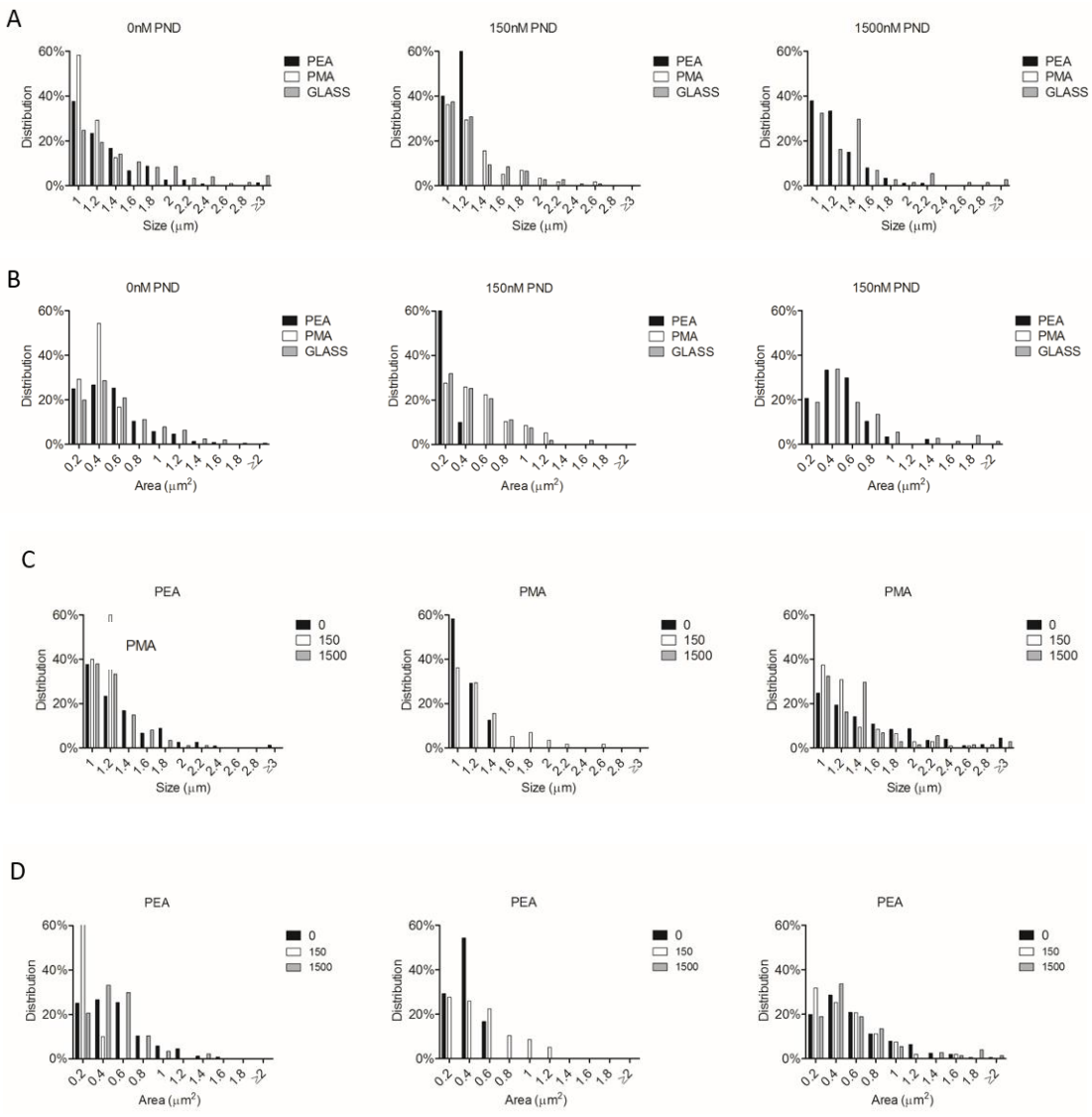

Figure 46: Size and area distribution of pFAK. (A)(B) Comparing PEA, PMA and glass (size and area respectively). (C)(D) Comparing PND-1186 concentration (size and area respectively). N = 5.

PEA has larger organised pFAK aggregates compared to PMA with no drug, however this does not appear to be the case with 150 nM of drug. With 1500 nM of PND-1186, organised pFAK is not present.

Fluorescent intensity of FAK and pFAK was also quantified using ImageJ. The following Figure 47 represents corrected total cell fluorescence of FAK and pFAK.

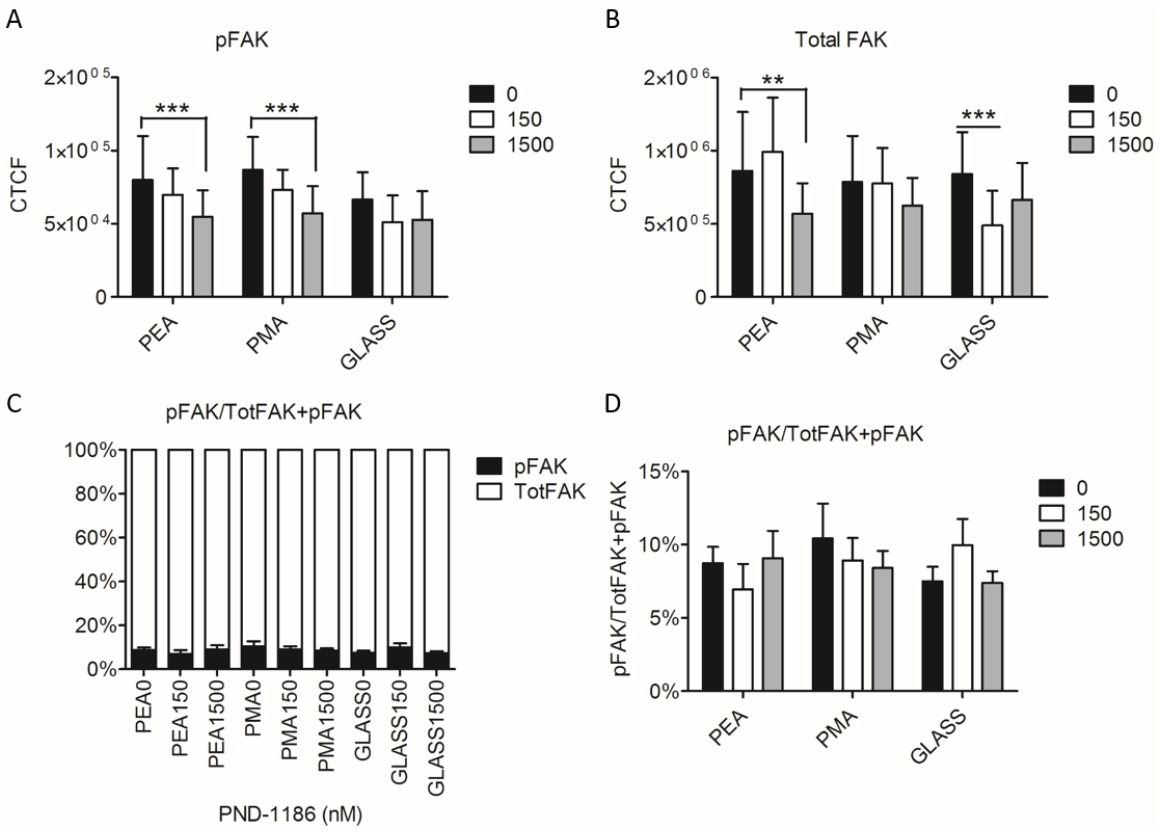

Figure 47: Corrected total cell fluorescence of cells on PEA, PMA and glass with 0 nM, 150 nM and 1500 nM of PND-1186. (A) pFAK fluorescent intensity. (B) Total FAK fluorescent intensity. (C)(D) Ratio of pFAK to total FAK. Total cell fluorescence only took into account FA-like structures. n = 20. ** $P < 0.01$, *** $P < 0.001$.

In cells on both PEA and PMA, there is a significant decrease in pFAK fluorescent intensity with increasing concentrations of PND-1186. There are no significant differences between polymers. In the case of total FAK, there is a decrease in cells on PEA between 0 nM and 1500 nM of drug. Although a similar trend is observed in cells on PMA, it is not significant. In comparing the ratio of pFAK to total FAK no noticeable differences were observed. The proportion of pFAK to total FAK remained constant at 7-10% in all conditions.

Fluorescent intensity measurements do no reveal differences between PEA and PMA in terms of the amount of pFAK compared to total FAK. However, pFAK is organised much differently on PEA with more structures resembling FAs, even with higher concentrations of drug compared to PMA.

3.4 Discussion

3.4.1 FN conformation and cell behaviour

Material-induced FN conformation has previously been shown to affect cell behaviour such as cell size and FA assembly in L929 fibroblasts[5]. Similar effects are seen in DU145 with cells being more spread and having a larger FA count on PEA leading to higher moment of inertia value (Figure 32).

Upon blocking the $FNIII_9$ and $FNIII_{10}$ domains of FN with mAb1937 and HFN7.1 monoclonal antibodies, clear differences could be seen in short term cell attachment (Figure 31) and FA formation *(*Figure 34). The RGD cell binding domain is essential for cell binding and the formation of FAs whereas blocking the PHSRN synergy sequence with mAb1937 did not drastically affect cell attachment. With mAb1937 blocking alone, ~100% of cells on FN-coated PMA remained attached after rinsing with PBS compared to ~60% of cells on PEA. As previously demonstrated in chapter 2, the fibrillar conformation of FN allows for more exposure of the PHSRN synergy sequence on PEA compared to PMA. However, cells adhere equally to both surfaces when coated with FN. It is therefore feasible that, depending on the conformation of FN, DU145 cells adhere using different integrins for binding to FN. Knowing that $\alpha_5\beta_1$ and $\alpha_v\beta_3$ integrins are required to bind to RGD whereas only $\alpha_v\beta_3$ is required to bind PHSRN[50, 158], cells on PMA attach to FN preferentially via RGD sequence via $\alpha_v\beta_3$ therefore blocking mAb1937 has no effect on attachment. Cells on PEA however, attach via $\alpha_5\beta_1$ which requires both the RGD cell binding domain and the PHSRN synergy sequence. This theory is confirmed by the partial decrease in cell binding once the synergy sequence is blocked with mAb1937.

Furthermore, upon blocking RGD alone or in conjunction with PHSRN cells appeared to be more rounded with no visible FA formation (Figure 34). Nevertheless, when the synergy sequence alone is blocked, cells on PEA are able to spread and form FAs as opposed to cells on PMA and glass. Because FN has an extended fibrillar conformation on PEA, more domains for cell binding and FAs are available allowing cells to attach even when the synergy sequence is blocked[5].

Similar results were also seen with L929 fibroblasts (Figure 23 A) with cells not being able to attach when the RGD domain was blocked however, when the synergy sequence is blocked, fibroblasts attach partially to PEA and not fully as seen with

prostate cancer cells (Figure 31). Moreover, the same effect on cell attachment isn't observed when both domains are blocked with cancer cells not being able to attach whereas fibroblasts were able to partially attach to PEA. It is known that cell phenotype has an effect on integrin expression[57] with cancerous cells selectively secreting specific integrins involved in cell binding[53]. These discrepancies are most likely due to the expression of integrins in these two cell types with one cell type being healthy mouse fibroblast and the other being human metastatic epithelial cells.

At first glance, these findings using DU145 human prostate cancer cells appear to contradict Livant *et al.* who reported that the synergy sequence alone was needed for DU145 invasion[49]. However, in the aforementioned study cell motility was investigated whereas studies performed in this instance are for static cell properties such as attachment and adhesion. Many studies have looked into the effect of the PHSRN sequence on cell motility[191] as well as the effect of RGD on cell anchorage and inhibiting migration[192, 193]. A study carried out by Overstreet *et al*. showed that cell motility was impaired in WT15 T cells when β_1 was blocked, therefore blocking activity of $\alpha_5\beta_1$ which binds to both RGD and PHSRN sequences. Blocking β_3 which inactivates $\alpha_v\beta_3$ that binds RGD alone did not show as much of an effect on motility[191].

The hypothesis therefore suggesting being that the RGD domain is necessary for cell stability and anchorage whereas the PHSRN synergy sequence in vital for cell motility such as migration and invasion.

3.4.2 Cytotoxic studies and material-induced drug resistance

On glass and tissue culture plastic, DOC had an IC_{50} of 8.06 nM and 6.9 nM (Figure 30A) which were within the same order of magnitude of what has been previously reported for DU145 cells[190]. The IC_{50} of cells on PEA and PMA coated with FN was higher, at 28.6 nM and 20.21 nM respectively implying a form of material-induced drug resistance. This could possibly be due to the physico-chemical nature of the polymers. As with most drugs, docetaxel is partially insoluble in aqueous solutions and needs to first be dissolved in an organic solvent such as DMSO. The hydrophobic drug could potentially interact preferentially with the hydrophobic polymers instead of remaining in solution, therefore limiting its effectiveness.

PND-1186 is powerful FAK inhibitor with a cellular IC_{50} of ~100 nM. This was determined in breast carcinoma cells by anti-phospho-specific immunoblotting in a study by Tanjoni *et al.*[101]. Cytotoxicity studies were carried out here on tissue culture plastic with no apparent effect on cell viability at up to 10 times the reported IC_{50}. Moreover, although FAK is inhibited, this did not affect cellular adhesion which has also been previously reported by Tanjoni *et al.*

PND-1186 could therefore be considered as a cytostatic drug inhibiting migration and tumour progression and not cytotoxic[102].

3.4.3 Migration and traction forces

3.4.3.1 Cell migration

Wound healing assay (or scratch test) is a standard experiment used to assess cell motility[194-196]. It is a particularly useful screening method for the development of therapies and treatment of highly mobile cancerous cells. Without drugs, DU145 cells migrate significantly faster on PEA than on PMA (Figure 36), closing the gap within 15 hours whereas the 500 µm gap remains open after 18 hours on PMA. Both surfaces are sensed as “stiff” by the cell with Young’s moduli of ~400 kPa and ~800 kPa on PEA and PMA respectively (Table 8) which are well over physiologically ‘soft’ tissue (1 – 20 kPa)[12]. The difference in motility appears to be entirely due to the conformation of FN on the surface. FAs were shown to have comparable sizes with a larger number of FAs on PEA compared to PMA (Figure 32B and C). The increased availability of integrin binding sites of stretched out FN leads to the formation of more FAs. Although these serve as anchorage points for the cell they are equally as important in cell motility, notably in cancer cell migration and invasion[197-199]. This suggests that a larger number of FAs on PEA are due to higher activity (formation and disassociation of FAs) and therefore more mobile cells. Therefore FAs aid cell migration in the case of high turnover of FA association and disassociation and slow down migration with low turnover thus anchoring the cell.

FAK plays a commanding role in cell motility[62]. Therapeutic agents aimed at inhibiting this enzyme are therefore becoming more and more popular[104, 200, 201]. PND-1186 has previously been shown to reduce the motility of 4T1 breast cancer cells with 60% of inhibition at 400 nM while unaffecting cell binding to FN[101]. With

increasing amounts of PND-1186 (150 nM and 1500 nM) a decrease in cell motility was observed on PEA with cells not managing to close the gap after 18 hours with 1500 nM of drug. This effect was not seen in cells on PMA where the gap closure was unchanged. This can be explained due to the lack of pFAK organisation in cells on PMA (Figure 44) making it less sensitive to the effects of a FAK-inhibiting drug.

3.4.3.2 Traction forces

Traction forces were initially measured using standard CTFM. These results indicated that the stiffness used for the model play a determining role in the results obtained. Stress and force values proportionally reflect the stiffness measured by force spectroscopy. However, this raises the question as to the aptness of using force spectroscopy to measure the stiffness of the bi-layered system.

Polymer layers are sufficiently thin to allow the transfer of forces from the surface to the underlying hydrogel as seen by the bead displacement located in the PAA (Figure 37). However, it remains unclear if the stiffness measured on the surface of the polymer coated hydrogels are the correct values to use.

AFM nanoindentation was used to determine the stiffness of the polymer-hydrogel system. This method is a highly sensitive technique which consists of indenting the surface of the measured substrate with a cantilever (in this case with a tip consisting of a spherical bead between 5 – 20 µm in diameter) (Figure 48). A small area of interaction between the bead and the surface allows for it to be highly sensitive.

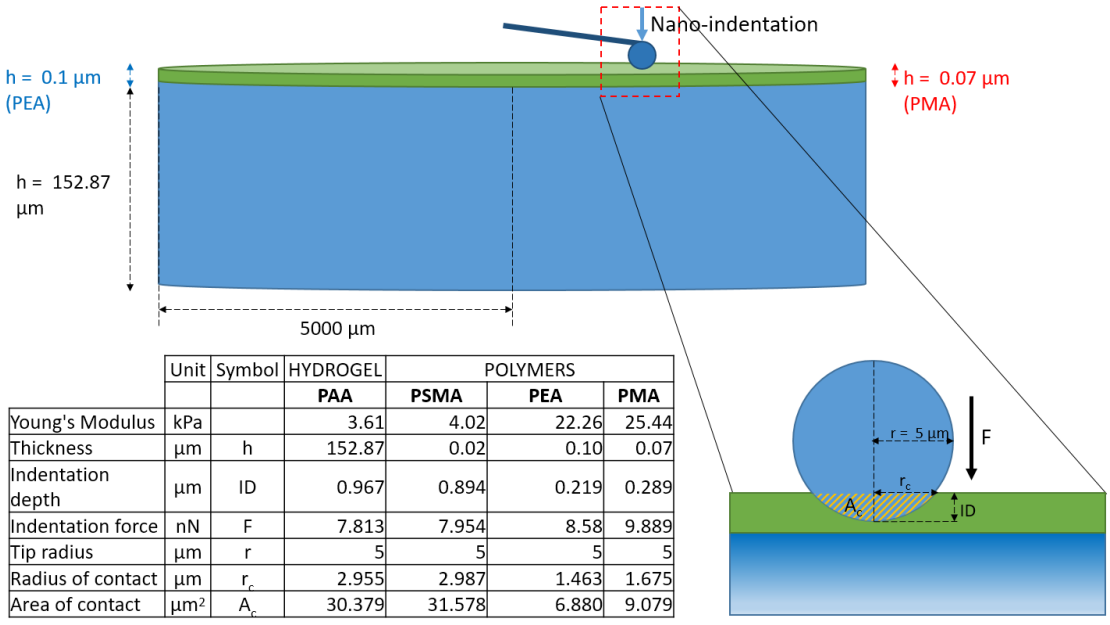

	Unit	Symbol	HYDROGEL	POLYMERS		
			PAA	**PSMA**	**PEA**	**PMA**
Young's Modulus	kPa		3.61	4.02	22.26	25.44
Thickness	µm	h	152.87	0.02	0.10	0.07
Indentation depth	µm	ID	0.967	0.894	0.219	0.289
Indentation force	nN	F	7.813	7.954	8.58	9.889
Tip radius	µm	r	5	5	5	5
Radius of contact	µm	r_c	2.955	2.987	1.463	1.675
Area of contact	µm²	A_c	30.379	31.578	6.880	9.079

Figure 48: Young's modulus of polyacrylamide alone and PSMA, PEA and PMA coated PAA along with nanoindentation parameters used.

The indentation depth *x* along with the spring constant *k* are used to determine indentation force *F* using Hooke's law:

Equation 5: Hooke's law used to determine nanoindentation force.

$$F = kx$$

Along with the indentation depth and force *F*, the radius of the sphere as well as the radius of contact are used in the Hertz model in order to deduce the Young's modulus *E*.

Equation 6: Hertz model used to deduce the Young's Modulus E

$$F = \frac{E}{1-\nu^2}\left[\frac{a^2+R_S^2}{2} ln \frac{R_S+a}{R_S-a} - aR_s\right] \Leftrightarrow E = \frac{F(1-\nu^2)}{\left[\frac{a^2+R_S^2}{2} ln \frac{R_S+a}{R_S-a} - aR_s\right]}$$

F: Indentation force

ν*:* Poisson's ratio

a: Radius of the contact circle

R_s*:* Radius of sphere

E: Young's modulus

This model assumes that the system measured is isotropic (having identical values of a property in all directions) meaning that vertical forces deduced by nanoindentation can be applied to lateral displacements (*i.e.* lateral cell forces and bead displacement within the PAA hydrogel). However, this method fails to take into account a bi-layered system in which, in the case of PEA and PMA coatings, a relatively stiff layer of polymer (400 – 800 kPa) with considerable thickness (70 – 100 nm) is covering a much softer layer of PAA hydrogel (3 – 4 kPa). A bi-layered system using different substrates with completely different mechanical properties poses a much more difficult problem when trying to measure traction forces of cells.

Finite element modelling was therefore used to determine forces exerted by cells on the polymer surface by modelling force transmission between the hydrogel-polymer interface. These results were then compared with values obtained using standard CTFM (Figure 49).

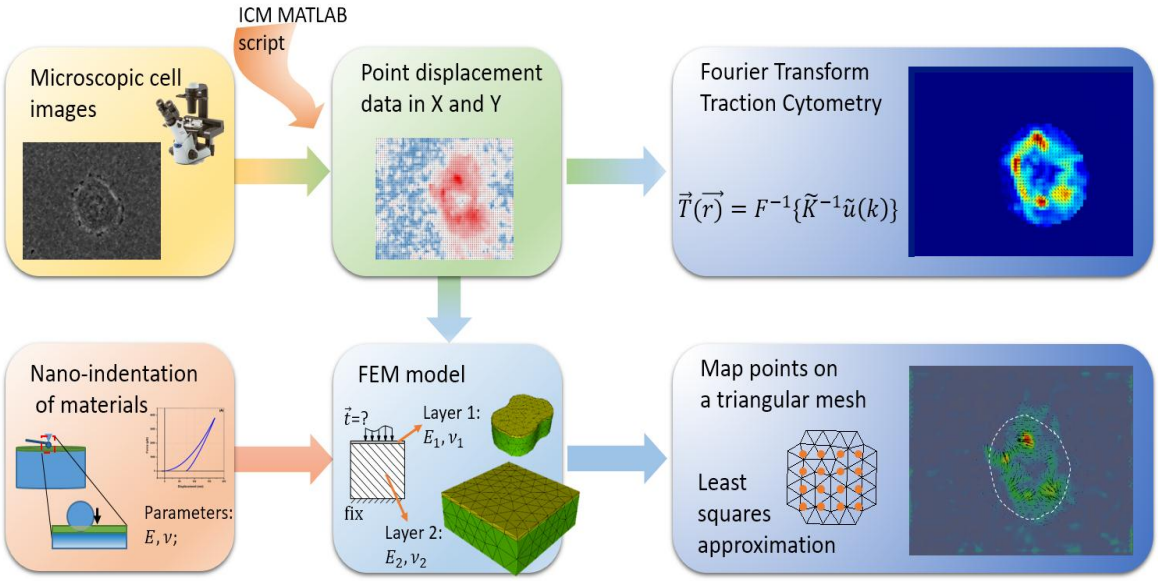

Figure 49: Finite element modelling traction field compared to standard traction field. Standard Fourier transform traction cytometry (top) uses the displacement of beads (or nanopillars) to obtain a displacement field which is converted to a traction field by knowing the mechanical properties of the system and applying the Green's function. This is especially useful when the substrate used is homogeneous. In the case of a heterogeneous bi-layered system, finite element modelling is used (bottom). This involves measuring the mechanical properties (Young's modulus *E* and Poisson's ratio *v*) of each layer, incorporating the previously obtained displacement field within a triangular mesh map and using the least squares approximation to obtain a traction field.

Standard CTFM is done by measuring bead displacement on the top layer of the PAA hydrogel. Only a negligibly soft and thin layer of PSMA (~4 kPa, 10 – 20 nm) separates the cells from the beads in the hydrogel which makes this system ideal for using the MATLAB algorithm to determine cell tractions. This is widely used for CTFM[184-186] which makes it a control experiment to compare FEM and CTFM. No

significant differences were observed between methods (Figure 39) which serves as a validation of the finite element model.

In contrast, differences in maximum tractions stress and total force were shown in cells on PEA and PMA when comparing FEM and CTFM, most remarkable in PMA. The standard method (CTFM) is highly dependent on the mechanical properties of the system as a whole (polymer and hydrogel). However, modelling takes into account several factors for every layer of the system individually. These include: stiffness, Poisson ration, and thickness of each component of the system.

When the stiffness of the polymer-hydrogel bi-layer were measured by force spectroscopy values were 22 and 25 kPa for PEA and PMA respectively. This is clearly a combination of the very thin and stiff polymer (70 – 100 nm; 400 – 800 kPa) with a relatively thicker, softer hydrogel (500 µm; 3.5 kPa). The proportions of which remain unclear. The FEM method was used to determine the forces on the surface of the FN-coated polymers by processing the transmission of forces from the surface of one substrate (polymers) to the surface of another (hydrogel).

It has been well documented that cells exert larger forces on stiffer surfaces[202-204]. With FEM, cells appear to exert more force on the PMA compared to PEA and PSMA with a maximum traction stress of ~790 Pa and total force of ~1350 nN (compared to ~300 Pa and ~535 nN on PEA). With a higher Young's modulus and thicker polymer layer on PMA, bead displacement in terms of distance was comparable to other surfaces.

Although there are clear differences in traction force measurements on PEA and PMA, it remains unclear if this is solely due to the difference in polymer stiffness (and thickness) or if the conformation of FN on the surface plays a role in cell forces.

3.4.4 FAK and downstream signalling

FAKis a protein-tyrosine kinase that is main component of FAs, and is responsible for signalling pathways involved in cell migration[62, 205]. The activated phosphorylated form of the protein (pFAK) is available in very little quantity and undetectable using certain techniques such as in-cell western[74] (Figure 40), but is a potent signalling protein[63, 206, 207]. Studies have shown that FAK, in conjunction with Src, contributes to integrin clustering which leads to: FA formation, MMP degradation leading to

cancer metastasis, and, actin polymerisation[208]. It is therefore a key factor in cancer progression and a potential therapeutic target.

In order to determine the effect of FA conformation on FAK/pFAK expression, standard Western blot and in-cell western techniques were used. However, pFAK is not expressed in large amounts within cells making protein quantification by these methods difficult (Figure 40 and Figure 43). Furthermore, previous studies measuring the expression of FAK/pFAK showed higher expression of pFAK in cells on fibrillar FN on PEA compared to globular FN on PMA[72,209].

Immunostaining of FAK and pFAK on both polymers revealed striking differences in pFAK organisation and distribution (Figure 44) while having similar amounts of the phosphorylated form (Figure 47). Phosphorylated FAK staining was more pronounced at the edges of cells on PEA compared to PMA, similarly to vinculin immunostaining. Interestingly, pFAK was localised mostly in the cytoplasm of cells on PMA and not organised in traditional FAs suggesting that globular FN is not conducive to integrin clustering and FA formation. This is translated to a lower FA count (Figure 32), and suppressed cell motility (Figure 36A) on PMA compared to PMA.

Furthermore, using PND-1186 to block FAK lead to a decrease in identifiable FA associated pFAK count as well as a decrease in fluorescent intensity on both polymers (Figure 45B and Figure 47A). This decrease in pFAK activity lead to supressed cell motility mostly in PEA (Figure 36) whereas mobility of cells on PMA was already limited due to the lack of organisation of phosphorylated FAK.

3.5 Conclusions

DU145 human prostate cancer cells have been shown to interact with FN via both $\alpha_5\beta_1$ and $\alpha_v\beta_3$ which are responsible for cell adhesion and migration. Both the RGD and PHSRN are needed to bind integrin $\alpha_5\beta_1$ whereas integrin $\alpha_v\beta_3$ binds solely to RGD. Although the RGD sequence is thought to be the main actor in cell attachment and motility whereas PHSRN is seen to be an auxiliary sequence, these studies demonstrate that both are equally important playing specific roles. The RGD cell binding domain being needed for cell anchorage, whereas the PHSRN sequence promotes migration.

In this study, it has been demonstrated that the use of materials capable of inducing differences in FN conformation and domain availability is capable of shedding light on the complex interactions between cells and a key protein of the ECM. The similar physico-chemical properties of PEA and PMA allow binding of FN, albeit in different conformations, and present similar cell behaviour such as cell attachment, FA size, drug resistance and traction forces. The value of using these materials are their ability to control the availability of specific sequences of FN leading to drastic changes in cell motility via changes in intracellular signalling.

4 Chapter 4: From 2D to 3D – DU145 invasion and degradation of functionalised PEG hydrogels

4.1 Introduction

4.1.1 The importance of 3D models in cancer research

Metastasis is the process by which tumour cells migrate away from the main tumour, using circulatory and lymphatic systems, and gets imbedded in a distant tissue. This requires for the cell to sustain various microenvironmental signals and influences. Determining factors in this process are the biochemical composition and mechanical properties of the surround tissue. Cells use these external cues to undergo the epithelial-mesenchymal transition which is a change in the cell phenotype causing the activation of transcription factors and an increase in the cell's ability to migrate and invade other tissue[110, 111]. Although this is a widely-understood process, many of the specific mechanisms involved remain unknown. The molecular and genetic mechanisms involved have been studied in 2D on a monolayer of cells but the biomechanical influences remain unclear. The use of 3D models in cancer research is therefore paramount for elucidating the roles of the ECM composition and structure, as well as the stiffness of the surrounding tissue[210, 211]. Many 3D models are currently being used to bridge the gap between 2D monolayer cell systems and *in vivo* studies[212]. Multicellular tumour spheroids are used to test chemotherapeutic agents and drug delivery systems[213, 214] whereas cell excreted ECM such as collagen, matrigel and hyaluronic acid (HA) as well as scaffolds such as silk protein, poly(ethylene glycol) (PEG), and poly(lactide-co-glycolide) (PLG) are used to study cell-cell and cell-ECM interactions in proliferation and migration[211, 215].

4.1.2 Advantages of functionalised PEG-based hydrogels

PEG-based hydrogels are highly tuneable systems that are used in regenerative medicine and drug delivery[216, 217]. This system also has the potential to help understand the interaction of cells with specific ECM protein sequences such as the RGD and PHSRN motifs on fibronectin as well as growth factors. It has the capabilities of mimicking the ECM, more specifically FN, with the possibility to tune biophysical and biochemical properties such as adhesion site density, MMP-degradable sites, as well as stiffness, all of which are intricately involved in cancer cells and their ability to migrate[218, 219].

A main advantage of using these synthetic hydrogels compared to natural matrices is that any changes to the stiffness by controlling protein concentration also leads

to variability in adhesive site quantity and density. PEG-based hydrogels, however, offer the possibility to modulate mechanical and biochemical properties independently of one another (Figure 50).

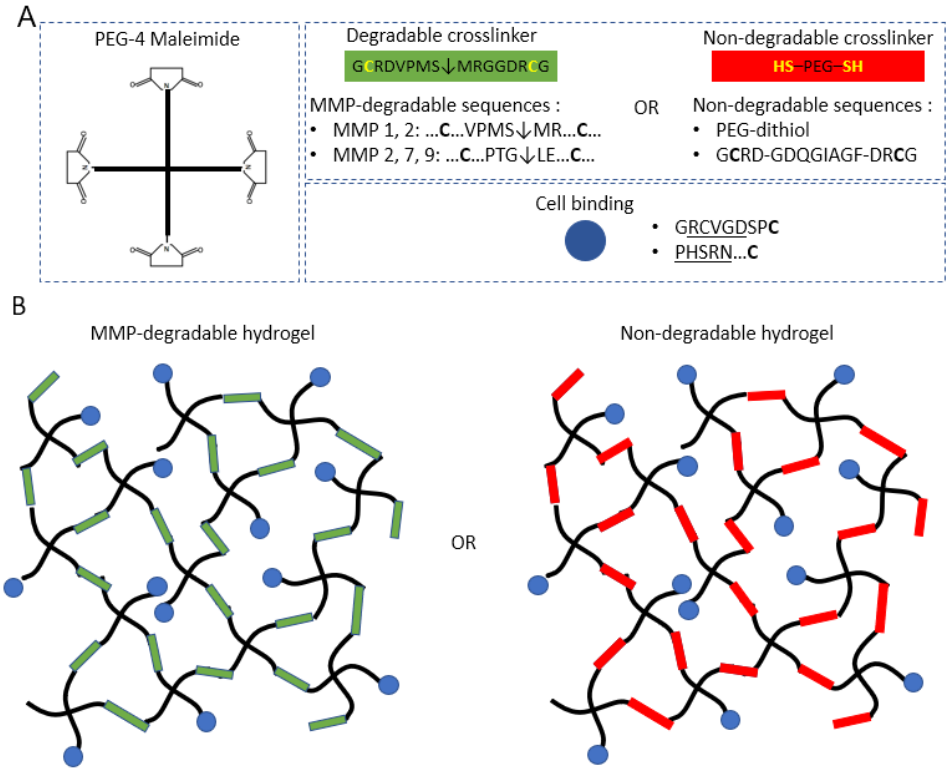

Figure 50: Schematic representation of PEG hydrogels with cross-linking and cell binding options. (A) PEG hydrogels consist of a PEG-4 maleimide backbone, a crosslinker that is either degradable (green) by MMPs secreted by the cell[220] or non-degradable (red)[221], and a cell binding sequence (blue) such as RGD of PHSRN. (B) Hydrogels obtained are either degradable by MMPs or non-degradable. Fine-tuning includes using a mix of degradable and non-degradable crosslinkers to control gel degradation time or modulating the amount of cell binding sequences to control cell binding.

These characteristics make this system ideal for understanding the specific interactions of cancer cells with the cell binding domain and synergy sequence of fibronectin as well as understanding cell migration via the degradation of ECM protein cleavable sites.

4.1.3 Hypothesis and experimental aims

We hypothesise that functionalised PEG-based hydrogels are an effective platform to study simple cell-ECM interactions within a 3D environment. The aims of this study are therefore to evaluate the potential of 4-arm PEG-based hydrogels with RDG (and eventually FN fragments) as a tool to understand cancer cell adhesion and invasion through the degradation of MMP-cleavable sites and to assess the limitations of this system.

4.2 Materials and methods

4.2.1 Hydrogel preparation

Hydrogels were made according to the protocol described by Andres Garcia[216]. 4-arm PEG-Maleimide (PEG-4MAL) macromer was first dissolved and mixed with RGD peptide with a 1:1 PEG-4MAL:RGD ratio allowing the binding of one RGD peptide to one arm of the 4-arm PEG therefore leaving 3 arms free for cross-linking. The cross-linker was then mixed in until gels were formed (Figure 51).

Figure 51: Principle of RGD-functionalised PEG-4-MAL with a MMP-degradable cross-linker. Gels are formed using 4-arm PEG-Maleimide (PEG-4MAL), and RGD sequence (GRGDSPC) and a cross-linker with a MMP-degradable sequence (-VPMSM-: degraded by MMP1 and MMP2[220]). Peptide sequences bind to 4-arm PEG via the thiol group of the cysteine amino acids which react with the maleimide group of PEG in a process known as Michael's addition reaction. It is possible to control gel stiffness by modulating the proportion of PEG-4MAL to the cross-linker.

The following Table 10 depicts the reagents used for the hydrogels.

Table 10: Reagents used for hydrogels

PEG used	PEG-4**MAL** (4 arm PEG with maleimide)
Cell binding sequence	G**RGD**SPC
Dithiol protease-cleavable cross-linker	GCRD**VPM**S↓MRGGDRCG

PEG-4MAL was first reacted with a constant concentration of 2 mM GRGDSPC cell binding sequence at different MAL:RGD ratios depending on desired gel stiffness. RGD-functionalised PEG was then cross-linked with the dithiol protease-cleavable cross-linking peptide (cleaved by MMP1 and MMP2[220]) at a 1:1 molar ratio of cysteine (2 per peptide) to remaining reactive group (MAL). All reactions were done in PBS in order to have a constant pH of 7.4. 50 µl gels were made at 4%, 7.5% and 10% wt/vol according to the following Table 11.

Table 11: Composition of gels

Gels (wt/vol)	4%	7.5%	10%
PEG-4MAL (20 µl)	36 mg/ml	67.5 mg/ml	90 mg/ml
2 mM RGD (10 µl)	1.4 mg/ml	1.4 mg/ml	1.4 mg/ml
VPM (20 µl)	2.6 mg/ml	6.1 mg/ml	8.6 mg/ml

PEG-4MAL and peptides were weighed, dissolved in PBS, mixed and left for 1h at room temperature in order to form gels.

4.2.2 Force spectroscopy

Force spectroscopy was attempted on functionalised PEG hydrogels. This was done by AFM using the Nanowizard 3 AFM from JPK in immersed conditions (water) with a 10 µm radius bead (spring constant 0.3 N/m). Due to the rough surfaces of hydrogels, force spectroscopy was only performed on 7.5 and 10% hydrogels.

4.2.3 Live/dead assay

Gels were prepared as previously described (Table 11) and seeded inside with $1.5x10^3$ cells/mm^3 of gel. Gels were then kept at 37°C with 5% CO_2 for up to 7 days, changing media every 2-3 days. Live/dead assay was then carried out on gels after 3 days and 7 days. Cells were seeded onto tissue culture plastic for a positive and negative control. Positive controls were incubated and stained normally whereas negative controls were treated with methanol for 5 minutes before being rinsed and stained.

After 3 or 7 days incubation, gels were rinsed with PBS and incubated with live/dead reagents. Images were then taken using an epifluorescent inverted microscope showing live cells in green and dead cells as red.

4.2.4 Cell invasion

In the case of cell invasion, gels were prepared as described (Table 11) in a 96-well tissue culture treated plate in an attempt to have a flat enough surface to seed cells upon. Gels were prepared at 4%, 7.5% and 10% w/v, left in PBS overnight, and seeded with DU145 human prostate cancer cells on top on the gels ($1.5x10^3$ cells/cm^2). Some cells were incubated using media containing 5 µM of MMP inhibitor (364205, Calbiochem).

Cell were then fixed with 4% formaldehyde and stained with DAPI. Images were then taken using an AxioObserver.Z1 with a scanning stage and a 10x objective. Images were taken for a maximum depth (*z*) between 300 – 900 µm with 10 µm *z* intervals. A 3D model was then reconstructed in post processing using the ZEN lite program from Zeiss microscopy.

4.2.5 Gel degradation

Gel degradation experiments were carried out on 7.5% gel only. Gels were prepared with $1.5x10^3$ cells/mm^3 (for 30 µl – 30 mm^3 gels) of hydrogel and weighed after seeding and every 3-4 hours for 30 to 72 hours using Eppendorf tubes with filter baskets. Tubes were first weighed empty and with gels right after they were formed with cells to establish the 'dry' weight of the gel without completely allowing it to dehydrate. Gels were then incubated with media for 3 – 4 hours before removing media by first centrifuging tubes to allow media to be drained through the pores of the filter and then removed (Figure 52). Tubes were then weighed with gels and this process was carried out for 1 to 3 days. This method is a complex and inaccurate way to indirectly determine gel degradation. Other methods such as using a rheometer to measure the mechanical properties of the gel until it is no longer detectable[222] or by the fluorescamine assay which detects primary amines at the picomole range[223] are more robust ways of measuring gel degradation.

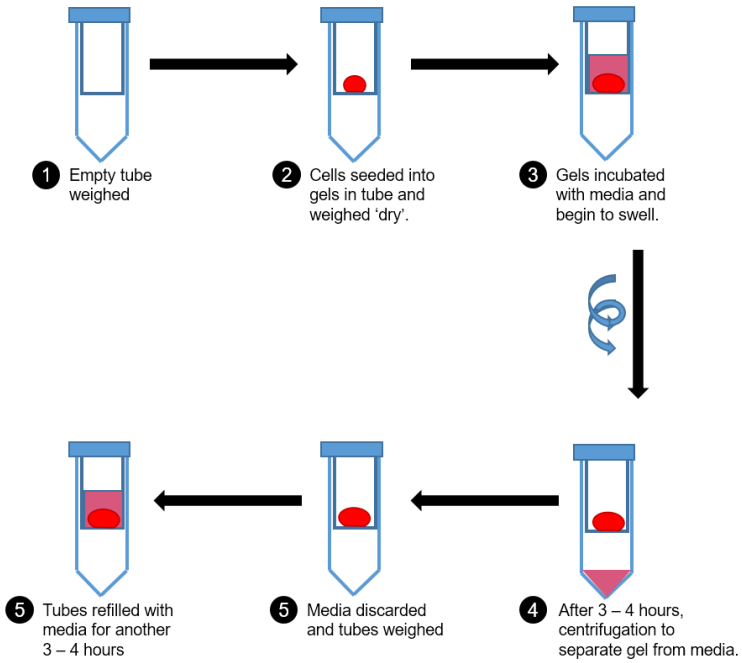

Figure 52: Gel degradation measurement process. Tubes were first weighed empty and gels were formed in the tubes in sterile conditions with or without cells seeded into them. Tubes were then incubated at 37°C with DU145 growth media and the weight of the gels were measured every 3-4 hours by carefully removing the media through centrifugation and pipetting and weighing in sterile conditions. Fresh media was then introduced to each tube until ready to measure again.

Experiments studying degradation of gels by cells were carried out using the VPM cleavable peptide but also PEG-Thiol (PEG-SH), an uncleavable cross-linker. The same ratio of PEG-4MAL:VPM was used for PEG-4MAL:PEG-SH, which was 1:3.

A control experiment was also carried out without cells but with the use of collagenase, a known ECM cleaving enzyme[224]. Collagenase was used at 10 µg/ml and 100 µg/ml RGD-PEG gels cross-linked with VPM and PEG-SH.

4.3 Results

4.3.1 Gel stiffness

Polymers with different wt/vol percentages have different mechanical properties. Modifying the PEG/Cross-linker ratio leads to differences in stiffness and even in the aspect of the gels. Higher wt/vol percentage gels are stiffer, more cloudy and easier to handle whereas lower percentage gels are translucent and much more difficult to handle (Figure 53).

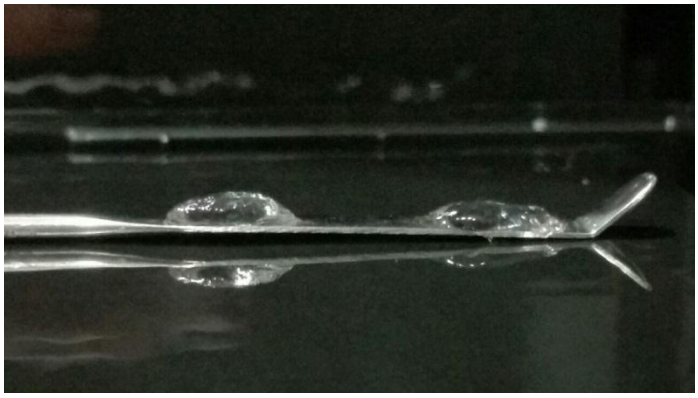

Figure 53: 10% wt/vol (left) and 7.5% wt/vol (right) functionalised PEG hydrogels.

The lowest percentage of hydrogel (4% wt/vol) was very liquid, making mechanical characterisation impossible as opposed to stiffer gels.

Higher percentage gels (10%) were measured to have a Young's modulus of ~2.8 kPa whereas 7.5% gels were approximately half that at ~1.4 kPa. Although this is not exactly in line with reports by Garcia *et al*., it has been demonstrated that gel stiffness can easily be modulated to mimic tissue stiffness for *in vitro* experiment closer resembling *in vivo* conditions (Figure 54).

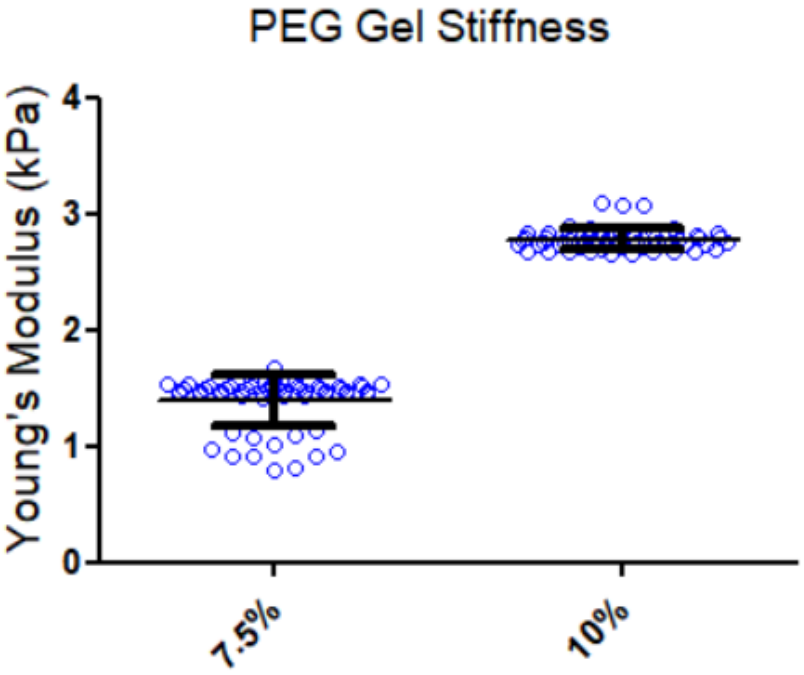

Figure 54: Young's modulus of 7.5% and 10% wt/vol PEG hydrogel functionalised with RGD, with MMP degradable cross-linkers.

4.3.2 Short term cell viability

Cell viability within hydrogels was measured by live/dead assay over a 1-week incubation. Only 7.5% gels were used in this instance.

After 3 days, 90% of cells were found to be alive within gels. After 7 days, no dead cells were detected with 5-10% of cells remaining compared to initial seeding (Figure 55). This is thought to be due to the degradation of the gel via cleavage of VPM sequences by MMPs secreted by the cells, allowing them to escape the hydrogel and be rinsed away during media changes.

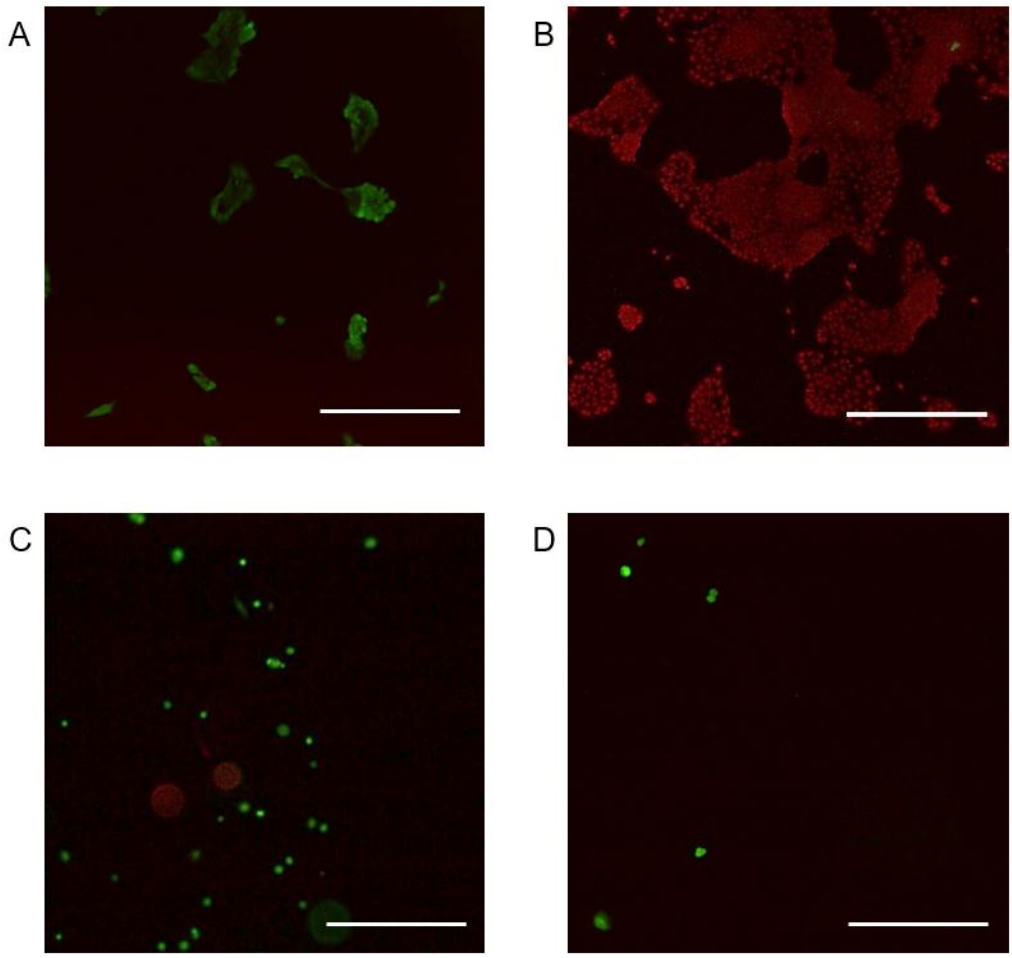

Figure 55: Live/dead assay of DU145 after 3 or 7 days incubation. (A) Positive control of cells on TCP. (B) Negative control of cells on TCP after being treated with methanol for 5 minutes. (C) Cell within gels after 3 days. (D) Cell within gels after 7 days. Scale bar: 500 µm.

4.3.3 Invasion and degradation

4.3.3.1 Cell invasion

Cells were seeded onto functionalised PEG hydrogels in a 96-well plate with and without a MMP inhibitor (Figure 56).

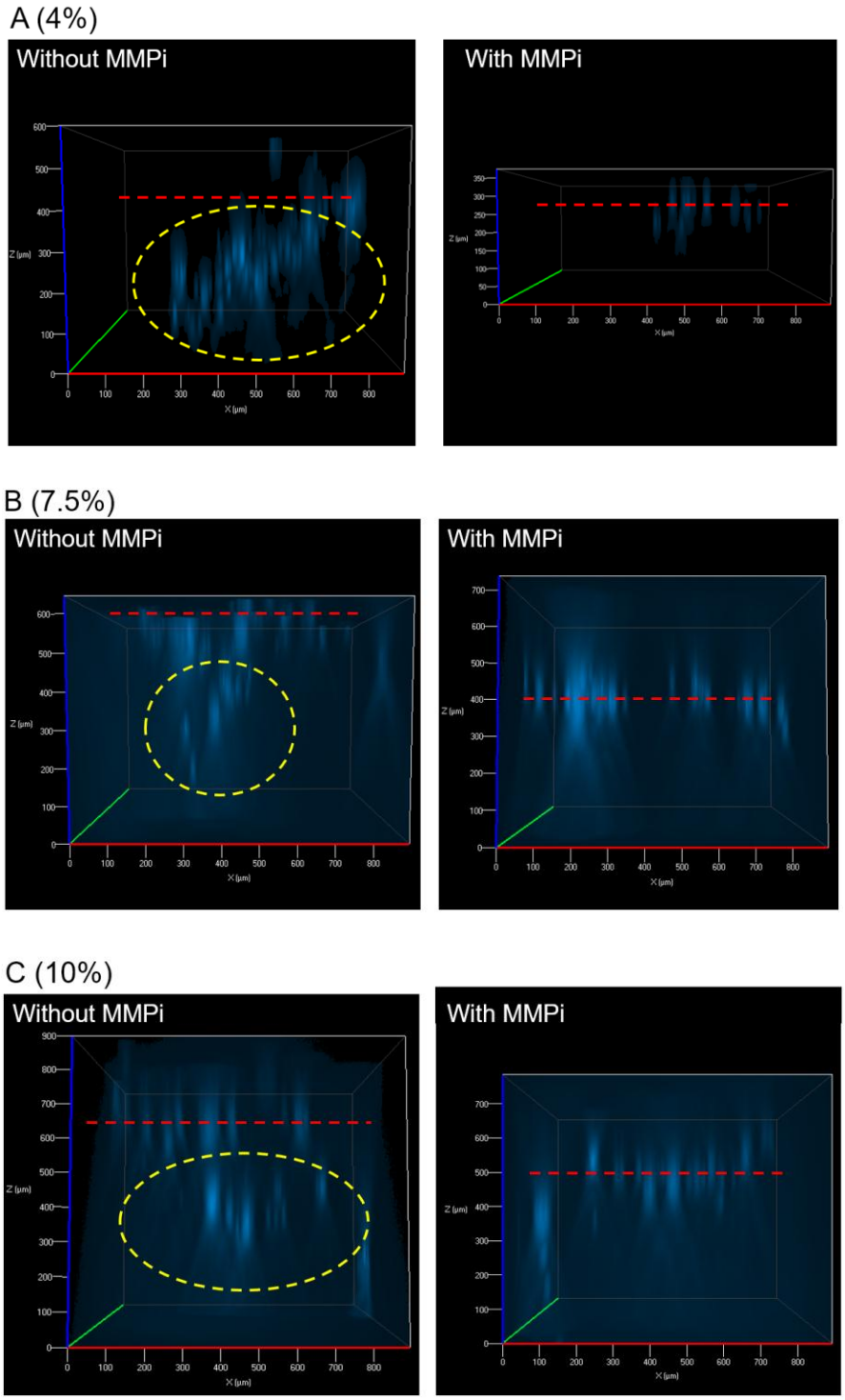

Figure 56: Invasion of DU145 cells stained with DAPI 24h after seeding onto PEG hydrogels of different wt/vol concentrations with and without MMP inhibitor. PEG gels were used at 4% (A), 7.5% (B) and 10% (C) wt/vol. The dotted red line represents the approximate gel surface whereas the dotted yellow oval indicates cells that have invaded the surface. With the MMP inhibitor cells remain at the designated gel surface, however, without the MMP inhibitor, cells penetrate the gel going lower than the designated gel surface

by degrading the gel. Although it is thought that the degradation occurs through the secretion of MMPs, the type of MMP is not clear.

In each case, cells appear to invade the gel in media with no MMPi whereas with MMPi cells appear to remain in the same plane. These results suggest that cell invasion within PEG hydrogels cross-linked with VPM is due to MMPs produced by the DU145 cells.

4.3.3.2 Gel degradation

Gel degradation by MMPs secreted by cells and also by collagenase was measured.

Hydrogels cross-linked with VPN swelled 3 – 5 times their original size and were able to maintain a consistent size for the first 30 hours after which cells began degrading to the point where gels were completely dissolved within 48 hours (Figure 57A and C). A similar trend was observed when cells were seeded into gels, however, degradation was evident with collagenase with gels losing mass after 24 hours with 10 µg/ml of collagenase and completely degraded hydrogels after 12 hours with 100 µg/ml.

Collagenase was shown to be ineffective on the PEG-SH cross-linked hydrogels with gels swelling 1.5 to 3 times original weight and maintained it over 30 hours even with the highest concentration of collagenase (Figure 57B). Strangely, the hydrogel degraded with or without cells after 48 hours (Figure 57D).

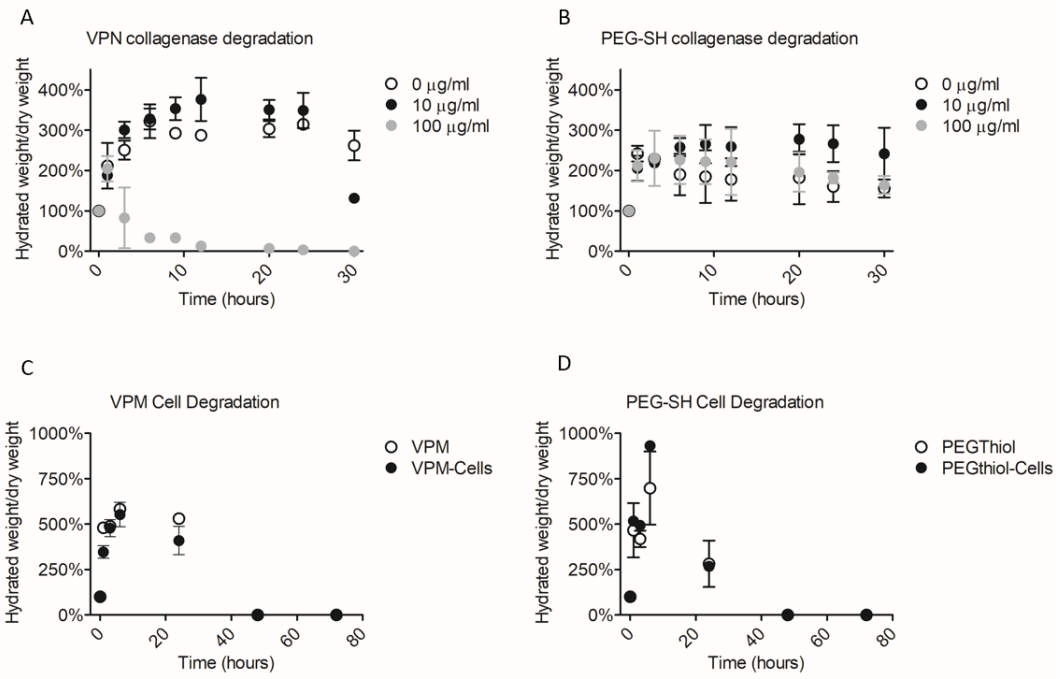

Figure 57: Degradation of functionalised PEG hydrogels with VPM or PEG-SH cross-linkers via (A) collagenase or (B) cell secreted MMPs. Lower concentrations of collagenase (10 µg/ml) started degrading the VPM cross-linked gels after 24 hours whereas the highest concentration (100 µg/ml) degraded gels almost immediately. Collagenase had no effect on PEG-SH cross-linked gels. VPN and PEG-SH cross-linked gels were both degraded by cells.

4.4 Discussion

4.4.1 Functionalised PEG gels as a 3D model

These gels provide a highly tuneable system as a viable 3D model in biomaterials research. Unlike natural networks and matrices such as Matrigel and collagen gels, it is possible to precisely determine the quantity of biological components capable of eliciting cellular response such a cell binding sequences and growth factors[216, 225, 226]. In this study the ratio and type of cross-linker was chosen while using a constant amount of RGD. However, studies have been carried out by binding FGF-2 and VEGF to PEG in order to modulate angiogenesis[225]. This can allow the study of potential peptide/growth factor combinations for increased cellular response[74]. Furthermore, the use of higher molecular weight PEG such as 8-arm PEG have

been shown to confer even more control on the hydrogel's composition with a broader range of possibilities in terms of combinations[227].

Just as with polyacrylamide hydrogels, mechanical properties of PEG hydrogels can be fine-tuned in order to mimic *in vivo* tissue conditions (Figure 54). This aspect is very useful in the study of cancer migration, the phenomenon of durotaxis, and, elucidating the cause and effect relationship between cancer progression and tumour stiffness.

4.4.2 Challenges and limitations

This is a preliminary study which has provided a general understanding of the use and potential of PEG hydrogels but has also highlighted many of its limitations. PEG hydrogels are a useful model for understanding specific cell-peptide or cell-growth factor interactions, which makes this 3D system very promising but the use of peptides as cross-linkers can become relatively costly. Furthermore, the ability to fine-tune this system is directly correlated to the number of arms the PEG backbone has. With 4-arm PEG in order to have consistent gels at least two arms are needed for cross-linking, therefore limiting functionalisation and degrees of degradation possibilities.

Results obtained in this study were mostly qualitative, showing the potential of this system as a 3D cancer model all while showing its limitations. Although it is possible to control gel stiffness, incorporating cells homogeneously within gels can prove to be challenging due to different polymerisations times.

4.5 Conclusions

In this study, PEG-based hydrogels have been shown to be a very adequate system to study the effects of specific peptides on cancerous cells in a 3D environment. It is possible to fine tune the degree of cell binding and gel degradation by simply changing the peptide content without sacrificing cross-linking density therefore compromising mechanical properties.

This is a simple and controlled method that offers the possibility to use numerous combinations of peptide sequences and is capable of completing a bigger picture alongside 2D systems in understand cell-protein interactions.

5 Discussions and outlook

5.1 Understanding and characterising the material-protein and protein-cell interfaces

The cell-protein interface is an important factor in determining cell behaviour. Cells are able to interact with their extracellular matrix via integrins. These allow bi-directional signalling between cells and their environment. Outside-in signalling occurs when specific sequences of ECM proteins or growth factors are presented to the cell, initiating downstream signalling which ultimately leads to changes in cell behaviour (proliferation, migration, apoptosis, etc.). Inside-out signalling is characterised by the effect cells have on their environment, leading to changes in ECM organisation via production of cell secreted ECM (collagen, FN) or degradation of the existing ECM by hydrolysis due to the secretion of MMP enzymes. Both forms of signalling are responsible for many of the processes involved in the formation and maintenance of the TME. These include cell growth and proliferation, angiogenesis, hypoxia, epithelial-mesenchymal transition, metastasis, and, drug resistance. In order to understand these behaviours, using the appropriate systems and materials is important.

Understanding that specific sequences of ECM proteins induces changes in cell behaviour highlights the importance of the choice of materials used to present the proteins to the cells. Conventionally, cell culture-treated tissue culture plastic is used which is usually coated with ECM proteins. However, the types of proteins used or their respective proportions remain unclear making it unfeasible to study specific cell-protein interactions. In order to do so, there is a need to be able to control ECM protein conformation and specific domain availability on the protein.

5.2 Controlling cell behaviour by using FN-coated poly(alkyl) acrylates

FN plays a vital role in cell signalling with various domains with which cells and other ECM protein can interact with. Many studies have shown its involvement cell binding, proliferation and migration mainly via the RGD and PHSRN synergy sequences located on the FN-III7-10 repeat domain (Figure 4). It is secreted as a soluble dimer which undergoes conformational changes, promoting its polymerization into insoluble fibres. This process occurs naturally and is cell-mediated. However, when adsorbed unto material surfaces they induce the unfolding of FN, it undergoes material-induced fibrillogenesis. We demonstrate that

upon adsorption to poly(ethyl acrylate) (PEA), FN undergoes fibrillogenesis leading to the formation of a fibrillous network. When adsorbed unto poly(methyl acrylate) (PMA), a substrate with very similar physico-chemical properties (Table 1), FN remains folded in a globular conformation (Figure 17). This leads to differences in the presentation of specific domains of FN when the protein is unfolded on PEA compared to when it is globular on PMA. We demonstrate that with similar amounts of protein are absorbed onto each surface, although the RGD cell binding domain is equally available the PHSRN synergy sequence is less available on PMA compared to PEA (Figure 19). This difference is the basis upon which cell studies were carried out by understanding that it has significant consequences on integrin biding and therefore cell behaviour. Cell attachment, FA formation and quantification were assessed using L929 mouse fibroblasts firstly and then using DU145 human prostate cancer cells. This human cancer cell line was subsequently used to study cell migration, cell traction, intracellular signalling and drug treatment when seeded onto FN-coated PEA and PMA.

5.3 Studying focal adhesion formation and cell migration

Cell attachment and FA formation are a direct response to contact with FN, the conformation of which is modulated by the underlying material it is presented to. Here we show that L929 mouse fibroblasts and DU145 human prostate cancer cells initially attach to the surface within the first 20 minutes of contact (Figure 23A and Figure31) via FN and that within a relatively short time of 2-3 hours are able to form FAs (Figure 21 and Figure 34). Furthermore, DU145 cells began migrating within the first 3 hours after seeding (Figure 36) indicating the mobile dynamic of FAs after initial attachment with continuous association of focal complexes which develop into FAs at the leading edge of the cell, coupled with disassociation of FAs at the opposite end leading to movement. This is commonly referred to as FA turnover and is responsible for cell motility[228].

FA characteristics such as size, amount and area were determined 2-3 hours after seeding and represent a fixed point in time. Here we looked at FA formation as well as cell migration of cells on PEA, PMA and glass coverslips coated with FN. FAs were more developed around the edges of the cells on the fibrillar FN of PEA and were also larger with more FAs compared to cells on globular FN on PMA. This is

thought to be a sign of cells being firmly attached to the surface on which FN is stretched out in a network conformation. Interestingly, upon studying the migration of DU145 cells on these substrates, cells were more mobile on PEA compared to PMA indicating that the more developed FAs on PEA are a result of higher activity in FA turnover leading to higher motility even when cells are treated with a FAK inhibiting cytostatic drug (Figure 36). This theory could be further developed by studying FA turnover using fluorescently-labelled FA proteins such as paxillin or vinculin in live imaging[228]. We can therefore conclude that the exposure of the RGD and PHSRN sequences of FN, due to the conformation taken upon adsorption to PEA and PMA, have a significant effect on FA formation and cell mobility. This brings into question the underlying mechanisms of the cell's interactions with these specific FN sequences.

5.4 Clarifying the underlying mechanisms involved in the cell's interaction with its environment

It is well known that the integrin $\alpha_5\beta_1$ interacts with both the RGD and PHSRN sequences whereas the $\alpha_v\beta_3$ integrin interacts preferentially with the RGD domain. The integrins, once bound to FN via these sequences, recruit other proteins such as talin and vinculin to form a focal complex which then develops into FAs by recruiting other FA proteins such as paxillin and FAK (Figure 6). FA being directly coupled to actin filaments are responsible for cell motility through their association and disassociation along the leading edge of the cell. FAK plays a critical role in the formation of FAs as its phosphorylated form (pFAK) is thought to be involved in the signalling pathways of migration such as MMP secretion and actin polymerisation making it a prominent therapeutic target. Both FAK and pFAK were shown to be expressed equally within DU145 cells on FN-coated PEA and PMA. The addition of a novel FAK inhibitor, PND-1186, was shown to decrease their expression in both cases. Although no differences were observed in pFAK expression with and without the addition of PND-1186, cells were more mobile on PEA.

Furthermore, blocking the RGD and PHSRN sequences of FN highlighted the role of integrins in cell adhesion and migration. Here we propose that cell anchorage and adhesion are dependent on the RGD cell binding domain via $\alpha_v\beta_3$ whereas cell motility is dependent on the combination of the RGD and PHSRN sequences via the

$\alpha_5\beta_1$ integrin. When cells attach to FN via RGD these integrins combined form a solid bond between the cell and the ECM protein. This was confirmed when the RGD domain was blocked with HFN7.1 leading to cell not attaching to surfaces (Figure 31). However, blocking the PHSRN synergy sequence partially affected cell attachment of cells on PEA. When motility was studied by wound healing assay, cells were shown to be more mobile on PEA (Figure 36) confirming that the PHSRN sequence, exposed more on fibrillar FN on PEA compared to globular FN on PMA, promotes cell migration along with the RGD cell binding domain via the $\alpha_5\beta_1$ integrin. When cells begin migrating we propose that the $\alpha_v\beta_3$ integrin detaches from the RGD sequence allowing cells to interact with FN using only one integrin heterodimer, allowing a more dynamic relationship between the cell and the ECM, leading to quicker FA turnover.

In order to further study the effect of the RGD and PHSRN sequences on cell adhesion and migration specific studies could be carried out such as the use of modified FN with inactivated sequences (RGE instead of RGD, PHSCN instead of PHSRN), assessing cell migration in a 3D setting, and studying cell tractions on polymers. These modified forms of FN would provide a more accurate study of cell-FN interactions. The use of the antibodies HFN7.1 and mAb1937 to block the RGD and PHSRN sequences respectively may pose an issue as they are relatively cumbersome (150 kDa) compared to FN (220 kDa). Furthermore, due to their size and the proximity of the domains they are blocking, it is not clear if blocking one domain with an antibody limits access to the other domain by the cell's integrins or even the other antibody. Removing these antibodies would therefore simplify the interactions between the cell and FN.

5.5 Developing novel methods for analysis of cell traction on polymers

CTFM is a common method used for the evaluation of the exertion of cellular forces on a given material surface such as functionalised polyacrylamide (PAA) or nanopillars[229]. These methods determine traction forces by simply knowing the mechanical properties of the material surface and the displacement induced by the cell at the cell-material interface (Figure 37). Here we use a bi-layered system consisting of a layer of PAA embedded with fluorescent polystyrene nanoparticles coated with a thin layer of PEA or PMA in order to compare the forces exerted by

cells on surfaces on which FN is in an extended fibrillar state on PEA or in a globular state on PMA. Nanobeads were not embedded directly into polymers due to the fact that they would dissolve in the polymer solution (prepared in toluene). This offers a unique opportunity to develop a method for measuring cell traction on a two-layered system that possesses vastly different mechanical properties between layers (Table 8) by using computational modelling. We can conclude from the results obtained that the majority of the force exerted by cells is due to the mechanical properties of the polymer-hydrogel system as there a clear correlation between the thickness and stiffness of the polymer layer and the maximum traction stress and total force exerted by the cell. However, an argument can be made that the conformation of FN on the surface plays a role in cell traction. Knowing that cells adhere to surfaces such as FN-coated PMA that present primarily the RGD sequence, via 2 sets of integrin heterodimers ($\alpha_5\beta_1$ and $\alpha_v\beta_3$), they are more firmly attached and exert more force on the surface. On surfaces such as FN-coated PEA that present RGD and PHSRN cells are more mobile thus exerting less force on its substrate.

The influence of the mechanical properties versus the protein conformation and binding domain presentation could be further elucidated by comparing the traction of cells on polymers with the same thickness and also by blocking the RGD and/or PHSRN sequences. The model does take into account the thickness and stiffness of the polymer layers however, they have no apparent linear correlation with the traction stresses exerted by cells on PEA and PMA.

Once fully developed and optimised, this model shows potential of being a more appropriate method for understanding cell traction on more complex surfaces such as the presented bi-layered system on which standard CTFM techniques are not possible. It also has other potential applications such as modelling cell traction and migration on stiff tissue like bone in tissue regeneration.

5.6 Studying cell behaviour in a simplified 3D model

3D models are often used to understand more complex phenomena within tissue such as vascularisation. They are representative on *in vivo* conditions but fail to shed light on specific cell-cell or cell-ECM interactions as with 2D systems. We propose the development of a model that takes into consideration the 3D aspect

which mimics *in vivo* conditions as well as looking at specific interaction between the cell and its microenvironment. These PEG-based hydrogels are highly tuneable and offer a wide range of possible combinations of mechanical properties, degradability, and peptide presentation to further understand the role of specific sequences of ECM proteins on cell behaviour in a controlled 3D setting.

Here we use PEG hydrogels functionalised with RGD and a MMP degradable cross-linker with controlled stiffness's and are able to maintain viable cells within them for up to 1 week, until cells completely degrade the gels (Figure 55C and D). Moreover, cells are shown to invade the gels through MMP secretion (Figure 56) highlighting its potential in further understanding the processes of metastasis and ECM degradation. The results presented in this study opens the door for understanding the role that the PHSRN synergy sequence of FN would play in cell encapsulation and behaviour. A proposed experiment would be to study cell migration within a non-degradable gel containing both the RGD and PHSRN sequences versus a non-degradable gel containing RGD only. This would shed light on the specific roles of both domains on cell mobility in a 3D system.

5.7 Future work

Although extensive research has been carried out into understanding material-protein and protein-cell interactions, there are many more mechanisms involved that have yet to be elucidated using both the FN-coated material platform as well as the functionalised PEG hydrogel system.

5.7.1 FN-coated polymer platform

This system can be further developed to take into account other ECM proteins that are involved in cancer progression or growth factors such as VEGF that bind to FN and may possibly alter cell behaviour.

Another avenue would be to study the reorganisation of the FN on the surface of the polymers by the cells. Knowing that the cells secrete MMPs as well their own FN it would be possible to stain and observe the secreted FN with a specific cellular-FN antibody. This would give insight into how cells interact with their surroundings depending on the conformation of FN.

Furthermore, studying the downstream signalling of FAK (pFAK, Src, PI3K,etc.) by Western blot or PCR would help to understand the effects of FN conformation on cell motility.

5.7.2 Functionalised PEG hydrogel system

This preliminary study of functionalised PEG with MMP-degradable crosslinkers shows promise in having a 3D system that is easily tuneable and offers many possibilities for further research.

Comparative studies with other established 3D systems such as Matrigel® and polymer scaffolds would further reveal the advantages and drawbacks of the system. Moreover, the use of 8-arm PEG would allow for more crosslinking and functionalising possibilities. This would be useful to study degradation speed (using a mixture of degradable and non-degradable crosslinker sequences), cell adhesion (modulating the amount of RGD) and cell proliferation. A more ambitious study would be attempting to use large sequences of FN or other ECM proteins as cross linkers. Incorporating growth factors within the system while controlling the degradation rate would allow cells to proliferate and possibly form their own ECM in 3D.

6 Conclusions

Advances in biomedical engineering have allowed for more in depth understanding of cell function. These have shown to be useful for the advancement of cancer research by providing further understanding of the specific processes involved through breaking down the TME.

Here, we used poly(alkyl acrylates) to be able to direct the conformation of FN, a key protein of the extracellular matrix. We have managed to show that these material substrates, with very similar physico-chemical properties, are able to modulate FN conformation and therefore cell behaviour. The change in FN organisation has shown to influence FA formation and organisation, cell migration, FAK/pFAK layout, and traction forces.

Furthermore, this has played an important part in clarifying the role of the RGD cell binding domain as well as the PHSRN synergy sequence in cell adhesion and migration. With the cell anchoring to the surface using the RGD sequence via integrin $\alpha_v\beta_3$ and cell motility being directed by both the RGD domain and PHSRN synergy sequence via integrin $\alpha_5\beta_1$. This can potentially lead to the development of new therapies specifically targeting cancerous cells at the FN-integrin interface to prevent cells from spreading.

Finally, we propose a 3D model that can replicate and study specific cell-FN interactions with RGD and PHSRN and provides a system that more closely mimics *in vivo* conditions.

References

1. Enderle, J. D.; Bronzino, J. D.; Blanchard, S. M., *Introduction to biomedical engineering*. 2. ed.; Elsevier Academic Press: Burlington, MA, 2005; p xxi, 1118 s.

2. Madihally, S. V., *Principles of biomedical engineering*. Artech house publishers: Norwood, 2010; p 481pp.

3. Saltzman, W. M., *Biomedical engineering : bridging medicine and technology*. Cambridge University Press ;: Cambridge

New York,, 2009; p xxi, 633 s.

4. Suh, S. C.; Gurupur, V. P.; Tanik, M. M., *Biomedical Engineering : Health Care Systems, Technology and Techniques*. Springer Science+Business Media, LLC: New York, NY, 2011.

5. Vanterpool, F. A.; Cantini, M.; Seib, F. P.; Salmerón-Sánchez, M., A material-based platform to modulate fibronectin activity and focal adhesion assembly. *Biores Open Access* **2014,** *3* (6), 286-96.

6. Edmondson, R.; Broglie, J. J.; Adcock, A. F.; Yang, L., Three-dimensional cell culture systems and their applications in drug discovery and cell-based biosensors. *Assay Drug Dev Technol* **2014,** *12* (4), 207-18.

7. Antoni, D.; Burckel, H.; Josset, E.; Noel, G., Three-dimensional cell culture: a breakthrough in vivo. *Int J Mol Sci* **2015,** *16* (3), 5517-27.

8. Hong, H.; Stegemann, J. P., 2D and 3D collagen and fibrin biopolymers promote specific ECM and integrin gene expression by vascular smooth muscle cells. *J Biomater Sci Polym Ed* **2008,** *19* (10), 1279-93.

9. Beningo, K. A.; Dembo, M.; Wang, Y. L., Responses of fibroblasts to anchorage of dorsal extracellular matrix receptors. *Proc Natl Acad Sci U S A* **2004,** *101* (52), 18024-9.

10. Watt, F. M.; Huck, W. T., Role of the extracellular matrix in regulating stem cell fate. *Nat Rev Mol Cell Biol* **2013,** *14* (8), 467-73.

11. Caliari, S. R.; Burdick, J. A., A practical guide to hydrogels for cell culture. *Nat Methods* **2016,** *13* (5), 405-14.

12. Wells, R. G., The role of matrix stiffness in regulating cell behavior. *Hepatology* **2008,** *47* (4), 1394-400.

13. Engler, A. J.; Sen, S.; Sweeney, H. L.; Discher, D. E., Matrix elasticity directs stem cell lineage specification. *Cell* **2006,** *126* (4), 677-89.

14. Discher, D. E.; Janmey, P.; Wang, Y. L., Tissue cells feel and respond to the stiffness of their substrate. *Science* **2005,** *310* (5751), 1139-43.

15. Shamir, E. R.; Ewald, A. J., Three-dimensional organotypic culture: experimental models of mammalian biology and disease. *Nat Rev Mol Cell Biol* **2014,** *15* (10), 647-64.

16. Goers, L.; Freemont, P.; Polizzi, K. M., Co-culture systems and technologies: taking synthetic biology to the next level. *J R Soc Interface* **2014,** *11* (96).

17. Zhang, W.; Zhuang, A.; Gu, P.; Zhou, H.; Fan, X., A review of the three-dimensional cell culture technique: Approaches, advantages and applications. *Curr Stem Cell Res Ther* **2016,** *11* (4), 370-80.

18. Duval, K.; Grover, H.; Han, L. H.; Mou, Y.; Pegoraro, A. F.; Fredberg, J.; Chen, Z., Modeling Physiological Events in 2D vs. 3D Cell Culture. *Physiology (Bethesda)* **2017,** *32* (4), 266-277.

19. Xu, X.; Farach-Carson, M. C.; Jia, X., Three-dimensional in vitro tumor models for cancer research and drug evaluation. *Biotechnol Adv* **2014,** *32* (7), 1256-68.

20. Lesniak, D.; Xu, Y.; Deschenes, J.; Lai, R.; Thoms, J.; Murray, D.; Gosh, S.; Mackey, J. R.; Sabri, S.; Abdulkarim, B., Beta1-integrin circumvents the antiproliferative effects of trastuzumab in human epidermal growth factor receptor-2-positive breast cancer. *Cancer Res* **2009,** *69* (22), 8620-8.

21. Pontiggia, O.; Sampayo, R.; Raffo, D.; Motter, A.; Xu, R.; Bissell, M. J.; Joffé, E. B.; Simian, M., The tumor microenvironment modulates tamoxifen resistance in breast cancer: a role for soluble stromal factors and fibronectin through β1 integrin. *Breast Cancer Res Treat* **2012,** *133* (2), 459-71.

22. Li, W. J.; Laurencin, C. T.; Caterson, E. J.; Tuan, R. S.; Ko, F. K., Electrospun nanofibrous structure: a novel scaffold for tissue engineering. *J Biomed Mater Res* **2002,** *60* (4), 613-21.

23. Yang, F.; Murugan, R.; Wang, S.; Ramakrishna, S., Electrospinning of nano/micro scale poly(L-lactic acid) aligned fibers and their potential in neural tissue engineering. *Biomaterials* **2005,** *26* (15), 2603-10.

24. Yoshimoto, H.; Shin, Y. M.; Terai, H.; Vacanti, J. P., A biodegradable nanofiber scaffold by electrospinning and its potential for bone tissue engineering. *Biomaterials* **2003,** *24* (12), 2077-82.

25. Katt, M. E.; Placone, A. L.; Wong, A. D.; Xu, Z. S.; Searson, P. C., In Vitro Tumor Models: Advantages, Disadvantages, Variables, and Selecting the Right Platform. *Front Bioeng Biotechnol* **2016,** *4*, 12.

26. Hulkower, K. I.; Herber, R. L., Cell migration and invasion assays as tools for drug discovery. *Pharmaceutics* **2011,** *3* (1), 107-24.

27. Kramer, N.; Walzl, A.; Unger, C.; Rosner, M.; Krupitza, G.; Hengstschläger, M.; Dolznig, H., In vitro cell migration and invasion assays. *Mutat Res* **2013,** *752* (1), 10-24.

28. Friedrich, J.; Seidel, C.; Ebner, R.; Kunz-Schughart, L. A., Spheroid-based drug screen: considerations and practical approach. *Nat Protoc* **2009,** *4* (3), 309-24.

29. LaBarbera, D. V.; Reid, B. G.; Yoo, B. H., The multicellular tumor spheroid model for high-throughput cancer drug discovery. *Expert Opin Drug Discov* **2012,** *7* (9), 819-30.

30. Mosadegh, B.; Lockett, M. R.; Minn, K. T.; Simon, K. A.; Gilbert, K.; Hillier, S.; Newsome, D.; Li, H.; Hall, A. B.; Boucher, D. M.; Eustace, B. K.; Whitesides, G. M., A paper-based invasion assay: assessing chemotaxis of cancer cells in gradients of oxygen. *Biomaterials* **2015,** *52*, 262-71.

31. Koch, T. M.; Münster, S.; Bonakdar, N.; Butler, J. P.; Fabry, B., 3D Traction forces in cancer cell invasion. *PLoS One* **2012,** *7* (3), e33476.

32. Bogorad, M. I.; DeStefano, J.; Karlsson, J.; Wong, A. D.; Gerecht, S.; Searson, P. C., Review: in vitro microvessel models. *Lab Chip* **2015,** *15* (22), 4242-55.

33. Butler, J. M.; Kobayashi, H.; Rafii, S., Instructive role of the vascular niche in promoting tumour growth and tissue repair by angiocrine factors. *Nat Rev Cancer* **2010,** *10* (2), 138-46.

34. Frantz, C.; Stewart, K. M.; Weaver, V. M., The extracellular matrix at a glance. *J Cell Sci* **2010,** *123* (Pt 24), 4195-200.

35. Stewart, D. A.; Cooper, C. R.; Sikes, R. A., Changes in extracellular matrix (ECM) and ECM-associated proteins in the metastatic progression of prostate cancer. *Reprod Biol Endocrinol* **2004,** *2*, 2.

36. Keeley, F. W.; Mecham, R. P., *Evolution of extracellular matrix*. Springer: Berlin ; New York, 2013.

37. Lu, P.; Weaver, V. M.; Werb, Z., The extracellular matrix: a dynamic niche in cancer progression. *J Cell Biol* **2012,** *196* (4), 395-406.

38. Burgeson, R. E.; Chiquet, M.; Deutzmann, R.; Ekblom, P.; Engel, J.; Kleinman, H.; Martin, G. R.; Meneguzzi, G.; Paulsson, M.; Sanes, J., A new nomenclature for the laminins. *Matrix Biol* **1994,** *14* (3), 209-11.

39. Hynes, R. O., The extracellular matrix: not just pretty fibrils. *Science* **2009,** *326* (5957), 1216-9.

40. Alberts B, J. A., Lewis J, et al., The Extracellular Matrix of Animals. In *Molecular Biology of the Cell*, 4th Ediion ed.; Garland Science: New York, 2002.

41. Byers, P. H.; Siegel, R. C.; Peterson, K. E.; Rowe, D. W.; Holbrook, K. A.; Smith, L. T.; Chang, Y. H.; Fu, J. C., Marfan syndrome: abnormal alpha 2 chain in type I collagen. *Proc Natl Acad Sci U S A* **1981,** *78* (12), 7745-9.

42. Lenselink, E. A., Role of fibronectin in normal wound healing. *Int Wound J* **2015,** *12* (3), 313-6.

43. Wierzbicka-Patynowski, I.; Schwarzbauer, J. E., The ins and outs of fibronectin matrix assembly. *J Cell Sci* **2003,** *116* (Pt 16), 3269-76.

44. Pankov, R.; Yamada, K. M., Fibronectin at a glance. *J Cell Sci* **2002,** *115* (Pt 20), 3861-3.

45. Schwarzbauer, J. E.; DeSimone, D. W., Fibronectins, their fibrillogenesis, and in vivo functions. *Cold Spring Harb Perspect Biol* **2011,** *3* (7).

46. Hynes, R. O., *Fibronectins*. 1 ed.; Springer New York, NY 1990; p 546.

47. Ochsenhirt, S. E.; Kokkoli, E.; McCarthy, J. B.; Tirrell, M., Effect of RGD secondary structure and the synergy site PHSRN on cell adhesion, spreading and specific integrin engagement. *Biomaterials* **2006,** *27* (20), 3863-74.

48. Zeng, Z. Z.; Yao, H.; Staszewski, E. D.; Rockwood, K. F.; Markwart, S. M.; Fay, K. S.; Spalding, A. C.; Livant, D. L., alpha(5)beta(1) Integrin Ligand PHSRN Induces Invasion and alpha(5) mRNA in Endothelial Cells to Stimulate Angiogenesis. *Transl Oncol* **2009,** *2* (1), 8-20.

49. Livant, D. L.; Brabec, R. K.; Pienta, K. J.; Allen, D. L.; Kurachi, K.; Markwart, S.; Upadhyaya, A., Anti-invasive, antitumorigenic, and antimetastatic activities of the PHSCN sequence in prostate carcinoma. *Cancer Res* **2000,** *60* (2), 309-20.

50. Mould, A. P.; Askari, J. A.; Aota, S.; Yamada, K. M.; Irie, A.; Takada, Y.; Mardon, H. J.; Humphries, M. J., Defining the topology of integrin alpha5beta1-fibronectin interactions using inhibitory anti-alpha5 and anti-beta1 monoclonal antibodies. Evidence that the synergy sequence of fibronectin is recognized by the amino-terminal repeats of the alpha5 subunit. *J Biol Chem* **1997,** *272* (28), 17283-92.

51. Leahy, D. J.; Aukhil, I.; Erickson, H. P., 2.0 A crystal structure of a four-domain segment of human fibronectin encompassing the RGD loop and synergy region. *Cell* **1996,** *84* (1), 155-64.

52. Redick, S. D.; Settles, D. L.; Briscoe, G.; Erickson, H. P., Defining fibronectin's cell adhesion synergy site by site-directed mutagenesis. *J Cell Biol* **2000,** *149* (2), 521-7.

53. Elosegui-Artola, A.; Bazellières, E.; Allen, M. D.; Andreu, I.; Oria, R.; Sunyer, R.; Gomm, J. J.; Marshall, J. F.; Jones, J. L.; Trepat, X.; Roca-Cusachs, P., Rigidity sensing and adaptation through regulation of integrin types. *Nat Mater* **2014,** *13* (6), 631-7.

54. Zhang, H.; Guo, M.; Chen, J. H.; Wang, Z.; Du, X. F.; Liu, P. X.; Li, W. H., Osteopontin knockdown inhibits αv,β3 integrin-induced cell migration and invasion and promotes apoptosis of breast cancer cells by inducing autophagy and inactivating the PI3K/Akt/mTOR pathway. *Cell Physiol Biochem* **2014,** *33* (4), 991-1002.

55. Michael, K. E.; Vernekar, V. N.; Keselowsky, B. G.; Meredith, J. C.; Latour, R. A.; Garcia, A. J., Adsorption-Induced Conformational Changes in Fibronectin Due to Interactions with Well-Defined Surface Chemistries. *Langmuir* **2003,** *19* (19), 8033-8040.

56. Kinbara, K.; Goldfinger, L. E.; Hansen, M.; Chou, F. L.; Ginsberg, M. H., Ras GTPases: integrins' friends or foes? *Nat Rev Mol Cell Biol* **2003,** *4* (10), 767-76.

57. Hynes, R. O., Integrins: bidirectional, allosteric signaling machines. *Cell* **2002,** *110* (6), 673-87.

58. Reading, U. o. Cell adhesion. (accessed June 12th, 2017).

59. Wu, C., Focal adhesion: a focal point in current cell biology and molecular medicine. *Cell Adh Migr* **2007,** *1* (1), 13-8.

60. Wozniak, M. A.; Modzelewska, K.; Kwong, L.; Keely, P. J., Focal adhesion regulation of cell behavior. *Biochim Biophys Acta* **2004,** *1692* (2-3), 103-19.

61. Kim, D. H.; Wirtz, D., Focal adhesion size uniquely predicts cell migration. *FASEB J* **2013,** *27* (4), 1351-61.

62. Mitra, S. K.; Hanson, D. A.; Schlaepfer, D. D., Focal adhesion kinase: in command and control of cell motility. *Nat Rev Mol Cell Biol* **2005,** *6* (1), 56-68.

63. Schlaepfer, D. D.; Mitra, S. K., Multiple connections link FAK to cell motility and invasion. *Curr Opin Genet Dev* **2004,** *14* (1), 92-101.

64. Cao, X.; Lin, Y.; Driscoll, T. P.; Franco-Barraza, J.; Cukierman, E.; Mauck, R. L.; Shenoy, V. B., A Chemomechanical Model of Matrix and Nuclear Rigidity Regulation of Focal Adhesion Size. *Biophys J* **2015,** *109* (9), 1807-17.

65. Balaban, N. Q.; Schwarz, U. S.; Riveline, D.; Goichberg, P.; Tzur, G.; Sabanay, I.; Mahalu, D.; Safran, S.; Bershadsky, A.; Addadi, L.; Geiger, B., Force and focal adhesion assembly: a close relationship studied using elastic micropatterned substrates. *Nat Cell Biol* **2001,** *3* (5), 466-72.

66. Geiger, B.; Spatz, J. P.; Bershadsky, A. D., Environmental sensing through focal adhesions. *Nat Rev Mol Cell Biol* **2009,** *10* (1), 21-33.

67. Cantini, M.; González-García, C.; Llopis-Hernández, V.; Salmerón-Sánchez, M., Material-Driven Fibronectin Fibrillogenesis. In *Proteins at Interfaces III State of the Art*, Horbett, T.; Brash, J. L.; Norde, W., Eds. 2012; Vol. 1120, pp 471-496.

68. Salmerón-Sánchez, M.; Rico, P.; Moratal, D.; Lee, T. T.; Schwarzbauer, J. E.; García, A. J., Role of material-driven fibronectin fibrillogenesis in cell differentiation. *Biomaterials* **2011,** *32* (8), 2099-105.

69. Llopis-Hernández, V.; Rico, P.; Moratal, D.; Altankov, G.; Salmerón-Sánchez, M., Role of Material-Driven Fibronectin Fibrillogenesis in Protein Remodeling. *BioResearch Open Access* **2013,** *2* (5), 364-373.

70. Mao, Y.; Schwarzbauer, J. E., Fibronectin fibrillogenesis, a cell-mediated matrix assembly process. *Matrix Biol* **2005,** *24* (6), 389-99.

71. Bathawab, F.; Bennett, M.; Cantini, M.; Reboud, J.; Dalby, M. J.; Salmerón-Sánchez, M., Lateral Chain Length in Polyalkyl Acrylates Determines the Mobility of Fibronectin at the Cell/Material Interface. *Langmuir* **2016,** *32* (3), 800-9.

72. Llopis-Hernández, V.; Rico, P.; Moratal, D.; Altankov, G.; Salmerón-Sánchez, M., Role of material-driven fibronectin fibrillogenesis in protein remodeling. *Biores Open Access* **2013,** *2* (5), 364-73.

73. Briz, N.; Antolinos-Turpin, C. M.; Alió, J.; Garagorri, N.; Ribelles, J. L.; Gómez-Tejedor, J. A., Fibronectin fixation on poly(ethyl acrylate)-based copolymers. *J Biomed Mater Res B Appl Biomater* **2013,** *101* (6), 991-7.

74. Llopis-Hernández, V.; Cantini, M.; González-García, C.; Cheng, Z. A.; Yang, J.; Tsimbouri, P. M.; García, A. J.; Dalby, M. J.; Salmerón-Sánchez, M., Material-driven fibronectin assembly for high-efficiency presentation of growth factors. *Sci Adv* **2016,** *2* (8), e1600188.

75. UK, C. R. Worldwide cancer statistics. (accessed February 28th).

76. UK, C. R. Worldwide cancer mortality statistics. (accessed February 2017).

77. Du, Y. X.; Liu, Z. W.; You, L.; Wu, W. M.; Zhao, Y. P., Advances in understanding the molecular mechanism of pancreatic cancer metastasis. *Hepatobiliary Pancreat Dis Int* **2016,** *15* (4), 361-70.

78. Takebe, N.; Nguyen, D.; Yang, S. X., Targeting notch signaling pathway in cancer: clinical development advances and challenges. *Pharmacol Ther* **2014,** *141* (2), 140-9.

79. Topalian, S. L.; Taube, J. M.; Anders, R. A.; Pardoll, D. M., Mechanism-driven biomarkers to guide immune checkpoint blockade in cancer therapy. *Nat Rev Cancer* **2016,** *16* (5), 275-87.

80. Muñoz-Nájar, U. M.; Neurath, K. M.; Vumbaca, F.; Claffey, K. P., Hypoxia stimulates breast carcinoma cell invasion through MT1-MMP and MMP-2 activation. *Oncogene* **2006,** *25* (16), 2379-92.

81. Gilkes, D. M.; Semenza, G. L.; Wirtz, D., Hypoxia and the extracellular matrix: drivers of tumour metastasis. *Nat Rev Cancer* **2014,** *14* (6), 430-9.

82. Muz, B.; de la Puente, P.; Azab, F.; Azab, A. K., The role of hypoxia in cancer progression, angiogenesis, metastasis, and resistance to therapy. *Hypoxia (Auckl)* **2015,** *3*, 83-92.

83. Sudhakar, A., History of Cancer, Ancient and Modern Treatment Methods. *J Cancer Sci Ther* **2009,** *1* (2), 1-4.

84. DeVita, V. T.; Chu, E., A history of cancer chemotherapy. *Cancer Res* **2008,** *68* (21), 8643-53.

85. Chemocare Types of chemotherapy. http://chemocare.com/chemotherapy/what-is-chemotherapy/types-of-chemotherapy.aspx (accessed July).

86. Partridge, A. H.; Burstein, H. J.; Winer, E. P., Side effects of chemotherapy and combined chemohormonal therapy in women with early-stage breast cancer. *J Natl Cancer Inst Monogr* **2001,** (30), 135-42.

87. Fabbrocini, G.; Cameli, N.; Romano, M. C.; Mariano, M.; Panariello, L.; Bianca, D.; Monfrecola, G., Chemotherapy and skin reactions. *J Exp Clin Cancer Res* **2012,** *31*, 50.

88. Cancer.org Chemotherapy Side Effects. https://www.cancer.org/treatment/treatments-and-side-effects/treatment-types/chemotherapy/chemotherapy-side-effects.html (accessed July).

89. Housman, G.; Byler, S.; Heerboth, S.; Lapinska, K.; Longacre, M.; Snyder, N.; Sarkar, S., Drug resistance in cancer: an overview. *Cancers (Basel)* **2014,** *6* (3), 1769-92.

90. Gottesman, M. M., Mechanisms of cancer drug resistance. *Annu Rev Med* **2002,** *53*, 615-27.

91. Holohan, C.; Van Schaeybroeck, S.; Longley, D. B.; Johnston, P. G., Cancer drug resistance: an evolving paradigm. *Nat Rev Cancer* **2013,** *13* (10), 714-26.

92. Borghaei, H.; Smith, M. R.; Campbell, K. S., Immunotherapy of cancer. *Eur J Pharmacol* **2009,** *625* (1-3), 41-54.

93. Couzin-Frankel, J., Breakthrough of the year 2013. Cancer immunotherapy. *Science* **2013,** *342* (6165), 1432-3.

94. Porter, D. L.; Levine, B. L.; Kalos, M.; Bagg, A.; June, C. H., Chimeric antigen receptor-modified T cells in chronic lymphoid leukemia. *N Engl J Med* **2011,** *365* (8), 725-33.

95. Topalian, S. L.; Hodi, F. S.; Brahmer, J. R.; Gettinger, S. N.; Smith, D. C.; McDermott, D. F.; Powderly, J. D.; Carvajal, R. D.; Sosman, J. A.; Atkins, M. B.; Leming, P. D.; Spigel, D. R.; Antonia, S. J.; Horn, L.; Drake, C. G.; Pardoll, D. M.; Chen, L.; Sharfman, W. H.; Anders, R. A.; Taube, J. M.; McMiller, T. L.; Xu, H.; Korman, A. J.; Jure-Kunkel, M.; Agrawal, S.; McDonald, D.; Kollia, G. D.; Gupta, A.; Wigginton, J. M.; Sznol, M., Safety, activity, and immune correlates of anti-PD-1 antibody in cancer. *N Engl J Med* **2012,** *366* (26), 2443-54.

96. Rosenberg, S. A., A new era for cancer immunotherapy based on the genes that encode cancer antigens. *Immunity* **1999,** *10* (3), 281-7.

97. Boon, T.; van der Bruggen, P., Human tumor antigens recognized by T lymphocytes. *J Exp Med* **1996,** *183* (3), 725-9.

98. Rosenberg, S. A., Progress in human tumour immunology and immunotherapy. *Nature* **2001,** *411* (6835), 380-4.

99. Yu, P.; Fu, Y. X., Tumor-infiltrating T lymphocytes: friends or foes? *Lab Invest* **2006,** *86* (3), 231-45.

100. Tang, H.; Qiao, J.; Fu, Y. X., Immunotherapy and tumor microenvironment. *Cancer Lett* **2016,** *370* (1), 85-90.

101. Tanjoni, I.; Walsh, C.; Uryu, S.; Tomar, A.; Nam, J. O.; Mielgo, A.; Lim, S. T.; Liang, C.; Koenig, M.; Sun, C.; Patel, N.; Kwok, C.; McMahon, G.; Stupack, D. G.; Schlaepfer, D. D., PND-1186 FAK inhibitor selectively promotes tumor cell apoptosis in three-dimensional environments. *Cancer Biol Ther* **2010,** *9* (10), 764-77.

102. Walsh, C.; Tanjoni, I.; Uryu, S.; Tomar, A.; Nam, J. O.; Luo, H.; Phillips, A.; Patel, N.; Kwok, C.; McMahon, G.; Stupack, D. G.; Schlaepfer, D. D., Oral delivery of PND-1186 FAK inhibitor decreases tumor growth and spontaneous breast to lung metastasis in pre-clinical models. *Cancer Biol Ther* **2010,** *9* (10), 778-90.

103. Zhang, Y.; Moschetta, M.; Huynh, D.; Tai, Y. T.; Zhang, W.; Mishima, Y.; Ring, J. E.; Tam, W. F.; Xu, Q.; Maiso, P.; Reagan, M.; Sahin, I.; Sacco, A.; Manier, S.; Aljawai, Y.; Glavey, S.; Munshi, N. C.; Anderson, K. C.; Pachter, J.; Roccaro, A. M.; Ghobrial, I. M., Pyk2 promotes tumor progression in multiple myeloma. *Blood* **2014,** *124* (17), 2675-86.

104. Dunn, K. B.; Heffler, M.; Golubovskaya, V. M., Evolving therapies and FAK inhibitors for the treatment of cancer. *Anticancer Agents Med Chem* **2010,** *10* (10), 722-34.

105. Jabłońska-Trypuć, A.; Matejczyk, M.; Rosochacki, S., Matrix metalloproteinases (MMPs), the main extracellular matrix (ECM) enzymes in collagen degradation, as a target for anticancer drugs. *J Enzyme Inhib Med Chem* **2016,** *31* (sup1), 177-183.

106. Overall, C. M.; López-Otín, C., Strategies for MMP inhibition in cancer: innovations for the post-trial era. *Nat Rev Cancer* **2002,** *2* (9), 657-72.

107. Coussens, L. M.; Fingleton, B.; Matrisian, L. M., Matrix metalloproteinase inhibitors and cancer: trials and tribulations. *Science* **2002,** *295* (5564), 2387-92.

108. Cathcart, J.; Pulkoski-Gross, A.; Cao, J., Targeting Matrix Metalloproteinases in Cancer: Bringing New Life to Old Ideas. *Genes Dis* **2015,** *2* (`1), 26-34.

109. Mammoto, T.; Ingber, D. E., Mechanical control of tissue and organ development. *Development* **2010,** *137* (9), 1407-20.

110. Hay, E. D., An overview of epithelio-mesenchymal transformation. *Acta Anat (Basel)* **1995,** *154* (1), 8-20.

111. Kalluri, R.; Weinberg, R. A., The basics of epithelial-mesenchymal transition. *J Clin Invest* **2009,** *119* (6), 1420-8.

112. Kalluri, R.; Neilson, E. G., Epithelial-mesenchymal transition and its implications for fibrosis. *J Clin Invest* **2003,** *112* (12), 1776-84.

113. Lee, J. M.; Dedhar, S.; Kalluri, R.; Thompson, E. W., The epithelial-mesenchymal transition: new insights in signaling, development, and disease. *J Cell Biol* **2006,** *172* (7), 973-81.

114. Stone, R. C.; Pastar, I.; Ojeh, N.; Chen, V.; Liu, S.; Garzon, K. I.; Tomic-Canic, M., Epithelial-mesenchymal transition in tissue repair and fibrosis. *Cell Tissue Res* **2016,** *365* (3), 495-506.

115. Gonzalez, D. M.; Medici, D., Signaling mechanisms of the epithelial-mesenchymal transition. *Sci Signal* **2014,** *7* (344), re8.

116. Zeisberg, M.; Neilson, E. G., Biomarkers for epithelial-mesenchymal transitions. *J Clin Invest* **2009,** *119* (6), 1429-37.

117. Acloque, H.; Adams, M. S.; Fishwick, K.; Bronner-Fraser, M.; Nieto, M. A., Epithelial-mesenchymal transitions: the importance of changing cell state in development and disease. *J Clin Invest* **2009,** *119* (6), 1438-49.

118. Okada, H.; Danoff, T. M.; Kalluri, R.; Neilson, E. G., Early role of Fsp1 in epithelial-mesenchymal transformation. *Am J Physiol* **1997,** *273* (4 Pt 2), F563-74.

119. Hanahan, D.; Weinberg, R. A., The hallmarks of cancer. *Cell* **2000,** *100* (1), 57-70.

120. Thiery, J. P., Epithelial-mesenchymal transitions in tumour progression. *Nat Rev Cancer* **2002,** *2* (6), 442-54.

121. Fidler, I. J.; Poste, G., The "seed and soil" hypothesis revisited. *Lancet Oncol* **2008,** *9* (8), 808.

122. Karlsson, M. C.; Gonzalez, S. F.; Welin, J.; Fuxe, J., Epithelial-Mesenchymal transition in cancer metastasis through the lymphatic system. *Mol Oncol* **2017**.

123. Fidler, I. J.; Balch, C. M., The biology of cancer metastasis and implications for therapy. *Curr Probl Surg* **1987,** *24* (3), 129-209.

124. Luzzi, K. J.; MacDonald, I. C.; Schmidt, E. E.; Kerkvliet, N.; Morris, V. L.; Chambers, A. F.; Groom, A. C., Multistep nature of metastatic inefficiency: dormancy of solitary cells after successful extravasation and limited survival of early micrometastases. *Am J Pathol* **1998,** *153* (3), 865-73.

125. Gupta, P. B.; Mani, S.; Yang, J.; Hartwell, K.; Weinberg, R. A., The evolving portrait of cancer metastasis. *Cold Spring Harb Symp Quant Biol* **2005,** *70*, 291-7.

126. Mani, S. A.; Yang, J.; Brooks, M.; Schwaninger, G.; Zhou, A.; Miura, N.; Kutok, J. L.; Hartwell, K.; Richardson, A. L.; Weinberg, R. A., Mesenchyme Forkhead 1 (FOXC2) plays a key role in metastasis and is associated with aggressive basal-like breast cancers. *Proc Natl Acad Sci U S A* **2007,** *104* (24), 10069-74.

127. Mani, S. A.; Guo, W.; Liao, M. J.; Eaton, E. N.; Ayyanan, A.; Zhou, A. Y.; Brooks, M.; Reinhard, F.; Zhang, C. C.; Shipitsin, M.; Campbell, L. L.; Polyak, K.; Brisken, C.; Yang, J.; Weinberg, R. A., The epithelial-mesenchymal transition generates cells with properties of stem cells. *Cell* **2008,** *133* (4), 704-15.

128. Trerotola, M.; Jernigan, D. L.; Liu, Q.; Siddiqui, J.; Fatatis, A.; Languino, L. R., Trop-2 promotes prostate cancer metastasis by modulating β(1) integrin functions. *Cancer Res* **2013,** *73* (10), 3155-67.

129. Ruoslahti, E., Fibronectin in cell adhesion and invasion. *Cancer Metastasis Rev* **1984,** *3* (1), 43-51.

130. Ruoslahti, E., Fibronectin and its integrin receptors in cancer. *Adv Cancer Res* **1999,** *76*, 1-20.

131. Fornaro, M.; Plescia, J.; Chheang, S.; Tallini, G.; Zhu, Y. M.; King, M.; Altieri, D. C.; Languino, L. R., Fibronectin protects prostate cancer cells from tumor necrosis factor-alpha-induced apoptosis via the AKT/survivin pathway. *J Biol Chem* **2003,** *278* (50), 50402-11.

132. Thant, A. A.; Nawa, A.; Kikkawa, F.; Ichigotani, Y.; Zhang, Y.; Sein, T. T.; Amin, A. R.; Hamaguchi, M., Fibronectin activates matrix metalloproteinase-9 secretion via the MEK1-MAPK and the PI3K-Akt pathways in ovarian cancer cells. *Clin Exp Metastasis* **2000,** *18* (5), 423-8.

133. Wang, J. P.; Hielscher, A., Fibronectin: How Its Aberrant Expression in Tumors May Improve Therapeutic Targeting. *J Cancer* **2017,** *8* (4), 674-682.

134. Lee, H. A.; Park, I.; Byun, H. J.; Jeoung, D.; Kim, Y. M.; Lee, H., Metastasis suppressor KAI1/CD82 attenuates the matrix adhesion of human prostate cancer cells by suppressing fibronectin expression and β1 integrin activation. *Cell Physiol Biochem* **2011,** *27* (5), 575-86.

135. McNicol, L. A.; Kelley, C. A.; Sipe, J. D.; National Institutes of Health (U.S.). Bioengineering Consortium., *Reparative medicine*

growing tissues and organs. New York Academy of Sciences: New York, N. Y., 2002.

136. Griffith, L. G.; Naughton, G., Tissue engineering--current challenges and expanding opportunities. *Science* **2002,** *295* (5557), 1009-14.

137. Pompe, T.; Markowski, M.; Werner, C., Modulated fibronectin anchorage at polymer substrates controls angiogenesis. *Tissue Eng* **2004,** *10* (5-6), 841-8.

138. Werner, C.; Garcia, A. J., Interfaces to Control Cell-Biomaterial Adhesive Interactions. In *Polymers for Regenerative Medicine*, Werner, C., Ed. Springer: Berlin Heidelberg, 2006; Vol. 203, pp 171-190.

139. Salmerón-Sánchez, M.; Altankov, G., Cell-protein-material interaction in tissue engineering. In *Tissue Engineering*, Eberli, D., Ed. InTech: Vienna, Austria, 2010; pp 77-102.

140. Erickson, H. P.; Carrell, N.; McDonagh, J., Fibronectin molecule visualized in electron microscopy: a long, thin, flexible strand. *J Cell Biol* **1981,** *91* (3 Pt 1), 673-78.

141. Erickson, H. P.; Carrell, N. A., Fibronectin in extended and compact conformations. Electron microscopy and sedimentation analysis. *J Biol Chem* **1983,** *258* (23), 14539-44.

142. Geiger, B.; Bershadsky, A.; Pankov, R.; Yamada, K. M., Transmembrane crosstalk between the extracellular matrix--cytoskeleton crosstalk. *Nat Rev Mol Cell Biol* **2001,** *2* (11), 793-805.

143. Toworfe, G. K.; Composto, R. J.; Adams, C. S.; Shapiro, I. M.; Ducheyne, P., Fibronectin adsorption on surface-activated poly(dimethylsiloxane) and its effect on cellular function. *J Biomed Mater Res A* **2004,** *71* (3), 449-61.

144. Baugh, L.; Vogel, V., Structural changes of fibronectin adsorbed to model surfaces probed by fluorescence resonance energy transfer. *J Biomed Mater Res A* **2004,** *69* (3), 525-34.

145. Grinnell, F.; Feld, M. K., Fibronectin adsorption on hydrophilic and hydrophobic surfaces detected by antibody binding and analyzed during cell adhesion in serum-containing medium. *J Biol Chem* **1982,** *257* (9), 4888-93.

146. Altankov, G.; Thom, V.; Groth, T.; Jankova, K.; Jonsson, G.; Ulbricht, M., Modulating the biocompatibility of polymer surfaces with poly(ethylene glycol): effect of fibronectin. *J Biomed Mater Res* **2000,** *52* (1), 219-30.

147. Keselowsky, B. G.; Collard, D. M.; García, A. J., Surface chemistry modulates fibronectin conformation and directs integrin binding and specificity to control cell adhesion. *J Biomed Mater Res A* **2003,** *66* (2), 247-59.

148. Marco, C.; Cristina, G.-G.; Virginia, L.-H.; Manuel, S.-S., Material-Driven Fibronectin Fibrillogenesis. In *Proteins at Interfaces III State of the Art*, American Chemical Society: 2012; Vol. 1120, pp 471-496.

149. Smith, P. K.; Krohn, R. I.; Hermanson, G. T.; Mallia, A. K.; Gartner, F. H.; Provenzano, M. D.; Fujimoto, E. K.; Goeke, N. M.; Olson, B. J.; Klenk, D. C., Measurement of protein using bicinchoninic acid. *Anal Biochem* **1985,** *150* (1), 76-85.

150. Humphries, M. J., Cell adhesion assays. In *Methods Mol Biol*, 2009; Vol. 522, pp 203-10.

151. Selinummi, J.; Seppälä, J.; Yli-Harja, O.; Puhakka, J. A., Software for quantification of labeled bacteria from digital microscope images by automated image analysis. *Biotechniques* **2005,** *39* (6), 859-63.

152. Scientific, T. **How Zenon Labeling Technology works**. https://www.thermofisher.com/uk/en/home/life-science/cell-analysis/labeling-chemistry/protein-and-antibody-chemical-labeling/antibody-protein-labeling-kits/zenon-antibody-labeling-kits.html (accessed March).

153. ME, B.; SM, G. Focal Adhesion Analysis Server. http://faas.bme.unc.edu/ (accessed January).

154. Berginski, M. E.; Gomez, S. M., The Focal Adhesion Analysis Server: a web tool for analyzing focal adhesion dynamics. *F1000Res* **2013,** *2*, 68.

155. Zaidel-Bar, R.; Cohen, M.; Addadi, L.; Geiger, B., Hierarchical assembly of cell-matrix adhesion complexes. *Biochem Soc Trans* **2004,** *32* (Pt3), 416-20.

156. Keselowsky, B. G.; Collard, D. M.; García, A. J., Surface chemistry modulates focal adhesion composition and signaling through changes in integrin binding. *Biomaterials* **2004,** *25* (28), 5947-54.

157. Keselowsky, B. G.; Collard, D. M.; García, A. J., Integrin binding specificity regulates biomaterial surface chemistry effects on cell differentiation. *Proc Natl Acad Sci U S A* **2005,** *102* (17), 5953-7.

158. García, A. J.; Schwarzbauer, J. E.; Boettiger, D., Distinct activation states of alpha5beta1 integrin show differential binding to RGD and synergy domains of fibronectin. *Biochemistry* **2002,** *41* (29), 9063-9.

159. Galbraith, C. G.; Yamada, K. M.; Sheetz, M. P., The relationship between force and focal complex development. *J Cell Biol* **2002,** *159* (4), 695-705.

160. Dumbauld, D. W.; Lee, T. T.; Singh, A.; Scrimgeour, J.; Gersbach, C. A.; Zamir, E. A.; Fu, J.; Chen, C. S.; Curtis, J. E.; Craig, S. W.; García, A. J., How vinculin regulates force transmission. *Proc Natl Acad Sci U S A* **2013,** *110* (24), 9788-93.

161. Chan, C. E.; Odde, D. J., Traction dynamics of filopodia on compliant substrates. *Science* **2008,** *322* (5908), 1687-91.

162. Yim, E. K.; Darling, E. M.; Kulangara, K.; Guilak, F.; Leong, K. W., Nanotopography-induced changes in focal adhesions, cytoskeletal organization, and mechanical properties of human mesenchymal stem cells. *Biomaterials* **2010,** *31* (6), 1299-306.

163. Dalby, M. J.; Gadegaard, N.; Oreffo, R. O., Harnessing nanotopography and integrin-matrix interactions to influence stem cell fate. *Nat Mater* **2014,** *13* (6), 558-69.

164. Handorf, A. M.; Zhou, Y.; Halanski, M. A.; Li, W. J., Tissue stiffness dictates development, homeostasis, and disease progression. *Organogenesis* **2015,** *11* (1), 1-15.

165. Ferlay, J.; Steliarova-Foucher, E.; Lortet-Tieulent, J.; Rosso, S.; Coebergh, J. W.; Comber, H.; Forman, D.; Bray, F., Cancer incidence and mortality patterns in Europe: estimates for 40 countries in 2012. *Eur J Cancer* **2013,** *49* (6), 1374-403.

166. Siegel, R. L.; Miller, K. D.; Jemal, A., Cancer statistics, 2015. *CA Cancer J Clin* **2015,** *65* (1), 5-29.

167. UK, C. R. Prostate Cancer. https://www.cancerresearchuk.org/about-cancer/prostate-cancer/ (accessed June).

168. Massie, C. E.; Lynch, A.; Ramos-Montoya, A.; Boren, J.; Stark, R.; Fazli, L.; Warren, A.; Scott, H.; Madhu, B.; Sharma, N.; Bon, H.; Zecchini, V.; Smith, D. M.; Denicola, G. M.; Mathews, N.; Osborne, M.; Hadfield, J.; Macarthur, S.; Adryan, B.; Lyons, S. K.; Brindle, K. M.; Griffiths, J.; Gleave, M. E.; Rennie, P. S.; Neal, D. E.; Mills, I. G., The androgen receptor fuels prostate cancer by regulating central metabolism and biosynthesis. *EMBO J* **2011,** *30* (13), 2719-33.

169. Hååg, P.; Bektic, J.; Bartsch, G.; Klocker, H.; Eder, I. E., Androgen receptor down regulation by small interference RNA induces cell growth inhibition in androgen sensitive as well as in androgen independent prostate cancer cells. *J Steroid Biochem Mol Biol* **2005,** *96* (3-4), 251-8.

170. Hara, T.; Miyazaki, H.; Lee, A.; Tran, C. P.; Reiter, R. E., Androgen receptor and invasion in prostate cancer. *Cancer Res* **2008,** *68* (4), 1128-35.

171. Snoek, R.; Cheng, H.; Margiotti, K.; Wafa, L. A.; Wong, C. A.; Wong, E. C.; Fazli, L.; Nelson, C. C.; Gleave, M. E.; Rennie, P. S., In vivo knockdown of the androgen receptor results in growth inhibition and regression of well-established, castration-resistant prostate tumors. *Clin Cancer Res* **2009,** *15* (1), 39-47.

172. Lee RJ, S. M., *Hormone Therapy for Prostate Cancer.* 5th ed ed.; Sultan Qaboos University Sultan Qaboos University 2011.

173. Kumar, S.; Shelley, M.; Harrison, C.; Coles, B.; Wilt, T. J.; Mason, M. D., Neo-adjuvant and adjuvant hormone therapy for localised and locally advanced prostate cancer. *Cochrane Database Syst Rev* **2006,** (4), CD006019.

174. Visakorpi, T.; Hyytinen, E.; Koivisto, P.; Tanner, M.; Keinänen, R.; Palmberg, C.; Palotie, A.; Tammela, T.; Isola, J.; Kallioniemi, O. P., In vivo amplification of the androgen receptor gene and progression of human prostate cancer. *Nat Genet* **1995,** *9* (4), 401-6.

175. Steinkamp, M. P.; O'Mahony, O. A.; Brogley, M.; Rehman, H.; Lapensee, E. W.; Dhanasekaran, S.; Hofer, M. D.; Kuefer, R.; Chinnaiyan, A.; Rubin, M. A.; Pienta, K. J.; Robins, D. M., Treatment-dependent androgen receptor mutations in prostate cancer exploit multiple mechanisms to evade therapy. *Cancer Res* **2009,** *69* (10), 4434-42.

176. Stone, K. R.; Mickey, D. D.; Wunderli, H.; Mickey, G. H.; Paulson, D. F., Isolation of a human prostate carcinoma cell line (DU 145). *Int J Cancer* **1978,** *21* (3), 274-81.

177. van Golen, K. L.; Bao, L.; Brewer, G. J.; Pienta, K. J.; Kamradt, J. M.; Livant, D. L.; Merajver, S. D., Suppression of tumor recurrence and metastasis by a combination of the PHSCN sequence and the antiangiogenic compound tetrathiomolybdate in prostate carcinoma. *Neoplasia* **2002,** *4* (5), 373-9.

178. Yao, H.; Veine, D. M.; Zeng, Z. Z.; Fay, K. S.; Staszewski, E. D.; Livant, D. L., Increased potency of the PHSCN dendrimer as an inhibitor of human prostate cancer cell invasion, extravasation, and lung colony formation. *Clin Exp Metastasis* **2010,** *27* (3), 173-84.

179. Mosmann, T., Rapid colorimetric assay for cellular growth and survival: application to proliferation and cytotoxicity assays. *J Immunol Methods* **1983,** *65* (1-2), 55-63.

180. John, C. K., Place of the Methylene Blue and Resazurin Reduction Tests in a Milk Control Program. *Am J Public Health Nations Health* **1939,** *29* (3), 239-47.

181. Hernández-Vargas, H.; Palacios, J.; Moreno-Bueno, G., Molecular profiling of docetaxel cytotoxicity in breast cancer cells: uncoupling of aberrant mitosis and apoptosis. *Oncogene* **2007,** *26* (20), 2902-13.

182. Ridley, A.; Peckham, M.; Peter, C., *Cell Motility : From Molecules to Organisms*. 3 ed.; John Wiley & Sons: 2005; p 364.

183. Tse, J. R.; Engler, A. J., Preparation of hydrogel substrates with tunable mechanical properties. *Curr Protoc Cell Biol* **2010,** *Chapter 10*, Unit 10.16.

184. Müller, C.; Pompe, T., Distinct impacts of substrate elasticity and ligand affinity on traction force evolution. *Soft Matter* **2016,** *12* (1), 272-80.

185. Pompe, T.; Kaufmann, M.; Kasimir, M.; Johne, S.; Glorius, S.; Renner, L.; Bobeth, M.; Pompe, W.; Werner, C., Friction-controlled traction force in cell adhesion. *Biophys J* **2011,** *101* (8), 1863-70.

186. Pompe, T.; Glorius, S.; Bischoff, T.; Uhlmann, I.; Kaufmann, M.; Brenner, S.; Werner, C., Dissecting the impact of matrix anchorage and elasticity in cell adhesion. *Biophys J* **2009,** *97* (8), 2154-63.

187. Butler, J. P.; Tolić-Nørrelykke, I. M.; Fabry, B.; Fredberg, J. J., Traction fields, moments, and strain energy that cells exert on their surroundings. *Am J Physiol Cell Physiol* **2002,** *282* (3), C595-605.

188. Tolić-Nørrelykke, I. M.; Butler, J. P.; Chen, J.; Wang, N., Spatial and temporal traction response in human airway smooth muscle cells. *Am J Physiol Cell Physiol* **2002,** *283* (4), C1254-66.

189. McCloy, R. A.; Rogers, S.; Caldon, C. E.; Lorca, T.; Castro, A.; Burgess, A., Partial inhibition of Cdk1 in G 2 phase overrides the SAC and decouples mitotic events. *Cell Cycle* **2014,** *13* (9), 1400-12.

190. Institute, W. T. S. Genomics of Drug Sensitivity in Cancer. http://www.cancerrxgene.org/translation/Drug/1007 (accessed May).

191. Overstreet, M. G.; Gaylo, A.; Angermann, B. R.; Hughson, A.; Hyun, Y. M.; Lambert, K.; Acharya, M.; Billroth-Maclurg, A. C.; Rosenberg, A. F.; Topham, D. J.; Yagita, H.; Kim, M.; Lacy-Hulbert, A.; Meier-Schellersheim, M.; Fowell, D. J., Inflammation-induced interstitial migration of effector $CD4^+$ T cells is dependent on integrin αV. *Nat Immunol* **2013,** *14* (9), 949-58.

192. Georgoulis, A.; Havaki, S.; Drosos, Y.; Goutas, N.; Vlachodimitropoulos, D.; Aleporou-Marinou, V.; Kittas, C.; Marinos, E.; Kouloukoussa, M., RGD binding to integrin alphavbeta3 affects cell motility and adhesion in primary human breast cancer cultures. *Ultrastruct Pathol* **2012,** *36* (6), 387-99.

193. Maheshwari, G.; Brown, G.; Lauffenburger, D. A.; Wells, A.; Griffith, L. G., Cell adhesion and motility depend on nanoscale RGD clustering. *J Cell Sci* **2000,** *113 (Pt 10)*, 1677-86.

194. Rodriguez, L. G.; Wu, X.; Guan, J. L., Wound-healing assay. *Methods Mol Biol* **2005,** *294*, 23-9.

195. Yarrow, J. C.; Perlman, Z. E.; Westwood, N. J.; Mitchison, T. J., A high-throughput cell migration assay using scratch wound healing, a comparison of image-based readout methods. *BMC Biotechnol* **2004,** *4*, 21.

196. Liang, C. C.; Park, A. Y.; Guan, J. L., In vitro scratch assay: a convenient and inexpensive method for analysis of cell migration in vitro. *Nat Protoc* **2007,** *2* (2), 329-33.

197. Hauck, C. R.; Hsia, D. A.; Schlaepfer, D. D., The focal adhesion kinase--a regulator of cell migration and invasion. *IUBMB Life* **2002,** *53* (2), 115-9.

198. Serrels, A.; McLeod, K.; Canel, M.; Kinnaird, A.; Graham, K.; Frame, M. C.; Brunton, V. G., The role of focal adhesion kinase catalytic activity on the proliferation and migration of squamous cell carcinoma cells. *Int J Cancer* **2012,** *131* (2), 287-97.

199. Frisch, S. M.; Vuori, K.; Ruoslahti, E.; Chan-Hui, P. Y., Control of adhesion-dependent cell survival by focal adhesion kinase. *J Cell Biol* **1996,** *134* (3), 793-9.

200. Schultze, A.; Fiedler, W., Therapeutic potential and limitations of new FAK inhibitors in the treatment of cancer. *Expert Opin Investig Drugs* **2010,** *19* (6), 777-88.

201. McLean, G. W.; Carragher, N. O.; Avizienyte, E.; Evans, J.; Brunton, V. G.; Frame, M. C., The role of focal-adhesion kinase in cancer - a new therapeutic opportunity. *Nat Rev Cancer* **2005,** *5* (7), 505-15.

202. Brooke N. Mason , J. P. C., Cynthia A. Reinhart-King, Matrix Stiffness: A Regulator of Cellular Behavior and Tissue Formation. In *Engineering Biomaterials for Regenerative Medicine*, Bhatia, S. K., Ed. Springer: New york, 2012; pp 19-37.

203. Yip, A. K.; Iwasaki, K.; Ursekar, C.; Machiyama, H.; Saxena, M.; Chen, H.; Harada, I.; Chiam, K. H.; Sawada, Y., Cellular response to substrate rigidity is governed by either stress or strain. *Biophys J* **2013,** *104* (1), 19-29.

204. Lo, C. M.; Wang, H. B.; Dembo, M.; Wang, Y. L., Cell movement is guided by the rigidity of the substrate. *Biophys J* **2000,** *79* (1), 144-52.

205. Zhao, X.; Guan, J. L., Focal adhesion kinase and its signaling pathways in cell migration and angiogenesis. *Adv Drug Deliv Rev* **2011,** *63* (8), 610-5.

206. Parsons, J. T., Focal adhesion kinase: the first ten years. *J Cell Sci* **2003,** *116* (Pt 8), 1409-16.

207. Siesser, P. M.; Hanks, S. K., The signaling and biological implications of FAK overexpression in cancer. *Clin Cancer Res* **2006,** *12* (11 Pt 1), 3233-7.

208. Hauck, C. R.; Hsia, D. A.; Puente, X. S.; Cheresh, D. A.; Schlaepfer, D. D., FRNK blocks v-Src-stimulated invasion and experimental metastases without effects on cell motility or growth. *EMBO J* **2002,** *21* (23), 6289-302.

209. Mnatsakanyan, H.; Rico, P.; Grigoriou, E.; Candelas, A. M.; Rodrigo-Navarro, A.; Salmeron-Sanchez, M.; Sabater i Serra, R., Controlled Assembly of Fibronectin Nanofibrils Triggered by Random Copolymer Chemistry. *ACS Appl Mater Interfaces* **2015,** *7* (32), 18125-35.

210. Hutmacher, D. W., Biomaterials offer cancer research the third dimension. *Nat Mater* **2010,** *9* (2), 90-3.

211. Loessner, D.; Stok, K. S.; Lutolf, M. P.; Hutmacher, D. W.; Clements, J. A.; Rizzi, S. C., Bioengineered 3D platform to explore cell-ECM interactions and drug resistance of epithelial ovarian cancer cells. *Biomaterials* **2010,** *31* (32), 8494-506.

212. Nyga, A.; Cheema, U.; Loizidou, M., 3D tumour models: novel in vitro approaches to cancer studies. *J Cell Commun Signal* **2011,** *5* (3), 239-48.

213. Sutherland, R. M., Cell and environment interactions in tumor microregions: the multicell spheroid model. *Science* **1988,** *240* (4849), 177-84.

214. Monazzam, A.; Razifar, P.; Ide, S.; Rugaard Jensen, M.; Josephsson, R.; Blomqvist, C.; Langström, B.; Bergström, M., Evaluation of the Hsp90 inhibitor NVP-AUY922 in multicellular tumour spheroids with respect to effects on growth and PET tracer uptake. *Nucl Med Biol* **2009,** *36* (3), 335-42.

215. Lee, G. Y.; Kenny, P. A.; Lee, E. H.; Bissell, M. J., Three-dimensional culture models of normal and malignant breast epithelial cells. *Nat Methods* **2007,** *4* (4), 359-65.

216. Phelps, E. A.; Enemchukwu, N. O.; Fiore, V. F.; Sy, J. C.; Murthy, N.; Sulchek, T. A.; Barker, T. H.; García, A. J., Maleimide cross-linked bioactive PEG hydrogel exhibits improved reaction kinetics and cross-linking for cell encapsulation and in situ delivery. *Adv Mater* **2012,** *24* (1), 64-70, 2.

217. Phelps, E. A.; Templeman, K. L.; Thulé, P. M.; García, A. J., Engineered VEGF-releasing PEG-MAL hydrogel for pancreatic islet vascularization. *Drug Deliv Transl Res* **2015,** *5* (2), 125-36.

218. Enemchukwu, N. O.; Cruz-Acuña, R.; Bongiorno, T.; Johnson, C. T.; García, J. R.; Sulchek, T.; García, A. J., Synthetic matrices reveal contributions of ECM biophysical and biochemical properties to epithelial morphogenesis. *J Cell Biol* **2016,** *212* (1), 113-24.

219. Raeber, G. P.; Lutolf, M. P.; Hubbell, J. A., Molecularly engineered PEG hydrogels: a novel model system for proteolytically mediated cell migration. *Biophys J* **2005,** *89* (2), 1374-88.

220. Eckhard, U.; Huesgen, P. F.; Schilling, O.; Bellac, C. L.; Butler, G. S.; Cox, J. H.; Dufour, A.; Goebeler, V.; Kappelhoff, R.; Keller, U. A. D.; Klein, T.; Lange, P. F.; Marino, G.; Morrison, C. J.; Prudova, A.; Rodriguez, D.; Starr, A. E.; Wang, Y.; Overall, C. M., Active site specificity profiling of the matrix metalloproteinase family: Proteomic identification of 4300 cleavage sites by nine MMPs explored with structural and synthetic peptide cleavage analyses. *Matrix Biol* **2016,** *49*, 37-60.

221. Zisch, A. H.; Lutolf, M. P.; Ehrbar, M.; Raeber, G. P.; Rizzi, S. C.; Davies, N.; Schmökel, H.; Bezuidenhout, D.; Djonov, V.; Zilla, P.; Hubbell, J. A., Cell-demanded release of VEGF from synthetic, biointeractive cell ingrowth matrices for vascularized tissue growth. *FASEB J* **2003,** *17* (15), 2260-2.

222. Zustiak, S. P.; Leach, J. B., Hydrolytically degradable poly(ethylene glycol) hydrogel scaffolds with tunable degradation and mechanical properties. *Biomacromolecules* **2010,** *11* (5), 1348-57.

223. Deshmukh, M.; Singh, Y.; Gunaseelan, S.; Gao, D.; Stein, S.; Sinko, P. J., Biodegradable poly(ethylene glycol) hydrogels based on a self-elimination degradation mechanism. *Biomaterials* **2010,** *31* (26), 6675-84.

224. Solomonov, I.; Zehorai, E.; Talmi-Frank, D.; Wolf, S. G.; Shainskaya, A.; Zhuravlev, A.; Kartvelishvily, E.; Visse, R.; Levin, Y.; Kampf, N.; Jaitin, D. A.; David, E.; Amit, I.; Nagase, H.; Sagi, I., Distinct biological events generated by ECM proteolysis by two homologous collagenases. *Proc Natl Acad Sci U S A* **2016,** *113* (39), 10884-9.

225. Zieris, A.; Prokoph, S.; Levental, K. R.; Welzel, P. B.; Grimmer, M.; Freudenberg, U.; Werner, C., FGF-2 and VEGF functionalization of starPEG-heparin hydrogels to modulate biomolecular and physical cues of angiogenesis. *Biomaterials* **2010,** *31* (31), 7985-94.

226. Kloxin, A. M.; Kloxin, C. J.; Bowman, C. N.; Anseth, K. S., Mechanical properties of cellularly responsive hydrogels and their experimental determination. *Adv Mater* **2010,** *22* (31), 3484-94.

227. Singh, S. P.; Schwartz, M. P.; Lee, J. Y.; Fairbanks, B. D.; Anseth, K. S., A peptide functionalized poly(ethylene glycol) (PEG) hydrogel for investigating the influence of biochemical and biophysical matrix properties on tumor cell migration. *Biomater Sci* **2014,** *2* (7), 1024-1034.

228. Cavalcanti-Adam, E. A.; Volberg, T.; Micoulet, A.; Kessler, H.; Geiger, B.; Spatz, J. P., Cell spreading and focal adhesion dynamics are regulated by spacing of integrin ligands. *Biophys J* **2007,** *92* (8), 2964-74.

229. Roca-Cusachs, P.; Conte, V.; Trepat, X., Quantifying forces in cell biology. *Nat Cell Biol* **2017,** *19* (7), 742-751.

Appendices

Publications

Vanterpool, F. Cantini, M. Seib, FP, Salmerón-Sánchez M., A material-based platform to modulate fibronectin activity and focal adhesion assembly. Bioresearch Open Access 2014, 3 (6), 286-96.

Van Duong, H. Thahn Dang, NT. Tran, HT. Vanterpool, F. Salmerón-Sánchez M., Lizundia, E. Nguyen, VL. Nguyen TD., Biocompatible Chitosan-functionalized Upconverting Nanocomposites. Submitted.

Vanterpool, F. Cantini, M. Seib, FP, Salmerón-Sánchez M., Effect of fibronectin on cancer cell adhesion and mechanics. *Submitted.*

Presentations

(2016) Poster presentation at the British Orthapaedic Research Society (BORS), Glasgow, UK: Vanterpool, F. Cantini, M. Seib, FP, Salmerón-Sánchez M., Fibronectin-Based Microenvironments to Understand the Migration and Biomechanics of Cells.

(2015) Poster presentation at the Controlled Release Society (CRS), Edinburgh, UK: Vanterpool, F. Cantini, M. Seib, FP, Salmerón-Sánchez M., Deconstructing the tumour microenvironment – the role of fibronectin.